Stian Ismar
Morten Olsen Osvik

Detecting Gear and Bearing Faults in Wind Turbines Using Vibration Analysis

A Practical Application of Spectral Analysis and K-Means Clustering

Master's thesis

NTNU
Norwegian University of Science and Technology
Faculty of Engineering
Department of Mechanical and Industrial Engineering

NTNU
Norwegian University of
Science and Technology

Stian Ismar
Morten Olsen Osvik

Detecting Gear and Bearing Faults in Wind Turbines Using Vibration Analysis

A Practical Application of Spectral Analysis and K-Means Clustering

NTNU
Norwegian University of
Science and Technology

Preface

This thesis was carried out during the spring semester of 2020 and concludes our Master of Science in Engineering and ICT at the Norwegian University of Science and Technology (NTNU). The thesis was conducted in collaboration with the Norwegian power company TrønderEnergi.

Data from wind turbines situated at Skomakerfjellet, Norway has been analysed throughout this thesis. The preliminary project thesis provided an introduction to the wind turbine domain and fault detection methods, without using vibration data. In this master thesis however, vibration data was provided by TrønderEnergi, allowing for a different fault detection approach.

We would like to thank TrønderEnergi for sharing data and allowing us to visit the wind park at Skomakerfjellet. Special thanks to Zhenyou Zhang and Hans Kjetil Stein at TrønderEnergi for valuable insight into condition monitoring of wind turbines. Finally, we would like to thank our supervisors Bjørn Haugen and Odd Erik Gundersen for continuous guidance, valuable feedback, and motivation to work with the thesis.

<div align="center">Trondheim, June 2020</div>

Morten Olsen Osvik

Stian Ismar

Abstract

Monitoring wind turbine components through vibration signals enable operators to detect faults at an early stage, reducing operation and maintenance costs and improving reliability. Consequently, operators such as TrønderEnergi wish to implement monitoring systems utilising vibration signals. This thesis examined vibration signals from four wind turbines owned by TrønderEnergi in order to detect faults and fault development of gears and bearings. In addition, the research explored whether a relationship between start-stop cycles and degradation existed. Most research relies on component dimensions and state when monitoring conditions to validate their results. This study, however, aims to demonstrate the potential for exploratory analysis using only vibration and operational data, when component dimensions and component status is unavailable from the manufacturer.

The signals, recorded from August 2018 to January 2020, were analysed using two approaches. The first was a traditional vibration analysis consisting of order analysis used to inspect gears and an envelope order analysis applied to study bearings. The traditional approach was used to detect faults and fault development over time by inspecting spectrums. Spectrum comparison was carried out. The second approach was a data-driven clustering method using the K-means clustering algorithm, with the aim of detecting fault development over time. Documented features from previous literature were extracted from the signals, enabling the clustering method to identify transient signals and non-linearities, thus detecting fault development over time.

The results of the traditional vibration analysis suggested that one of the turbines could have an early parallel gear and a bearing fault. The same turbine had the highest number of start-stop cycles, which suggested a relation between start-stop cycles and faults. The traditional vibration analysis and the clustering results indicated that no fault development had occurred during the time period. This either suggested that the proposed fault development methods were unable to detect an actual deterioration over time, or that no fault development existed in the signals. The missing information regarding the component dimensions limited the conclusiveness of the results. This study would greatly benefit from knowing this information, and it is recommended that efforts are made to obtain it from the wind turbine manufacturers in future projects.

Sammendrag

Overvåking av vindturbinkomponenter ved bruk av vibrasjonssignaler tillater operatører å detektere tidlige feil. Dette bidrar til å redusere kostnader tilknyttet drift og vedlikehold samt redusere driftstans. Operatører som TrønderEnergi ønsker derfor å implementere overvåkningssystemer for vibrasjonssignaler. Denne masteroppgaven undersøker vibrasjonssignaler fra fire vindturbiner eid av TrønderEnergi for å oppdage feil og feilutvikling av komponenter i girboksen og kulelager tilknyttet høyhastighetsakslingen. Studiet undersøker også om det finnes et forhold mellom antall start-stopp sykluser og feil. Tidligere relevant forskning støtter seg på informasjon om komponentenes dimensjoner og tilstand for å validere resultatene. Denne oppgaven skiller seg fra andre ved at denne informasjonen var utilgjengelig fra produsenten.

Vibrasjonssignalene var hentet fra august 2018 til januar 2020 og ble analysert med to metoder. Den første metoden var en tradisjonell vibrasjonsanalyse besående av en *order* analyse for å oppdage girfeil og en *evelope order* analyse for å finne feil i kulelager. Den overordnede hensikten med den tradisjonelle metoden var å oppdage feil og feilutvikling over tid. Her var spektrum-analyse et sentralt verktøy. Den andre metoden var en datadreven clustering-teknikk implementert med K-means algoritmen. For å kunne skille ut transiente signaler og ikke-lineære sammenhenger som kunne indikere feil, ble veldokumenterte attributter trukket ut fra signalene. Målet med clustering-teknikken var å oppdage feilutvikling over tid.

Resultatene fra den tradisjonelle vibrasjonsanalysen indikerte at en av turbinene hadde en tidlig kulelager- og girfeil. Ettersom den samme turbinen hadde betydelig flere start-stopp sykluser enn de andre, pekte det på en sammenheng mellom start-stopp sykluser og feil. Resultatene fra den tradisjonelle og den datadrevne metoden viste ingen tegn på feilutvikling. Dette tydet enten på at de to foreslåtte metodene ikke var i stand til å oppdage noen feilutvikling, eller at det faktisk ikke eksisterte noen feilutvikling. På bakgrunn av de manglende komponentdimensjonene, kunne ikke en endelig konklusjon tas med sikkerhet. Denne studien viser at det er svært hensiktsmessig å innhente denne informasjonen for fremtidige prosjekter.

Table of Contents

List of Tables

List of Figures

Abbreviations

AI	=	Artificial Intelligence
ANN	=	Artificial Newral Network
BPFO	=	Ball Pass Frequency Outer race
CF	=	Characteristic Frequency
CM	=	Condition Monitoring
DFT	=	Discrete Fourier Transformation
EMD	=	Empirical Mode Decomposition
EEMD	=	Ensamble Empirical Mode Decomposition
EOA	=	Envelope Order Analysis
FFT	=	Fast Fourier Transformation
GMF	=	Gear Mesh Frequency
HOS	=	Higher Order Statistics
HSS	=	High Speed Shaft
IRENA	=	The International Renewable Energy Agency
IMF	=	Intrinsic Mode Function
ML	=	Machine Learning
OA	=	Order Analysis
OFB	=	Optimal Frequency Band
O&M	=	Operation and Maintenance
PCA	=	Principle Component Analysis
REB	=	Rolling Element Bearing
RMS	=	Root Mean Square
RQ	=	Research Question
SD	=	Standard Deviation
SK	=	Spectral Kurtosis
TVA	=	Traditional Vibration Analysis
WT	=	Wind Turbine

Chapter 1

Introduction

1.1 Topic and Context

The past decade has seen a rapid development of wind parks as renewable energy sources, both on-shore and off-shore (Lee and Zhao, 2020). Along with this growth, finding ways to minimise costs and maximise performance has become a key concern within the field. One area of interest is the operation and maintenance (O&M) of wind turbines (WTs) which, as estimated by The International Renewable Energy Agency (IRENA) (2012), accounts for up to 25 % of the levelised cost of energy (LCOE: the cost of the power produced).

Norwegian wind power production is estimated to increase from 2,85 TWh in 2017 to 25 TWh in 2030 (Bartnes et al., 2018). Norwegian power company TrønderEnergi has a clear ambition to be a part of the development. TrønderEnergi currently operates and maintains four wind parks consisting of 51 WTs and is the co-owner of several other wind parks. Early next year, TrønderEnergi will also add Roan wind park, Norway's second largest wind farm comprising of 71 WTs, to its portfolio. The expansion heightens the need for cost-effective and efficient O&M of the firm's WTs (Viseth, 2018).

WTs are subject to extreme and varying loads due to varying winds, start-ups, shutdowns and emergency stops. These conditions cause significant amounts of strain on the mechanical components. Gearbox components, with a design life of 20 years, have been reported to fail prematurely; after only 5-7 years (Barszcz and Randall, 2009; Coultate and Hornemann, 2018). Research suggests that a high number of start-stop cycles may degrade gearbox components (Drago, 2007). Additionally, Commission (2019)[1] informs that WTs are designed for 50 start/stop cycles per year. Early gearbox failure is also attributed to the heavy duty gearboxes used in WTs, designed for other industry applications with different load

---

[1]Section 7.4.4 (Start-up (DLC 3.1 to 3.3)) in Commission (2019)

patterns (Barszcz, 2019; Musial et al., 2007).

Condition monitoring (CM) works by observing mechanical components to identify changes that can indicate an emerging fault (Randall, 2011). CM aims to replace or repair components ahead of failure, saving time and costs. Vibration analysis of mechanical components is effectively paired with CM, and highly-developed signal processing techniques allows for weak fault impulses to be detected even in the presence of large noise from other rotating components.

Vibration from WT gearboxes are valuable to monitor due to their high failure rate (Musial et al., 2007). Components in the gearbox that are vulnerable to failure are bearings, parallel gears and planetary gears. High failure rates are also prominent in bearings connected to the power-producing high-speed shaft (HSS) (Musial et al., 2007). The HSS is connected to the gearbox, thus HSS vibration measurements will also contain any gearbox fault impulses.

Traditional vibration analysis (TVA) utilises signal processing and frequency analysis to detect faults and changes in vibration signals from CM systems. TVA provides a visual interpretation easily understood by vibration analysts (Barszcz and Randall, 2009). However, TVA often requires specific information regarding the components, e.g. bearing dimensions, to support the analysis. This kind of information is not always provided by manufacturers. Domain knowledge is also advantageous with TVA.

TVA is applied across many different industries. Zhao et al. (2013) discovered bearing faults from real, noisy locomotive vibrations and Barszcz and Randall (2009) detected planetary gear faults in real, noisy WT vibration data. Guo et al. (2012a) detected bearing faults in an experimental setup. The common denominator with these applications was that the faults were known, and the components' dimensions were familiar. Hence, the methods and results could be validated.

Data-driven approaches using machine learning (ML), a sub-field within artificial intelligence (AI), can be used to detect changes in large amounts of vibration data. The accessibility of powerful computing hardware has accelerated such analysis methods. However, results from ML methods often lack interpretability (Ribeiro et al., 2016), and may be difficult to rely on if the results are not validated.

Data-driven methods with ML are used in a variety of settings. Ben Ali et al. (2018) used machine learning to detect WT bearing faults in HSS, Liu et al. (2016) detected imbalance faults in WTs. The research was validated in both papers using WT vibration data with known faults. Yiakopoulos et al. (2011) and Huitao et al. (2018) applied data-driven methods to detect bearing and gear faults using laboratory set ups. The methods were validated using known faults.

1.2 Focus and Scope

The data to be examined in this thesis was streamed from four WTs located at Skomakerfjellet. The WTs have been operating since 2016. The data consisted of vibration signals from a Vestas Condition Monitoring (CM) system, sampled at 25.6 kHz from August 2018 to January 2020. Access to the data was provided by the Norwegian power company TrønderEnergi.

In addition to TrønderEnergi wanting to expand their CM systems, the four WTs being analysed had logged between 350 - 700 start-stop cycles per year, with one of them having approximately twice as many in total as the other three. On-site WT operators had not reported any faults on the WTs. With this information in mind, TrønderEnergi requested for a vibration analysis to be carried out on the WTs, to look for indications of early mechanical faults.

As mentioned, gears and bearings in gearboxes, as well as bearings associated with the high-speed shaft, have the highest failure rates in WTs. Thus, gear and bearing faults were selected for further analysis. Specifically, the vibration measurements recorded on the HSS were studied.

Three crucial pieces of information regarding the WTs in this thesis were lacking. (i) The dimensions of the gears and bearings were unknown. (ii) The state of the gearboxes and bearings were not given. (iii) Even though the turbines were assembled by Vestas at the same time, there was uncertainty whether the same drive-train components were used.

1.2.1 Research Questions

Other researchers usually rely on the two first aforementioned factors to validate that their methods indeed did *detect* present faults. Contrarily, this thesis aimed to demonstrate the potential for exploratory analysis regarding early fault detection in gearboxes and shafts using only vibration data and operational data (wind speed, power production etc.). The findings are potentially valuable in scenarios where power companies lack information from the WT manufacturer.

In particular, this thesis will examine three main research questions (RQs): Do the vibration signals recorded on the high-speed shaft on the WTs:

1. Indicate fault characteristics suggesting faulty gears or bearings?

2. Indicate any gear or bearing fault development over time (August 2018 to December 2019)?

3. Reveal any relationship between the number of start-stop cycles and gear or bearing faults?

1.2.2 Procedure

In this thesis, two exploratory methods were applied (Figure 1.1); traditional vibration analysis and a data-driven analysis using *clustering*. The traditional vibration analysis focused on manually inspecting selected vibration signals, and aimed to answer all three research questions. The data-driven clustering approach analysed and grouped hundreds of signals, using extracted fault-detection features. This allowed for the detection of potential fault development over time, since similar signals would be grouped together. Research question 2 was answered through the clustering approach. Research question 1 and 3 were out of the scope for this method, since it was only able to detect changes. This is brought up in the Discussion, Chapter 6.
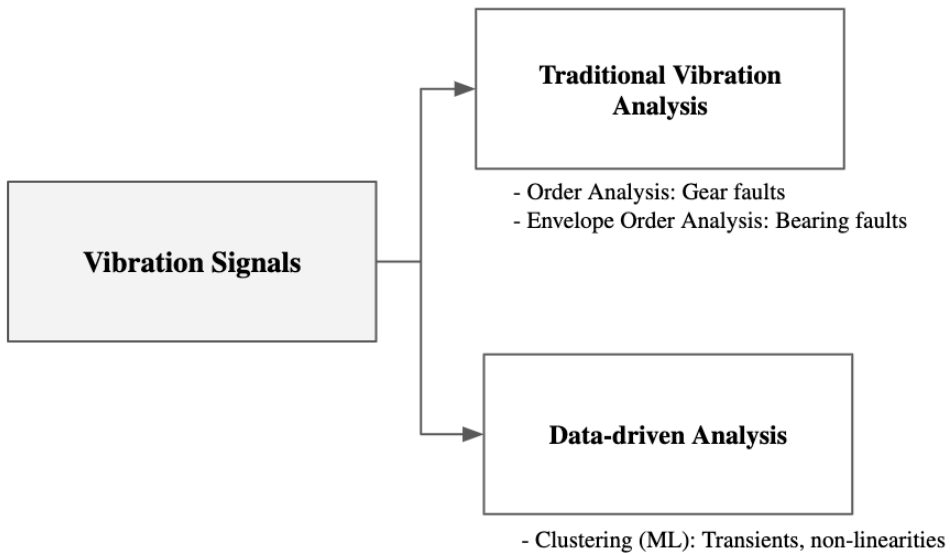
Figure 1.1: Overview of analysis procedure and what each method is capable of detecting.

Research question 2 was explored using two separate approaches, primarily to strengthen the analysis. The data-driven approach is capable of analysing *all* signals from a single WT at once, whilst the TVA relies on manual, visual inspection of some selected signals. A comparison of these methods is presented in the Discussion, Chapter 6.

As seen in the procedure overview in Figure 1.1, the TVA applied two sub-methods to detect gear faults and bearing faults; order analysis was applied for detecting gear faults, and envelope order analysis was applied to detect bearing faults. The clustering method was not specified towards any faults in particular, but was able to detect transients and non-linearities in vibration signals, which are both related to mechanical faults in vibration (Fackrell et al., 1995a,b; Rivola and White, 1999).

1.3 Outline

This thesis is structured as follows. Chapter 2 defines the relevant theoretical framework. Chapter 3 provides an overview of relevant research where the theory was applied. Chapter 4 describes the data, the chosen methods along with advantages and disadvantages of these. Chapter 5 presents the results along with a brief analysis. Chapter 6 discusses the results and considers the research questions. Future work is also presented in the Discussion. Chapter 7 presents the conclusion.

Chapter 2

Theory

2.1 Maintenance Strategies

Maintenance strategies are often categorised into three main groups; reactive, preventive and predictive (Randall, 2011; Stetco et al., 2019; Tchakoua et al., 2014). In this thesis, predictive maintenance is the focus, and is used with condition monitoring.

A reactive maintenance strategy performs repairs or replacements *after* a defect has occurred. A preventive strategy aims to perform maintenance at decided intervals, to limit the likelihood of a fault between checks. A predictive maintenance strategy uses component data from a condition monitoring system to decide if a component is due to fail. Maintenance is therefore performed at the optimal time. Figure 2.20 shows the cost associated with each approach as well as the desired goal of predictive maintenance (Tchakoua et al., 2014).
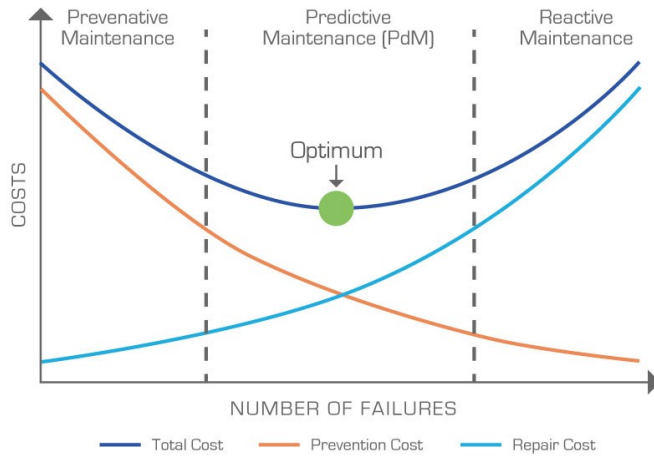
Figure 2.1: Cost associated with the three maintenance approaches (Sanger, 2017).

2.1.1 Condition Monitoring

Condition monitoring is an important tool within predictive maintenance. It involves observing components to identify their conditions and changes in operation that could indicate development of a fault.

Signs of mechanical faults are detectable through different monitoring methods, shown in Figure 2.2. Vibration based monitoring is able to detect failure at the earliest stage, 1-9 months prior to failure (Barszcz and Randall, 2009; Stetco et al., 2019). Oil analysis and thermography is capable of detecting faults 1-6 months and 3-12 weeks ahead of failure, respectively.
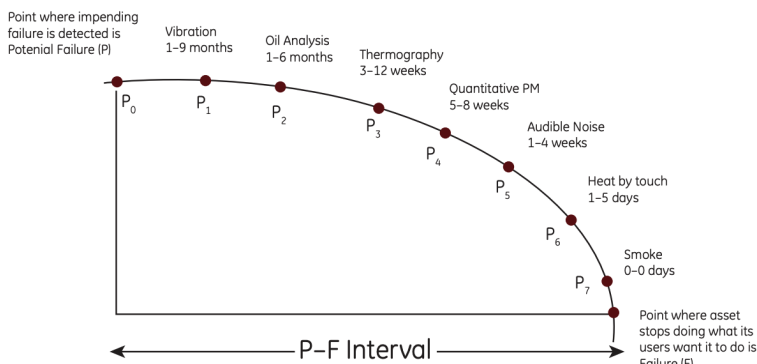
Figure 2.2: Detection stages of mechanical faults using different monitoring methods (Basics, 2009).

Additionally, vibration analysis has other advantages compared to the other meth-

ods in Figure 2.2; change is immediately visible, it can pinpoint the location of faults, and most importantly, powerful signal processing techniques can be applied to the signals to extract even weak fault indicators (Randall, 2011). Consequently, vibration monitoring is the preferred analysis method for detecting gearbox faults in this thesis.

2.1.2 Fault Detection, Fault Diagnosis and Fault Prediction

The literature distinguishes between three types of CM applications (Stetco et al., 2019):

- **Fault detection** is a binary analysis; determining whether the system is in a faulty state or not.

- **Fault diagnosis** separates the different fault types and aims to classify which is present.

- **Fault prediction** analyses data to find a pattern leading up to a fault, and aims to predict if and when a fault will happen in the future.

Fault detection is the focus for this thesis. Diagnosis and prediction is not possible due to the lack of information.

2.2 Vibration Signals

2.2.1 Discrete-Time and Continuous Signals

There are two types of signals- *continuous-time* signals and discrete-time signals. Measured vibration signals are discrete-time signals consisting of a sequence measurement. Vibration signals are often measured by either a displacement sensor, a velocity sensor or an accelerometer. Displacement sensors are capable of measuring low-frequency vibration, velocity sensors measure low to medium frequencies, and accelerometers measure high frequency ranges (Verbruggen, 2003). Accelerometer measurements are preferred for gearbox fault detection (Randall, 2011).

Discrete signals have two parameters; sampling frequency f_s and the number of samples N. The sampling frequency is the time between each sample, given by $T_s = \frac{1}{f_s}$. The duration of the signal is given in $T = N \cdot T_s$.

2.2.2 Filtering

Filters are used to remove unwanted components from a signal, for example when focusing on higher frequencies in a vibration signal. Three common types of filters are lowpass, highpass and bandpass filters. The *idealised* filters can be seen in Figure 2.3. *Pass band* denotes the range of frequencies from a signal that are passed through the filter, and *band stop* is the range that is rejected.
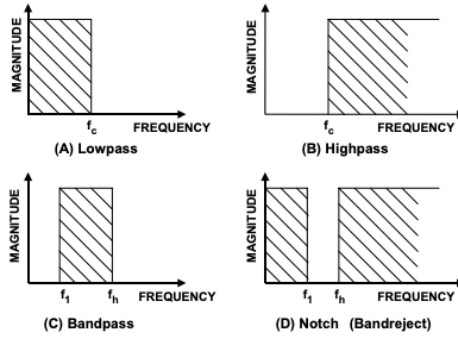
Figure 2.3: Idealised filter responses (Uhrmann et al., 2014).

In Figure 2.3, the transition from pass band to stop band is illustrated as instantaneous. This will not be the case in reality, as there will exist a transition region (Figure 2.4). Filters therefore aim to approximate the ideal filter responses (Uhrmann et al., 2014).

Filters are either designed for continuous-time signals or discrete-time signals. The most common filter families for continuous-time signals include Butterworth, Chebyshev, and elliptic filters (Jackson, 2002).
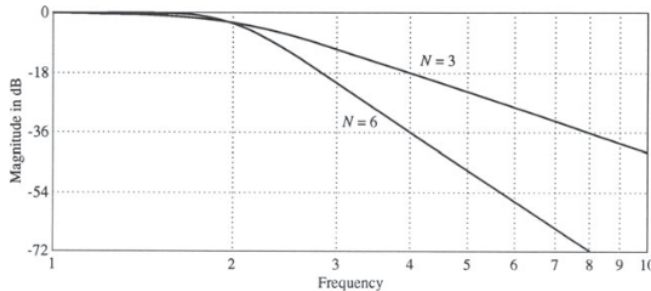
Figure 2.4: Butterworth low pass filter response (Jackson, 2002).

The filters mentioned above can in most cases be transformed and applied to discrete-time signals. After a transformation, these filters are characterised as *digital filters*. The discrete-time filters resulting from a transformation from a continious-time filter are infinite impulse response (IIR) filters (Jackson, 2002). Digital transformations of the Butterworth filter approximation will be implemented in this thesis for lowpass, highpass and bandpass filters.

2.3   Wind Turbines

WTs drive-trains are complex machines designed to transform kinetic wind energy to a generator to produce electricity. Relevant drive-train components from a vibration monitoring point of view are presented, followed by challenges associated with WT vibrations.

2.3.1   Wind Turbine Components

Interesting mechanical components are shafts, rotor with blades, couplings, gears, and rolling element bearings (REBs). Gearbox components, i.e. parallel gears, planetary gears and gearbox bearings, have recorded high failure rates (Barszcz, 2019; Coultate and Hornemann, 2018). Bearings associated with the HSS are also known to fail prematurely (Musial et al., 2007). On the basis of this, gear and bearing faults are the most interesting components to analyse in terms of an early fault exploratory study. An illustration of WT components is shown in Figure 2.5 and an illustration of Vestas' gearbox is shown in Figure 2.6.
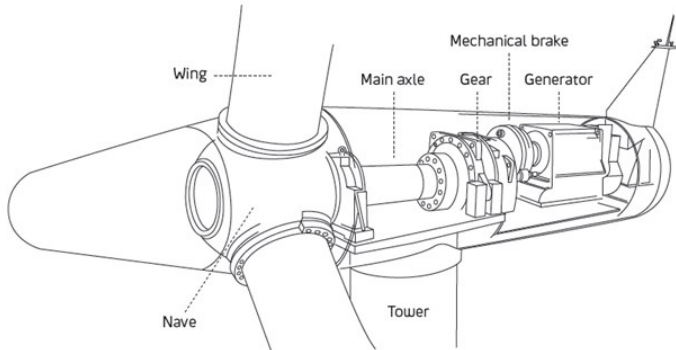
Figure 2.5: Illustration of the main components inside a WT (Statkraft).
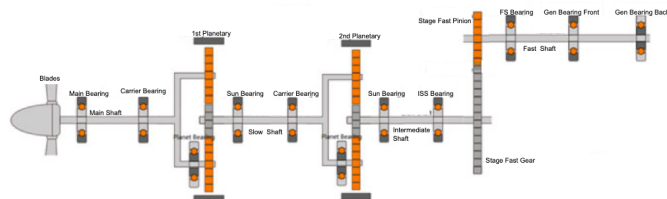
Figure 2.6: Illustration of the gearbox used in Vestas WT, consisting of two planetary gears, one parallel gear and several bearings. The illustration is a modification of a gearbox shown in Barszcz (2019).

2.3.2   Challenges with Wind Turbine Signals

Signals are Non-Stationary

Wind speed varies during operation and the rotation of WT components and generator output varies with it. In some cases, wind speed changes dramatically and suddenly. There are events when wind speed can increase from 3 m/s to 11 m/s in only 60 s, making WTs non-stationary systems. Such changes in operating conditions present a challenge when applying standard vibration analysis techniques (Barszcz, 2019).

Noise-to-Signal Ratio is High

Vibration from WTs are dominated by strong signals associated with shafts, rotor bars and parallel gears (Ben Ali et al., 2018). Thus, weaker vibration from faults in components such as bearings are hidden in the vibration data, making fault detection challenging (Liu, 2005). Early fault detection in environments with high noise-to-signal ratio is a widely researched field (Wei et al., 2019). Before a fault is fully developed, resonances will first appear in the higher frequency ranges (Liu, 2005), shown in Figure 2.7. Consequently, a number of the methods implemented in this thesis will focus on the higher frequency ranges.
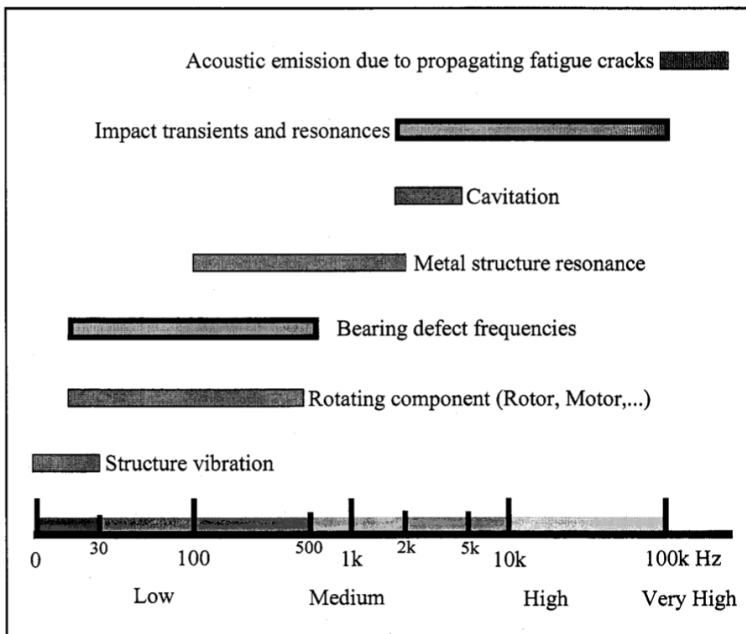
Figure 2.7: Typical vibration sources of rotating machinery in a frequency spectrum (Liu, 2005).

2.4   WT Component Characteristics

All rotating machinery components produce a specific vibration signal with a distinctive trait (Barszcz, 2019; Randall, 2011) known as a component's *characteristic frequency* (CF). The CFs are related to the component's condition, and it is possible to identify and track them using different methods (Section 2.5). Identifying components without CFs is very difficult and sometimes impossible. However, some are easier to identify for instance by recognising a pattern (Barszcz, 2019). This section describes the characteristic frequencies for each relevant component. Parallel gears are presented in this section, followed by planetary gears and bearings.

2.4.1   Parallel Gear Characteristics

In the Vestas WTs studied, the parallel gear in the gearbox was connected to the high-speed shaft. The speed ratio is given in Equation 2.3. The process of tooth meshing generates vibration and its CF is called the gear mesh frequency (GMF). It is given in Equation 2.2:

$$f_1 = \frac{N_2}{N_1} f_2 \tag{2.1}$$

$$f_{GMF} = N_1 \cdot f_1 = N_2 \cdot f_2 \tag{2.2}$$

where N_i is the number of teeth and f_i is the rotational speed of wheel i (Barszcz, 2019).
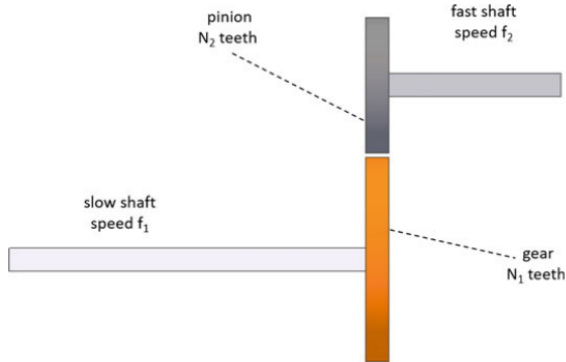
Figure 2.8: Illustration of a parallel gear (Barszcz, 2019).

2.4.2   Planetary Gear Characteristics

The first and second stage of the Vestas gearboxes consisted of planetary gears. An illustration of a planetary gear is shown in Figure 2.9. The gear ratio is given in Equation 2.3 and the speed ratio is given in equation 2.4.

$$n = \frac{N_s + N_r}{N_s} = 1 + \frac{N_r}{N_s} \tag{2.3}$$

$$f_s = n \cdot f_c = \left(1 + \frac{N_r}{N_s}\right) f_c \tag{2.4}$$

where N_s is the number of sun gear teeth, N_p is the number of planet gear teeth, N_r is the number of ring gear teeth, n_p is the number of planets, f_c is the rotational speed of the carrier and f_s is the rotational speed of the sun gear.
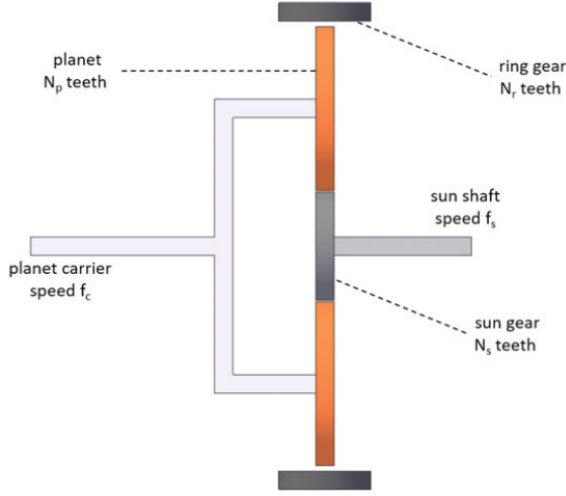
Figure 2.9: Ilustration of planetary gear (Barszcz, 2019).

Planetary gears are more complex than parallel, and have more CFs associated with them. Their CFs are listed in Table 2.1.

Table 2.1: Characteristic frequencies for planetary gears.

Fault description	Fault location	Characteristic frequency
Gear mesh frequency (GMF)	Present in majority of failures	$f_{GMF} = N_r \cdot f_c$
Ring over roll (ROR)	Ring gear	$f_{ROR} = n_p \cdot f_c$
Sun over roll (SOR)	Sun gear	$f_{SOR} = \frac{N_r \cdot n_p}{N_s} f_c$
Planet over roll (POR)	Planet gear	$f_{POR} = \frac{N_r}{N_p} f_c$
Planet rolling element bearing (PREB)	Bearing of the planet	$f_{POR} = \frac{N_r - 2N_p}{N_p} f_c$

2.4.3 Rolling Element Bearing Characteristics

As bearings deteriorate, a spall may emerge on the inner race, the outer race, the rolling elements, or a combination of these. When the spall impacts with another

surface during operation, an impulse is generated at a periodic repetition rate; the bearing's CF. The CF depends on the bearing geometry, load angle (θ), rotational speed (f_r) and the location of the spall. An illustration of bearing geometries is shown in Figure 2.10 and the CFs are show in Table 2.2. Note that n is the number of balls, d is the ball diameter, and p the pitch diameter.
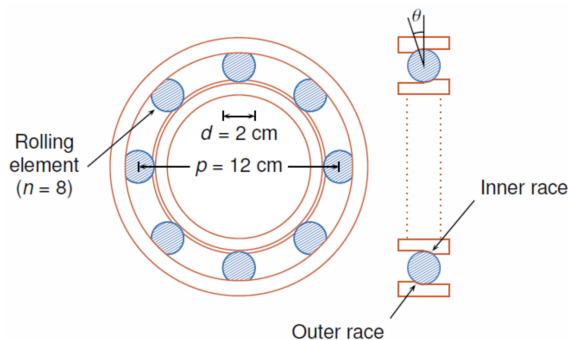
Figure 2.10: Illustration of bearing geometry (Barszcz, 2019).

Table 2.2: Characteristic bearing fault frequencies.

Fault description	Fault location	Characteristic frequency
Ball pass frequency of the outer race (BPFO)	Outer race	$f_{BPFO} = \frac{1}{2}f_r n \left(1 - \frac{d\cos\theta}{p}\right)$
Ball pass frequency of the inner race (BPFI)	Inner race	$f_{BPFI} = \frac{1}{2}f_r n \left(1 + \frac{d\cos\theta}{p}\right)$
Ball pass spinn frequency (BSF)	Rolling element	$f_{BSF} = f_r \frac{d}{p} \left(1 - \frac{d^2\cos^2\theta}{p^2}\right)$
Fundamental train frequency (FTF) picks up mechanical looseness	Cage	$f_{FTF} = \frac{1}{2}f_r \left(1 - \frac{d\cos\theta}{p}\right)$

2.5 Traditional Vibration Analysis Techniques

An important source of information reagarding TVA methods was Tomasz Barszcz's textbook *Vibration-Based Condition Monitoring of Wind Turbines* from 2019 (Barszcz, 2019).

This section will introduce the most common and effective Traditional Vibration Analysis (TVA) methods. The methods are traditional in the sense that they are widely applied across different industries. Their main advantage is that they have a real, physical interpretation, easily understood by most vibration analysts and experts (Barszcz and Randall, 2009).

Firstly, an overview of recommended TVA methods are presented. Secondly, the Fourier analysis is defined, providing a theoretical foundation to TVA methods. Lastly, the two relevant TVA methods for this thesis is presented; the *order analysis* (OA) and the *envelope order analysis* (EOA). They are used to detect gear deterioration and bearing deterioration, respectively.

2.5.1 Recommended Traditional Vibration Analysis Techniques

Recommended TVA methods depending on the component being analysed is presented in Table 2.3 (Barszcz, 2019). In the table, nX is the n$^{\text{th}}$ harmonic of the CF. Identifying faults using these CFs is described in Section 2.5.4 and 2.5.6.

Table 2.3: Recommended TVA techniques.

Component of interest	Analysing technique	Interesting characteristics
Parallel gears	Order analysis	GMF 1X, 2X, 3X, sidebands
Planetary gears	Order analysis	GMF 1X, 2X, 3X, sidebands
REBs	Envelope order analysis	REB CFs

Varying wind speeds causes the WT signals to behave non-stationary. Therefore, to correctly compare various vibration signals, it is common to define a generator power threshold of 80 % of nominal power (Barszcz, 2019).

2.5.2 Fourier Analysis

A Fourier analysis consists of a Fourier transformation and a frequency analysis and plays an essential part when analysing vibration from rotating machinery. The frequency spectrum from a Fourier transform reveals spectral lines showing the frequency content of a signal. These lines can be linked to mechanical components through the CFs discussed in Section 2.4. A Fourier transformation represents a signal as a summation of sinusoidal components and almost all signals, whether they are periodic, almost periodic or random, can be decomposed this way (Randall, 2011).

Analogue Fourier Transformation

The Fourier transformation of an analogue signal is given in equation 2.5 and the inverse Fourier transformation is presented in equation 2.6.

$$X(f) = \int_{-\infty}^{\infty} x(t)e^{-j2\pi ft}dt \tag{2.5}$$

$$x(t) = \int_{-\infty}^{\infty} X(f)e^{j2\pi ft}df \tag{2.6}$$

for an analogue signal x.

Discrete Fourier Transformation

When Fourier transforming discrete signals, the discrete Fourier transform (DFT) must be applied. It is given in Equation 2.7 and the inverse in 2.8. The fast Fourier transform (FFT) algorithm is considered the most efficient implementation of DFT (Barszcz, 2019). DFT plays an essential part in traditional vibration analysis methods described in 2.5.3 and 2.5.5. A more thorough mathematical study of Fourier transformations can be found in Randall (2011).

$$X(k) = \sum_{n=0}^{N-1} x(n) e^{-\frac{j2\pi}{N} nk} \tag{2.7}$$

$$x(n) = \sum_{k=0}^{N-1} X(k) e^{\frac{j2\pi}{N} nk} \tag{2.8}$$

where x is a discrete signal.

Frequency Analysis Example

Figure 2.11) shows how a simulated signal composed of two shafts and a parallel gear can be analysed using a Fourier Transform. Spectral lines corresponding to the components CFs are easily observed.

The two first spectral lines relate to the slow shaft rotating at 540 rpm (9 Hz), the fast shaft rotating at 1500 rpm (25 Hz). The last two spectral lines at 225 Hz and 450 Hz are the CF and the first harmonic of the gear. The gear has 25 teeth on its slow rotating wheel and 9 teeth on its fast rotating wheel and the CF can be calculated by the equation found in Section 2.4.1.
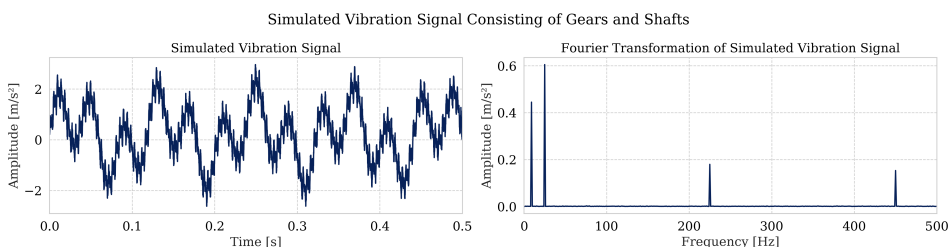
Figure 2.11: Left: simulated vibration signal of two shafts and a parallel gear with white noise added. Right: frequency spectrum after Fourier transformation is applied. The characteristic frequencies are easily identified.

Fourier analysis are most accurate when transforming vibrations from machinery rotating at constant speed. However, WTs are non-stationary, and all CFs are dependent on the rotational speed (Section 2.4). Consequently, when the rotational

speed changes, the CFs change as well, making it difficult to compare frequencies when the rotational speed is not exactly the same. In addition, acceleration and deceleration leads to frequency smearing and makes it difficult to separate the characteristic frequencies from noise. This makes regular Fourier analysis inaccurate for WTs. Yet, Fourier transformation and frequency analysis play an important part in the other methods and an overview is therefore valuable.

2.5.3 Order Analysis

Order analysis is recognised as a powerful tool for handling non-stationary vibration signals Barszcz (2019). To accurately Fourier transform a non-stationary signal, order analysis applies resampling. This means that a signal dependant of time is resampled to be a function of revolutions instead. This makes the signal independent of speed variations, which is defined as a cyclo-stationary signal. An illustration of the procedure is given in Figure 2.12 and an example of a simulated vibration signal from a parallel gear is provided in Figure 2.13.
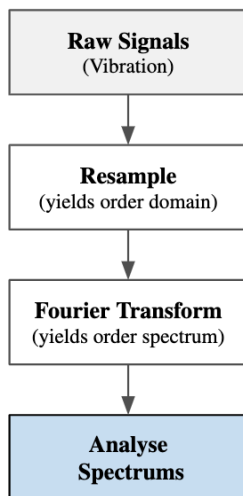
Figure 2.12: Illustration of the order analysis process.

A regularly sampled vibration signal has an equal number of data points for a given time period. Order analysis, on the other hand, requires an equal number of data points between each shaft revolution to make the vibration signal cyclo-stationary.
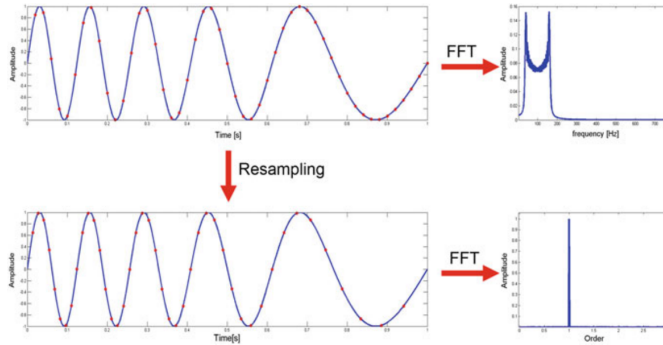
Figure 2.13: Top: Fourier analysis of a simulated non-stationary signal. Bottom: Order analysis of the same signal.

It is necessary to track the shaft's revolutions to resample correctly. This is commonly achieved with a tachometer, which delivers a pulse signal for each rotation. The actual resampling is often executed with a resampling algorithm, estimating the values between each rotation using interpolation. Cubic interpolation is the optimum interpolation method (McFadden, 1989). There are many rotating shafts within a wind turbine. However, Barszcz (2019) recommends using the high speed shaft's rotational speed measurements to resample with high resolution.

The next step involves Fourier transforming the resampled signal to reveal characteristic frequencies. This is performed using DFT. After resampling, the data points are not equidistant in time anymore and, after the Fourier transformation, it is no longer in the frequency domain. Instead, they are in the *order* domain where order 1 is the rotational frequency of the shaft.

The CFs become independent of speed variations and are only determined by the components geometry. This means that they are constant in the order domain. The spectral lines become much sharper and it is easier to identify the CFs.

2.5.4   Identifying Faults with Order Analysis

Order analysis is used to track parallel and planetary gear faults, which are typically visible in the first 50 orders of the spectrum. According to Barszcz (2019), "the existence and amplitude of gear mesh frequencies and sidebands is a very good indicator of the gearbox's health". The spectrum of a healthy gear shows clean spectral lines at the GMF and its harmonics.

Gear faults causes frequency/phase modulation in the signal and can be observed as series of sidebands around GMF and its harmonics. As wear increases, the amplitude and number of sidebands will increase. When a parallel gear is in poor condition, the GMFs are barely visible and the overall energy level of the frequency region has increased (Barszcz, 2019).

An advantage with order analysis is that some spectral lines are easier to link to components by recognising the pattern, even without knowing the CFs. Regarding fault development, it is possible to inspect if new spectral lines emerge, if new sidebands appear or if the general level of noise increases Barszcz (2019).

2.5.5 Envelope Order Analysis

Envelope order analysis (EOA) is a powerful tool capable of detecting weaker impulse signals concealed in a stronger signal (Barszcz, 2019; Zhao et al., 2013). Figure 2.14 shows a simulated complex vibration signal with a weak REB fault (BFPO), and the isolated weak signal. It is important to note that real WT vibration is much more complex than the simulated signal. EOA has proved effective at detecting these kinds of faults in REBs. It handles non-stationary signals by making them cyclo-stationary.
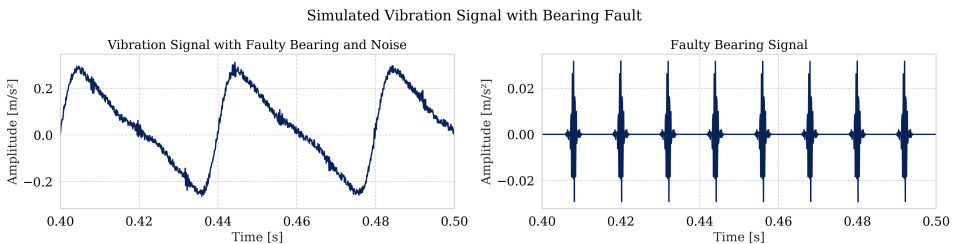
Figure 2.14: Left: A simulated, complex vibration signal with an early bearing fault masked by noise from shaft harmonics. Right: Bearing impulses isolated.

Weak impulse signals from REBs are often concealed by other components like gears and shafts, and are undetectable by order analysis Barszcz (2019). However, these signals can be observed as series if impulses, spaced at their CF, which EOA takes advantage of. The CFs are strongest around the resonance frequency.

Envelope Order Analysis Procedure

The simulated vibration signal shown in Figure 2.15 is used to explain the EOA procedure. The signal contains an early BPFO (Ball Pass Frequency Outer race) fault development. The CF is $f_{BPFO} \approx 83.33$ Hz and after resampling it is $f_{orderBPFO} \approx 3.33$.

The goal of envelope analysis is to demodulate the signal to easier reveal the characteristic frequencies of the bearing fault. There are two demodulating techniques used to obtain the envelope signal; the first uses a high-pass filter, rectification and a low-pass filter while the second is a *Hilbert transformation* (Barszcz, 2019). The first method is implemented in this thesis and thus further explained. The procedure follows the steps below. Each step corresponds to a row in Figure 2.15. The Fourier transformation is performed using DFT.

1. The vibration signal is obtained. After a Fourier transformation, the sought frequencies are barely visible on the frequency spectrum around 3 kHz. However, the shaft speed harmonics are easily visible.

2. The signal is high-pass filtered to reject vibration signals from shaft, gears, etc, which produce lower frequencies. The frequencies of interest are more evident, appearing in the high frequency region.

3. Next, the signal is rectified by taking the absolute value of the signal. This is the demodulating part. New spectral lines appear in the low frequency bands.

4. The rectified signal is low-pass filtered, removing noise. The envelope signal is obtained. We observe harmonics of the fault characteristic frequency f_{BPFO} at 83.33 Hz and its harmonics.

5. The envelope signal is resampled, producing the envelope order signal, suited for non-stationary systems. The signal's x axis become *order* and the order spectrum is obtained. We observe $f_{orderBPFO}$ at 3.33 and its harmonics.
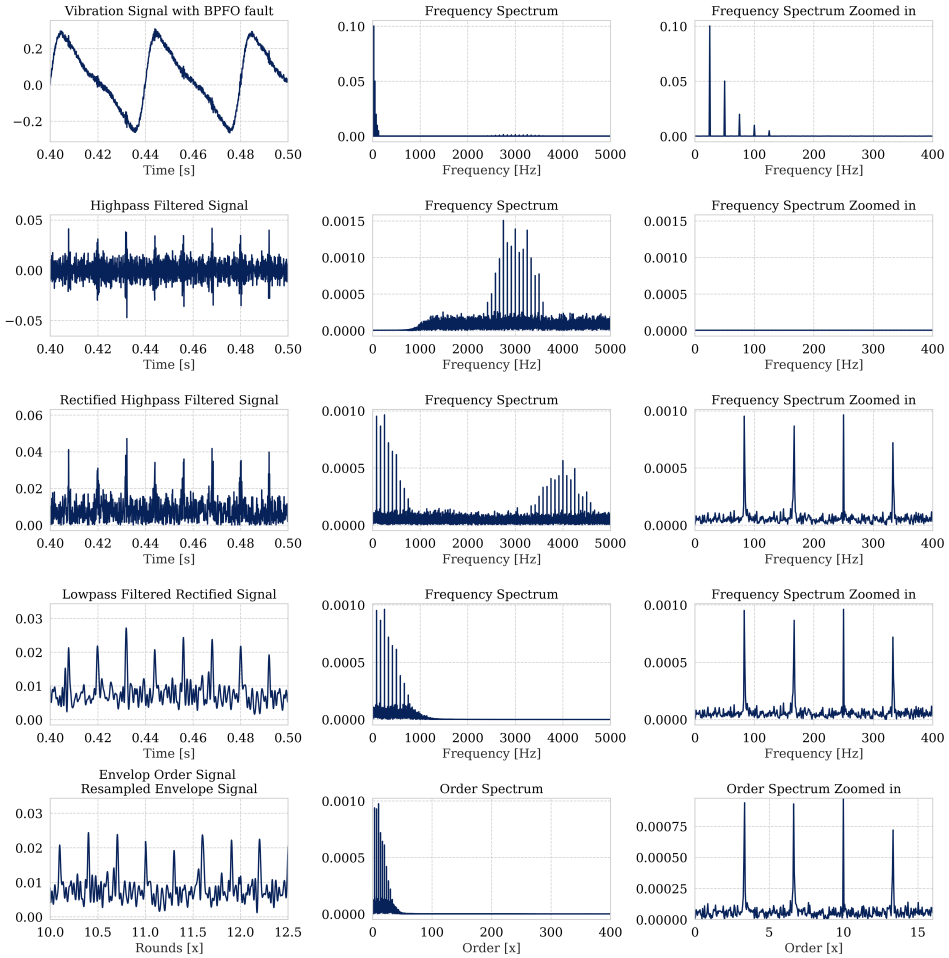
Figure 2.15: Envelope analysis procedure of a simulated signal with a REB BPFO fault. Each row corresponds to a step in EA procedure. Left figures: show the vibration signal zoomed in. Middle figures: show the frequency spectrums after Fourier transformation. Right figures: show the frequency spectrums zoomed in.

When performing envelope analysis, it is important to consider which frequency band should be demodulated (Step 3). Barszcz (2019) argues that it is generally sufficient to use a a high-pass filter with a cutoff frequency above the second or third gear mesh harmonic of the fastest gear. This is usually around 2 kHz for wind turbines (Barszcz, 2019). If the fault is in a very early stage and masked by other sources of impulses, this may not be enough. In this case, *Narrowband* envelope analysis is preferred. After selecting the *optimal frequency band* (OFB),

it uses a band-pass filter to demodulate the interesting part of the signal. However, defining the OBF is a challenging task. One of the efficient methods recommended by Barszcz (2019) is Spectral Kurtosis, which is further explained in Section 2.6.

2.5.6 Identifying Faults with Envelope Order Analysis

An illustration of REB fault development is shown in Figure 2.16. A healthy REB has not developed spalls, meaning that CFs are not present in the EOA spectrum and the level of vibration is low (Stage (a)). A REB with a fault developing means that a spall has emerged on the REB. This is seen as clear spectral lines at CF and otherwise low vibration in the EOA spectrum (Stage (b) and Stage (c)). As the spall grows and becomes larger than the rolling element, the overall vibration level increases in the EOA spectrum and impulses tend to mix (Stage (d)). At this stage the REB is in a poor state and should be replaced (Barszcz, 2019).
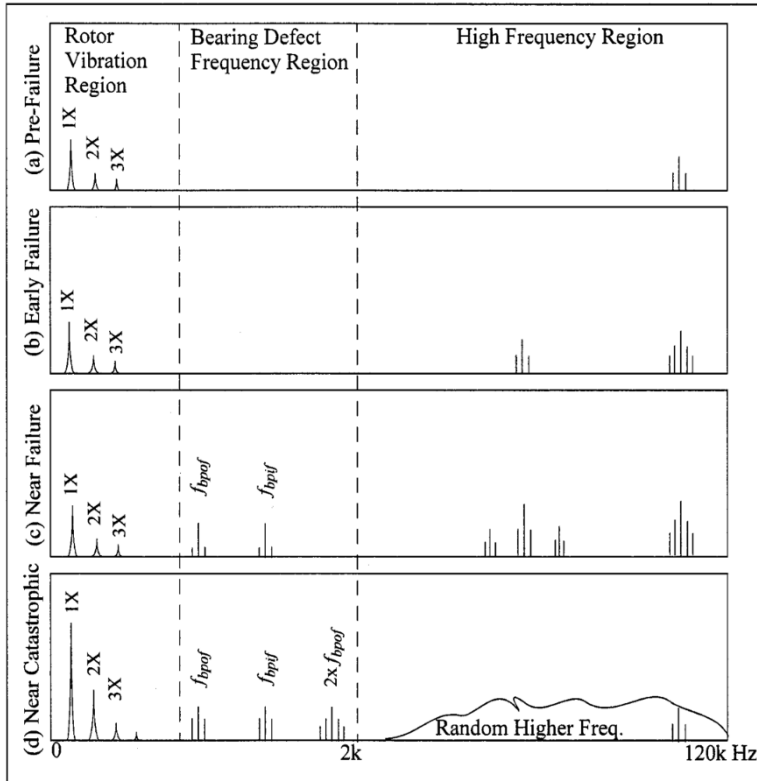
Figure 2.16: Fault regions for bearings in early fault detection. Early bearing faults produce resonances in the *high frequency region*, above 2000 Hz (Liu, 2005).

2.6 Spectral Kurtosis and the Kurtogram

Spectral kurtosis (SK) is powerful method for detecting weak fault impulses in noisy, non-stationary signals. SK finds the OFB by exploring different combinations of filter parameters; *center frequency* and *bandwidth*, and calculates the kurtosis for each combination. The kurtosis value is often used to indicate mechanical faults. The combination with the highest kurtosis value is the optimal frequency band.

Kurtosis is the 4-th moment of a distribution (vibration) x and is defined as

$$K = \frac{\int_{-\infty}^{+\infty}(x-\mu)^4 p(x))dx}{\sigma^4} \tag{2.9}$$

where μ is the mean value of x, $p(x)$ is the probability density of x and σ is the standard deviation. Kurtosis can also be used on a complete signal, without applying any filtering. The kurtosis of a Gaussian distribution equals three, thus values above 3 indicate transients in a vibration signal.

However, when the noise-to-signal ratio is high, the kurtosis-value fails to detect the weak fault impulses. In such cases, SK is useful and returns the OFB. The definition of SK is placed in Appendix A.1.

According to Barszcz (2019), there are two practical applications of SK; the Kurtogram proposed by Antoni and Randall (2006) and the Fast Kurtogram developed by Antoni. The original Kurtogram calculates all combinations of center frequencies and bandwidths, making it resource-intensive. The Fast Kurtogram calculates fewer combinations while achieving the same accuracy.

Regular kurtosis and SK with the Fast Kurtogram is used in this thesis.

2.7 Machine Learning

Machine learning (ML) is a collection of methods that can detect patterns in data with little human intervention, and use these patterns to understand new, unseen data (Murphy, 2012). With access to large amounts of vibration data, ML can be applied to detect changes over time.

2.7.1 Supervised and Unsupervised Learning

ML is mostly divided into two types, supervised and unsupervised learning (Murphy, 2012).

Supervised learning methods aim to learn a mapping function from a sample x to a target variable y. A data set D can be defined with N samples or observations on the form $D = \{(x_i, y_i)_{i=1}^N\}$, where x_i is the input and y_i the known target variable

(output). D can then be used to learn the mapping function. Each data sample x_i consists of S features. Each feature holds a numbered value. An example of target variable y_i could be *outer race bearing fault.* An approximation function or model $\hat{f}$ is the result from training on the data D. $\hat{f}$ is then capable of predicting target values for new samples $\hat{f}(x_0) = y_0$ (James et al., 2013).

In unsupervised learning, the target variable is unknown. The data only consists of inputs, $D = \{(x_i)_{i=1}^{N}\}$ (Murphy, 2012). The goal of unsupervised learning is to discover interesting patterns in the data. *Clustering* is a broad set of unsupervised learning techniques where the data samples x_i are grouped together (Jain, 2010; James et al., 2013).

Since the vibration data in this thesis was unlabelled, the machine learning method applied was unsupervised.

2.7.2 Clustering

Clustering can be used in exploratory data analysis of vibration data to group samples that share common characteristics (Yiakopoulos et al., 2011). Clustering methods are broadly divided into partitional and hierarchical clustering (Figure 2.18). A partitional clustering is a division of the data set samples into non-overlapping subsets (clusters). Hierarchical clustering organises clusters in a tree, and allows for clusters to have sub-clusters.
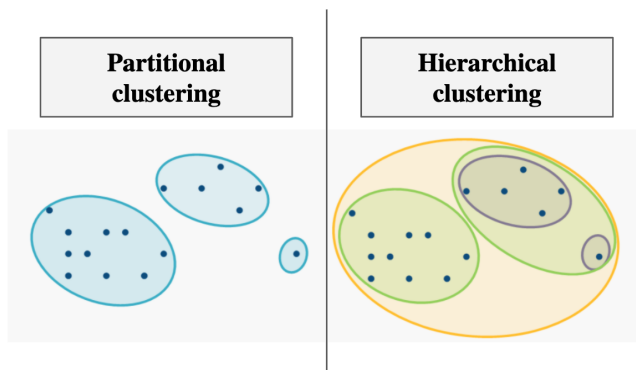
Figure 2.17: The two most common clustering types.

K-Means Clustering

K-means is a simple partitional clustering technique first introduced by Lloyd (1982) in 1957 (Elkan, 2003). Even though thousands of clustering algorithms has been published since then, K-means still remain popular (Berkhin, 2002; Jain, 2010). The procedure for K-means is described in the following section.

Given a data set $D = \{(x_i)_{i=1}^{N}\}$ with N samples $x_i...x_N$ and S features for each sample x_i, K-means clustering can be applied to group similar samples into K *clusters*. The clusters are denoted $C_1, ..., C_K$ and contain the indices of the samples in each cluster. It is desirable that each cluster C_k has a small *within-cluster variation* $W(C_k)$ (James et al., 2013). $W(C_k)$ states how much each sample within each cluster differ from each other. The samples should be partitioned into clusters so that the total within-cluster variation is minimised. This is defined as (James et al., 2013):

$$\min_{C_1,...,C_K} \left\{ \sum_{K=1}^{K} W(C_k) \right\} \tag{2.10}$$

where $W(C_k)$ is defined as

$$W(C_k) = \frac{1}{|C_k|} \sum_{i,i' \in C_k} \sum_{j=1}^{p} (x_{ij} - x_{i'j})^2 \tag{2.11}$$

The number of samples in each cluster is denoted $|C_k|$. As seen in equation 2.11, the within-cluster variation is calculated as the pairwise squared Euclidean distances between all the samples in the kth cluster.

Combining Equations 2.10 and 2.11 yields the optimisation problem defining K-means clustering (James et al., 2013).

$$\min_{C_1,...,C_K} \left\{ \frac{1}{|C_k|} \sum_{i,i' \in C_k} \sum_{j=1}^{p} (x_{ij} - x_{i'j})^2 \right\} \tag{2.12}$$

Minimising equation 2.12 is known to be a NP-hard problem (Drineas et al., 2004). However, it can converge to a *local minimum* using the following algorithm (Jain and Dubes, 1988):

1. Select an initial partitioning with K clusters and

2. Iterate until the cluster membership stops changing:

    (a) For each of the K clusters, compute the cluster centroid. The centroid is the mean value for all samples in the Kth cluster.

    (b) Re-assign each sample to its closest cluster centroid.
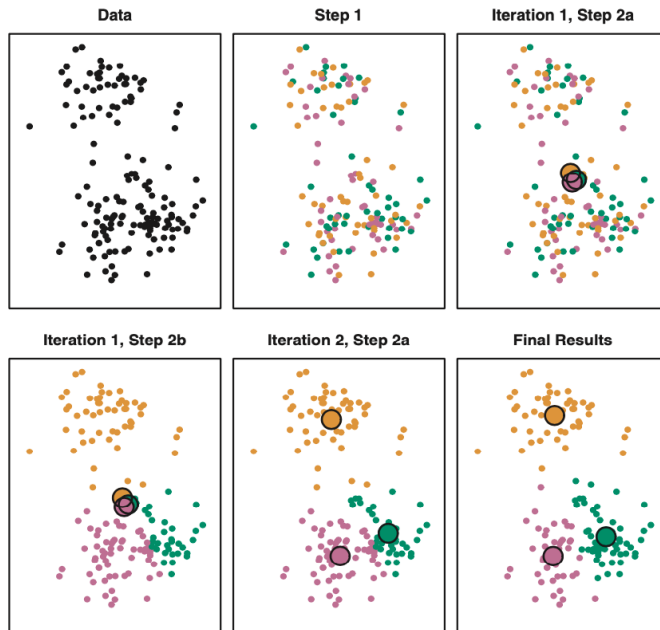
Figure 2.18: K-means clustering with $K = 3$ as described in equation 2.7.2. The large discs are the cluster centroids (James et al., 2013).

The K-means implementation in this thesis is performed with an acceleration of the K-means algorithm which avoids unnecessary distance calculations by applying the triangle inequality and distance bounds. It is described in detail in Elkan (2003).

Before clustering, the data needs to be normalised. This is because a proximity measure like euclidean distance will implicitly assign greater weight to large-ranged features (Jain and Dubes, 1988). Normalisation will be done in this thesis through scaling, where the range for each feature is set to $[0, 1]$.

K-Means User Decisions

The K-means algorithm requires three user-defined parameters, namely the number of clusters K the data should be partitioned into, the initial partitioning of the data samples, and the distance metric used. Of these three parameters, the selection of K is the most critical (Jain, 2010). K-means implementation in this thesis used Euclidean distance.

Generally, K can be selected by running K-means with different K's, and selecting the one which yields the most meaningful result to the domain expert (Jain, 2010). This is of course subjective, and increasingly difficult when clustering data in more than 2-dimensional space (Jain, 2010).

Another approach for selecting K is the *elbow method* (Huang, 2017). The elbow method works by running K-means with a range of Ks. For each K, the within-cluster-variation $W(C_k)$ decreases (Equation 2.12). The local optimal K is then selected where the incremental improvement of $W(C_k)$ is small. This thesis uses the common elbow method as well as an objective-driven criteria, presented in the Method chapter, Section 4.3.6.

The initial partitioning of the data samples (step 1. in 2.7.2) is often selected at random (James et al., 2013) or by using the K-means++ algorithm. The K-means++ uses a randomised seeding technique for selecting the initial clusters, and can be studied further in Arthur and Vassilvitskii (2007). K-means++ has been documented to greatly increase the speed and accuracy of K-means (Arthur and Vassilvitskii, 2007). The algorithm will be used with K-means in this thesis.

Cluster Validation

Jain and Dubes (1988) propose three criteria used to measure the validity of a cluster. The *external criteria* will be applied in this thesis. An *external criteria* measures performance of a partitioning by matching a clustering structure to a priori information. This can for example be a measure of the degree to which data confirms a defined objective. The two other criteria are described in Jain and Dubes (1988).

Challenges with K-Means

Jain and Dubes (1988) illuminated a range of important questions to bear in mind when clustering data (Appendix A.2). This list of questions will be addressed in the discussion, Chapter 6. James et al. (2013) recommended clustering the data on different subsets, in order to gain a sense of robustness of the resulting clusters.

2.7.3 Feature Extraction

To apply unsupervised ML to detect gearbox faults, features need to be extracted from the discrete vibration signals. Features are commonly extracted from three domains: the *time* domain, *time-frequency* domain, and the *frequency* domain.

Time Domain Features: Statistics

Time domain features can be extracted from a raw vibration signal x and often consists of statistical features such as mean, standard deviation (SD), and kurtosis. Frequently extracted time domain features for detecting faults gearboxes are presented in the Literary Survey (Chapter 3).

Frequency Domain Features: Bi-Spectrum

Frequency information within noisy vibration data can be derived from the bi-spectrum (Fackrell et al., 1995b; Nikias and Mendel, 1993; Saidi et al., 2015). Since mechanical faults are often present as nonlinearities in the vibration signature, bi-spectrum analysis can be used to detect such faults (Fackrell et al., 1995a,b; Hinich and Wilson, 1990; Rivola and White, 1999).

The bi-spectrum of a discrete signal is a higher order statistic (HOS) which can be used to analyse the interaction between frequencies. HOS provides higher order moments and nonlinear combinations of higher order moments called cumulants (Nikias and Mendel, 1993). HOS can be studied in greater detail in Nikias and Mendel (1993) and Mendel (1991).

Saidi et al. (2015) specify two properties which make the bi-spectrum applicable for vibration signal analysis; (i) Bi-spectrum is insensitive to noise since it is is theoretically zero for Gaussian noise and flat for non-Gaussian white noise, (ii) the bi-spectrum peaks only at frequency pairs corresponding to those related components with frequency and phase (Mendel, 1991; Nikias and Mendel, 1993). These properties makes the bi-spectrum a relevant tool for analysing non-linear and non-Gaussian vibration signals (Nikias and Mendel, 1993). However, bi-spectrum analysis requires the input signal to be stationary, which is not the case for WT vibration signals. This can be solved by using a short-period signal of the input signal.

For systems where weak fault impulses are masked by stronger periodic components and noise, traditional linear spectral analysis such as power spectral may fall short (Fackrell et al., 1995a). The power spectrum is one of the most common signal analysis tools, and is defined in Equation 2.13.

$$S(k) = E[X(k)X^*(k)] \tag{2.13}$$

E is the expectation operator and k is the discrete frequency variable. $X(k)$ is the DFT of the discrete signal $x(t)$ and $X(k)^*$ its conjugate. The power spectrum is considered the signals second moment (Rivola and White, 1999).

The signal's DFT is also used to describe the bi-spectrum as

$$B(f_1, f_2) = E[X(f_1)X(f_2)X^*(f_1 + f_2)] \tag{2.14}$$

where $B(f_1, f_2)$ is complex and is defined by two frequencies f_1 and f_2.

A DFT holds redundant information above the Nyquist frequency, $f_s/2$. Symmetries also exist in the f_1, f_2 plane (Fackrell et al., 1995a)]. The relevant region is called the principal domain (PD), defined as

$$PD = f_1, f_2 : 0 \le f_1 \le f_s/2, f_2 \le f_1, 2f_1 + 1 = f_s \tag{2.15}$$

Equation 2.14 can be estimated though a direct or indirect method (Nikias and Mendel, 1993). The direct estimation is given as

$$\hat{B}(f_1, f_2) = \frac{1}{K} \sum_{i=1}^{K} X_i(f_1) X_i(f_2) X_i^*(f_1 + f_2) \tag{2.16}$$

Here, K is the number of segments the discrete signal is split into, each segment consisting of M data points. The elaborated process can be seen in Nikias and Mendel (1993).

With the bi-spectrum estimated, a range of features can be extracted for use in clustering. Commonly extracted features are shown in the Literary Survey, Chapter 3.

Time-Frequency Domain Features: Ensemble Empirical Mode Decomposition

Time-frequency features can be extracted from non-stationary vibration signals using ensemble empirical mode decomposition (EEMD) to detect gearbox faults (Ben Ali et al., 2018, 2013; Chen et al., 2017; Yu et al., 2006). Commonly extracted features are highlighted in the literary survey. An example of a decomposition is shown in Figure 2.19. Following is a brief overview of the EEMD method.
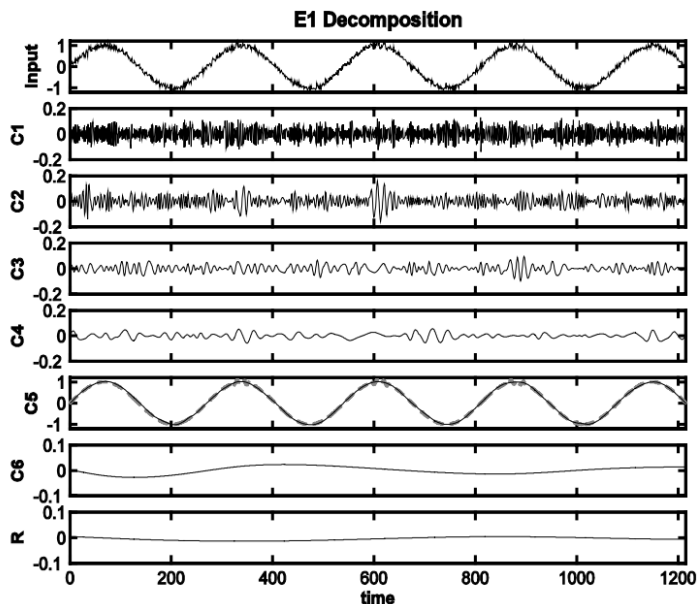
Figure 2.19: Example of a decomposition using EMD. C1-6 shows the IMFs to the input signal (Chang, 2010).

EEMD is an adaptive denoising technique that can be used to extract the weak fault characteristics from a vibration signal (Wei et al., 2019). EEMD is an improvement of empirical mode decomposition (EMD), and eliminates the problem of mode mixing in EMD (Chang, 2010). Both methods are proposed by Huang et al., and are applicable with nonlinear and non-stationary signals, since they are based on local characteristics of the signals (Chang, 2010).

EEMD and EMD decompose a signal $x(t)$ into a series of intrinsic mode functions (IMFs) without requiring any assumptions about the signal which is being decomposed (Figure 2.19). After acquiring the M IMFs for a signal, the original signal can be represented like so

$$x(t) = \sum_{m=1}^{M} c_m(t) + r_M(t) \tag{2.17}$$

where c_m is IMF number j, r_M is the residue of data after M IMFs have been extracted. The IMFs are extracted in an iterative fashion, where the repeated step is to find one IMF, subtract it from the original signal, and then use this resulting signal to find the next IMF.

Chang (2010) describes that each IMF has a unique instantaneous frequency at every instant of time and needs to satisfy the two conditions:

1. In the whole data set, the number of extrema and the number of zero crossings must either be equal or differ at most by one.

2. At any point in the times series, the mean value of the envelopes which is defined by local maxima (upper envelope) and local minima (lower envelope) is equal to zero.

In the EMD algorithm, the IMFs are obtained through a 5 step process termed the *sifting algorithm* (Gaci, 2016):

1. Identify the extrema (local maxima and minima) of the input signal $x(t)$.

2. Use cubic spline to interpolate the local extrema to find the upper and lower envelope functions, respectively $U(t)$ and $L(t)$.

3. Calculate the local mean $m(t)$ from the average of $U(t)$ and $L(t)$.

4. Subtract the mean $m(t)$ from the original signal to obtain h_1: $h_1(t) = x(t) - m(t)$

5. Replace the signal $x(t)$ by $h_1(t)$, and repeat steps 1-4 until the resulting signal satisfies the two IMF conditions.

The EEMD method improves on EMD by adding different realizations of white noise $w_n(t)$ to the input signal where n is the trial number, for $n = 1, 2, ..., N$ and N the number of ensembles or trials.

$$Y_n(t) = x(t) + w_n(t) \tag{2.18}$$

After the noise is added in one of the N trials, the steps for EMD are then carried out from step 1 with $Y_n(t)$ to get the decomposed signal

$$Y_n(t) = \sum_{m=1}^{M} c_m^n(t) + r_m^n(t) \tag{2.19}$$

where $\sum_{m=1}^{M} c_m^n(t)$ is the sum of the IMFs obtained in the n-th trial and $r_m^n(t)$ the residue in the same trial n, after M IMFs have been extracted from the signal.

After all trials with their corresponding IMFs (with the same number of IMFs for each trial), the ensemble mean is computed for each IMF.

$$c_m(t)^{average} = \frac{1}{N} \sum_{n=1}^{N} c_m^n(t) \tag{2.20}$$

Chang (2010) state that the added white noise will provide a relatively uniform reference scale distribution, which in turn will not affect the decomposition method. Chang (2010) also expresses that the added noise may assist in extracting interesting signal characteristics from the data. Additionally, taking the mean of the corresponding IMFs reduces the chance of mode mixing, which was the main problem for the EMD algorithm. EMD and EEMD is explained in further detail in (Chang, 2010).

2.7.4 Feature Selection

High dimensional data sets consist of many features or variables. Such data sets has provided a challenge to clustering approaches (Jain, 2010). Firstly, a high dimensional data set can cause the algorithm to run slowly. Secondly, clustering data on irrelevant features may cause the algorithm to fail to detect the underlying structures (Guyon et al., 2005; Jain, 2010).

Reducing the dimension of a data set can be done through *feature selection* or *feature extraction*. Feature selection selects a subset of the features for further analysis, whilst feature extraction constructs a smaller set of features from the original features (Boutsidis et al., 2009). Feature selection will be relevant for reducing the feature space in this thesis.

2.7.5 Data set Exploration Techniques

Cross-Correlation
Cross-correlation is a term used in statistics to measure the strength of a linear

relationship between two variables X and Y. One method for quantifying this relationship is through the Pearson correlation coefficient (PCC) (Benesty et al., 2009). It is defined as

$$\rho_{X,Y} = \frac{cov(X,Y)}{\sigma_X \sigma_Y} \tag{2.21}$$

Which is the co-variance of two variables divided by the product of their respective standard deviation. PCC is defined between -1 and 1. If the correlation value is 0, the two variables are uncorrelated. If $\rho_{X,Y} = 1$, the variables have a strong linear correlation, and a negative linear correlation if $\rho_{X,Y} = -1$ (anti-correlation) (Benesty et al., 2009).

Highly correlated variables hold the same information and can be considered redundant (Abu-Mostafa et al., 2012). On the other hand, Guyon and Elisseeff (2003) suggest that high variable correlation does not necessarily indicate absence of variable complementary.

Box Plots and Violin Plots
The box plot and violin plots are used to summarise the characteristics of a variable in a data set. The box plot shows four main features of a variable: centre, spread, asymmetry, and outliers. However, the distribution of samples in a box plot is not visible. The violin plot supplements the box plot by using a simple density estimator to show the distribution of data samples. The distribution of samples is useful for discovering clusters in the data (Hintze and Nelson, 1998).
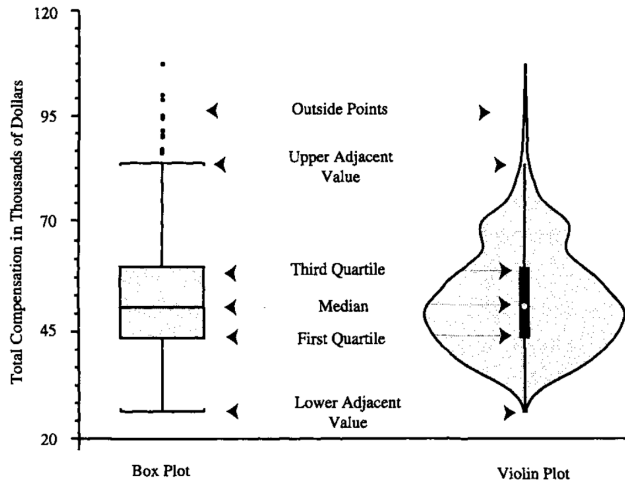
Figure 2.20: Components of box plot and violin plot (Hintze and Nelson, 1998).

Chapter 3

Literary Survey

This chapter demonstrates how the presented theory has been applied in other research. The key findings are presented as a summary in the final section of the chapter.

3.1 Applications of Traditional Vibration Analysis

Li et al. (2009) identified a cracked gear fault in a parallel gear using order analysis. The data was collected during speed-up of a gearbox in an experimental test rig. The components' dimensions and CFs were known and the results of order analysis were manually inspected where the fault was identified.

Zhao et al. (2013) explored EOA to identify a faulty REB in real vibration data, originating from a locomotive with a known BPFO fault. The geometric dimensions of the components were known, thus the CFs were known as well. The noise-to-signal ration was high. However, after SK was carried out and EOA was filtered with the OFB. Clear indications of a REB BPFO fault was discovered in the EOA spectrums.

Barszcz and Randall (2009) applied SK to detect tooth crack in a planetary gear of a wind turbine eight weeks before failure. The data was from a catastrophic gear failure on a wind turbine and the geometric dimensions and CFs were known. The authors filtered out low frequencies before applying SK. They were able to discover a shift in SK values from around 1.5 - 9 to 50 - 270 which indicated fault development. The authors localised the faulty signal by only using SK. However, the authors recommends using SK with envelope order analysis for automated detection.

Guo et al. (2012b) detected REB faults in a rotating machinery operating at variable speed by utilising EOA. The authors first analysed the vibration signals using

SK to obtain the OFB, next, the EOA spectrums were manually inspected and fault characteristics of REB faults were identified. As their data originated from an experimental test rig and all components' dimensions were known, they were able to validate their results.

3.2 Applications of Data-Driven Methods

This section will first show how K-means clustering has been used in previous literature to detect faults. Furthermore, commonly extracted features for fault detection is presented.

3.2.1 Fault Detection with K-Means clustering

Yiakopoulos et al. (2011) applied K-means to automate the detection of REB faults. The authors highlighted that the biggest advantage of K-means is that it is unsupervised, meaning that no previous data from faulty bearings is needed to *train* the model. Other mentioned benefits for selecting K-means is the ease of implementation and its simplicity. The method is tested on a laboratory test case with known bearing faults.

3.2.2 Extracted Features

Three domains are mostly used for extracting machine learning features for fault detection of vibration signals, namely the time domain, frequency domain and the time-frequency domain. This section will summarise some of the most relevant features from the literature. Several studies also deal with high noise-to-signal ratios.

Time Domain Features

Ben Ali et al. (2018) used the following features from the time domain; RMS, kurtosis, skewness, peak to peak, crest factor, shape factor, impulse factor, margin factor, mean, standard deviation, energy and energy entropy.

Yiakopoulos et al. (2011) classified bearing faults using similar time domain features as Ben Ali et al. (2018), without energy and energy entropy and adding clearance factor. Yiakopoulos et al. (2011) emphasised the potential of detecting "spiky" signals using crest factor and kurtosis.

Yiakopoulos et al. (2011) provided an explanation behind each chosen time domain feature: The RMS of a signal can be used to indicate the severity of a bearing defect. Kurtosis is a measure of how peaked or flat a signal is compared to a normal distribution. Skewness is a measure of symmetry/non-symmetry of a signal. Crest factor is the ratio of the peak value of a signal to its RMS value. Shape factor is the value that is being affected by an object's shape but is independent of its

dimensions.

Caesarendra and Tjahjowidodo (2017) provided an overview of time domain features to be used when classifying REB. The authors state that impulse factor is used to measure how much impact is generated from defects. Margin factor was used to measure the level of impact between REB and their raceways.

Frequency Domain Features: Bi-Spectrum

Features extracted from a bi-spectrum analysis has shown to be highly relevant in condition monitoring of vibration signals with noise present. Ben Ali et al. (2018) extracted features from the bi-spectrum from WT vibration data to classify a range of bearing faults. The extracted features from the bi-spectrum are shown in Table 3.1.

Table 3.1: The bi-spectrum features extracted by Ben Ali et al. (2018).

	Extracted bi-spectrum features
1	Sum of logarithmic amplitudes
2	Sum of logarithmic amplitudes of diagonal elements
3	k^{th}-order spectral moment of amplitudes of diagonal elements *(k=1,k=2,k=3)*
4	Normalized bi-spectral entropy
5	Normalized bi-spectral squared entropy
6	Bi-spectrum phase entropy
7	First axe weighted center of the bi-spectrum
8	Second axe weighted center of the bi-spectrum
9	Mean magnitude

Saidi et al. (2015) performed CM and fault diagnosis of four different faults in an induction motor based on extracted features from the bi-spectrum. The features were the same as in Table 3.1, with the exception of feature (9) as well as only using k=1 for feature (3). The feature space was then reduced from 8 features to 5 using a principal component analysis (PCA). PCA constructs new features based on input features using weighted sums in order to find orthogonal directions of maximum variance (Saidi et al., 2015).

Saidi et al. (2014) demonstrated how bi-spectral analysis of vibration signals can be coupled with EMD to diagnose bearing faults. The data used by the authors contained a high noise-to-signal ratio, which complicates classical frequency analysis. Because of the non-stationary signals in WTs, the authors proposed to first decompose the signals to stationary IMFs using EMD. Thereafter, they applied the bi-spectral analysis to these IMFs. The suggested method was able to diagnose 4 types of bearings states with an accuracy of 98.9 %. The states were *healthy bearing, Outer race fault, inner race fault* and *ball fault*.

Time-Frequency Domain Features: EMD/EEMD Features

Yu et al. (2006) proposed a method for diagnosing REB faults using Artificial Neural Networks (ANNs) using time-frequency features extracted from EMD (Section 2.7.3). Specifically, the authors extracted the energy entropy from each IMF by:

1. Calculating the energy from the first m IMFs:

$$E_i = \sum_N x_j^2 \tag{3.1}$$

   where $i = 1...m$ and N is the total number of samples in the considered IMF.

2. Construct a feature vector T with the calculated energy from each IMF

$$T = [E_1, E_2, ..., E_m] \tag{3.2}$$

3. Normalising the feature vector T by first calculating he total energy in the signal:

$$E = \left(\sum_{i=1}^m |E|^2 \right)^{0.5} \tag{3.3}$$

   and then dividing the feature vector by E, the authors get

$$T' = [E_1/E, E_2/E, ..., E_m/E] \tag{3.4}$$

which was then used to train the parameters of a machine learning classifier (ANN).

Ben Ali et al. (2018) used a similar approach as Yu et al. (2006) when extracting features from the time-frequency domain (they also used other features, discussed in Section 3.2.2 and 3.2.2. Ben Ali et al. (2018) selected the first five IMFs on the basis of previous research by the same authors (**?**), much like the features shown in Equation 3.4. The expression E_i/E was denoted the *energy rate p_i* for each IMF. Ben Ali et al. (2018) also extracted the energy entropy H_{en} from each IMF

$$H_{en} = -p_i log(p_i) \tag{3.5}$$

resulting in the two feature vectors shown in Equation 3.4 and 3.6:

$$[-p_1 log(p_1), -p_2 log(p_2), ..., -p_5 log(p_5)] \tag{3.6}$$

Thus, Ben Ali et al. (2018) extracted 10 features in the time-frequency domain.

3.3 Summary

To summarise the literature, applications of TVA has been thoroughly studied and is widely used for detecting gear and bearing faults. A key finding is that the

presented research uses known component dimensions in their analysis. These dimensions were, as stated, not available in this thesis, separating it from previous studies. In regards to the data-driven approach, Ben Ali et al. (2018) proposed a strong argument for extracting features from all three available domains; the time domain, the frequency domain and the time-frequency domain. These three domain were therefore explored in this research.

Chapter 4

Method

This chapter presents the methods applied in the thesis. First, the available data will be shown, followed by a traditional vibration analysis and a data-driven approach using clustering.

4.1 Available Data

Four Vestas V112 3.3 MW WTs were analysed in this thesis. They are located at Skomakerfjellet on the coast of Trønderlag in Norway. The wind farm is operated by TrønderEnergi and has produced power since March 2016. Skomakerfjellet wind farm has a yearly production of 36 GWh and supplies energy to 1800 households (TrønderEnergi). The data set used in this thesis was from August 2018 to December 2019.

The WTs' CM systems continuously store 165 different operational parameters such as wind speed, power outputs, temperatures, currents, and voltages It also stores different statistics related to vibration measurements. A small sample from the five first measurements of WT01 is shown in Table 4.1.

Vestas' WTs were equipped with 9 accelerometers measuring vibration at different locations. The full, raw vibration signals, were stored. In addition, the WTs were equipped with two tachometers measuring rotational speed of the low-speed shaft and the high-speed shaft. All vibration signals were sampled at 25.6 kHz and had a duration of 10 s. Every signal was recorded once or twice a day. The data set used contained approximately 400 measured signals from every sensor in each WT. The sensors are listed in Table 4.2. Information regarding start-stop cycles in the four WTs is presented in Table 4.3.

Table 4.1: WT01: Example of operational data.

Time stamp	Average power [kW]	Wind speed [m/s]	Ambient temp [C^o]	Gbx bearing oil temp [C^o]	Gbx Rotor Bearing ISOA [m/s^2]	...
04.08.18 18:51:17	543.4	5.5	14.0	60.0	0.3411	...
04.08.18 20:24:47	2500.9	13.0	15.0	71.0	0.7170	...
05.08.18 12:44:15	1839.5	9.5	10.0	70.0	0.5709	...
10.08.18 13:01:19	2565.2	9.9	15.0	69.0	0.5138	...
11.08.18 13:00:46	2861.5	12.0	13.0	71.0	0.6297	...

Table 4.2: Measurements i Vestas' WTs.

Name	Unit	Measuring device	Description
GnDe	m/s^2	Accelerometer	Generator vibration.
GnNDe	m/s^2	Accelerometer	Generator vibration.
MnBrg	m/s^2	Accelerometer	Main bearing vibration.
GbxRotBrg	m/s^2	Accelerometer	Gearbox vibration, low speed shaft.
Gbx1Ps	m/s^2	Accelerometer	Gearbox vibration, 1st planetary gear.
Gbx2Ps	m/s^2	Accelerometer	Gearbox vibration, 2nd planetary gear.
GbxIss	m/s^2	Accelerometer	Gearbox vibration, intermediate speed shaft.
GbxHssFr	m/s^2	Accelerometer	Gearbox vibration, high-speed shaft.
GbxHssRr	m/s^2	Accelerometer	Gearbox vibration, high-speed shaft.
HssShf	V	Tachometer	Measuring rotations of high-speed shaft.
LssShf	V	Tachometer	Measuring rotations of low-speed shaft.
Time	s	-	Time during measurement.

Table 4.3: Number of turbine start-stop cycles (TrønderEnergi).

Wind turbine	Start/ stop cycles	Number of signals	WT operating since
WT01	1148	410	March 2016
WT02	897	419	March 2016
WT03	1040	415	March 2016
WT04	1805	424	March 2016

4.1.1 Operational Data

The following operational parameters were selected; *time stamp*, *wind speed*, *average power* and *average rotational speed* of the high-speed shaft. Note that *average rotational speed* is denoted *AvgSpeed* throughout this thesis. The features above were all averaged over 10 s.

4.1.2 Vibration Data

Out of the 9 available vibration measurements presented in Table 4.2, GbxHssRr (Gearbox High-Speed Shaft) was selected for analysis in this thesis. This choice was made based on the vulnerability of the gearbox and the high-speed shaft bearings. Additionally, GbxHssRr measurements encapsulates potential gearbox and high-speed bearing faults, both of which were interesting to study. All GbxHssRr vibration signals for each WT are plotted consecutively in the Figure 4.2 and 4.1. The *HssShf* measurements, measuring rotational speed of high-speed shaft and used to resample the signals, was selected as well. It was selected because it measures the same shaft as GbxHssRr. In addition, resampling with the highest speed measurements gives the highest resolution, as described in Section 2.5.3.

Figure 4.2 and 4.1 suggested that the running conditions varied greatly among the measured 10 s vibration signals. Consequently, all signals were not comparable to each other. This is further described in Section 4.2.2.

(a)

(b)
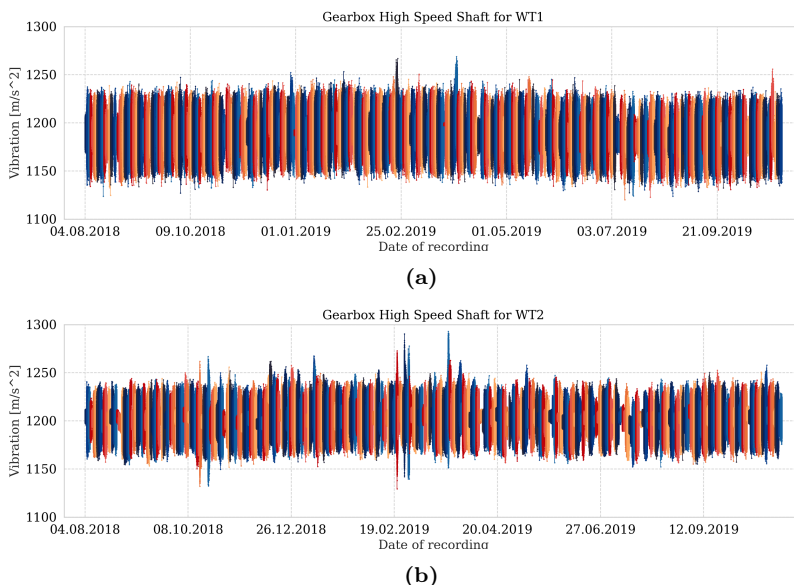
Figure 4.1: All 10 s vibration signals plotted after each other for (a) WT01 and (b) WT02.
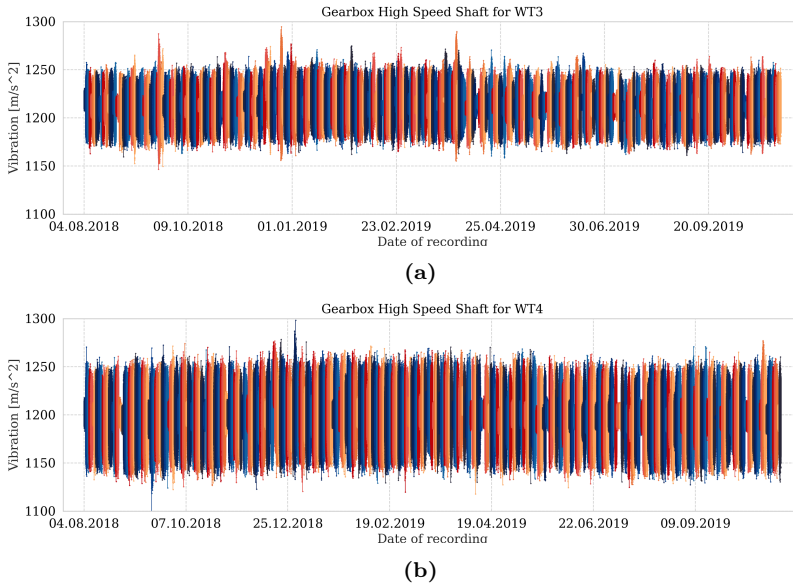
Figure 4.2: All 10 s vibration signals plotted after each other for (a) WT 3 and (b) WT 4.

4.2 PART 1: Traditional Vibration Analysis

Based on the literature study, the most effective TVA methods were determined to be OA for parallel and planetary gears and EOA for REBs, following the recommendations in Section 2.5.1.

The chosen TVA methods handle non-stationary vibration signals, enabling them to track the state of WT components, and to detect fault development during a time period. In addition, the analysis can be compared across WTs to investigate whether one has deteriorated more than another, given that the WTs are assembled with the same components. Thus, the methods were implemented in an attempt to answer all three research questions.

A disadvantage with TVA methods is that they require human inspection as the results must be interpreted by vibration experts. An in-depth analysis of all vibration signals was considered too extensive to be included. Thus, a smaller sub-sample was chosen to thoroughly investigate each WT.

4.2.1 Fourier Transformation of all WTs

In addition to the two chosen methods, a Fourier transformation was performed on all signals from each WT, regardless of the generated power during each measurement. As explained in Section 4.2.3, the vibration signals were non-stationary,

making the results from regular Fourier transformation inaccurate. However, they were used to inspect if any notable differences existed. The RMS of the amplitudes were taken to easier compare the spectrums.

4.2.2 Selecting Comparable Signals

A threshold was set to include signals measured while generator power output was greater than 80 % of nominal power (equivalent to 2640 kW) as recommended in Section 2.3. Out of the filtered signals, five signals were selected from each WT for further analysis. These five signals were evenly spaced out in time to detect changes in condition. The selected signals are presented in Table 4.4.

Table 4.4: Relevant information regarding the five chosen signals for each WT.

Wind turbine	Date	Time	Average power [kW]	Average rpm
	10.08.2018	13:01:19	2862	1499
	10.11.2018	01:56:57	3294	1532
WT01	17.03.2019	15:12:45	2915	1489
	26.06.2019	18:32:15	3305	1505
	25.10.2019	11:51:54	2906	1490
	19.08.2018	11:03:11	3066	1476
	09.11.2018	23:43:41	3298	1476
WT02	17.03.2019	15:16:30	2968	1481
	06.06.2019	18:43:42	2969	1493
	20.10.2019	06:05:54	2911	1519
	04.08.2018	20:22:58	2953	1489
	14.11.2018	22:49:56	3100	1470
WT03	05.03.2019	13:58:58	2856	1483
	21.06.2019	22:27:49	2887	1473
	25.10.2019	08:11:15	3207	1468
	11.08.2018	12:54:56	2853	1460
	10.11.2018	22:17:55	3315	1464
WT04	01.03.2019	02:40:08	3010	1505
	18.06.2019	12:42:55	2858	1493
	24.10.2019	06:19:54	3244	1511

4.2.3 Order Analysis

OA was applied to detect gear faults and is described in detail in Section 2.5.2 and 2.5.3. It involves resampling the signal and taking the Fourier transform.

Resampling Signal

As mentioned, the vibration signal was resampled according to the high-speed shafts rotational speed. The high-speed shaft normally completed approximately 250 revolutions during the recorded 10 s when generator power was above the threshold value.

The data points in between a revolution of the HSS was denoted a *segment*. It was decided that each segment should contain 2000 data points, corresponding to about twice as many as in the original segment, to increase interpolation precision. As concluded in Section 2.5.3, cubic interpolation is preferred and was implemented. This was done using SciPy's cubic interpolation technique; *scipy.interpolate* (Virtanen et al., 2020).

Fourier Transformation

The discrete Fourier transform was done using NumPy's Fast Fourier Transform implementation; *numpy.fft* (Van Der Walt et al., 2011). The Fourier transformed values were normalised by dividing it by the number of data points in the signal. Due to symmetry, only the first half of the frequencies were used.

Analysing Order Spectrums

As described in Section 2.5.1, OA is preferred when analysing parallel gears. The spectrums were analysed with regards to fault characteristics of gears (described in Section 2.5.4). As stated in Section 2.5.4, the CFs usually appears in the first 50 orders. To account for harmonics, the spectrums were filtered to show the first 200 orders. In addition, complete spectrums was inspected to detect changes in the whole spectrum.

The order spectrums of the five selected signals from each WT were thoroughly inspected. To compensate for missing vibration expertise and not knowing the CFs, the spectrums were compared across WTs to identify deviation which could indicate fault, thereby answering RQ1. To address RQ2 and detect fault development, the spectrums within each WT were compared over time.

Lastly the order spectrums were computed for all signals above the power threshold in each turbine. The median as well as the 5th and 95th percentile were plotted to better understand how much the order spectrums varied across measurements.

4.2.4   Envelope Order Analysis

Implementation of EOA followed the same steps described in Section 2.5.5. The procedure is illustrated in Figure 4.3.
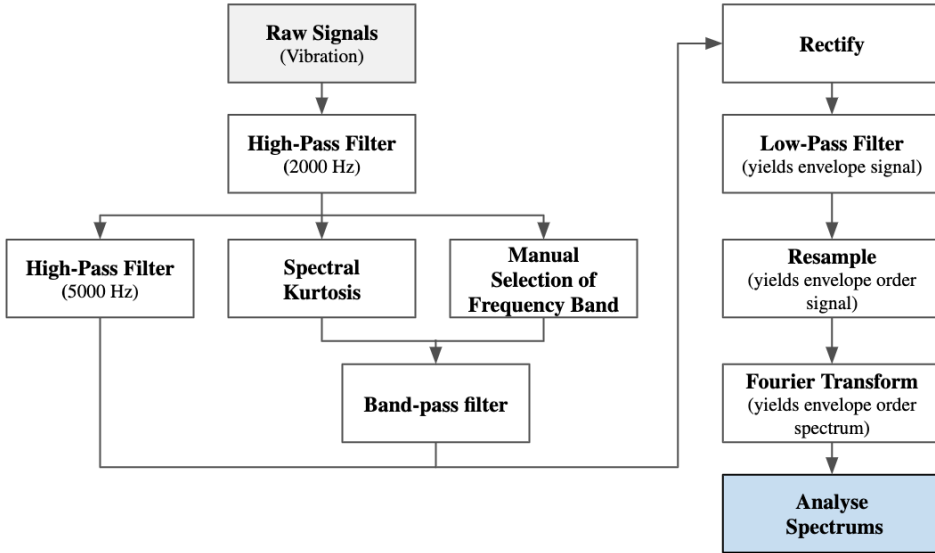
Figure 4.3: Schema of the EOA process.

An initial filtering was performed using a highpass filter with a cutoff frequency of 2000 Hz to remove vibration signals originating from shafts and gears. Obtaining the optimal frequency band for further filtering is known as a challenging task and three methods were explored:

1. Highpass filter.

2. Narrow-band filter based on Optimal SK Values.

3. Narrow-band filter based on manual selection.

Highpass Filter

The signals were highpass filtered with a cutoff frequency at 2500 Hz. This threshold was chosen to remove gear CFs and harmonics, since REBs faults are analysed in EOA (Barszcz, 2019; Liu, 2005). Because all signals were filtered the same way, they were easily compared. However, it might be difficult to detect early failure if the faulty signal is masked by other components (Section 2.3.2).

Narrowband Filter Based on Optimal SK Values

The signals were bandpass filtered using the OFB reccomended by SK. Calculating SK was performed using MatLab's implementation; *kurtogram* (MATLAB, 2019),

which utilises the Fast Kurtogram algorithm mentioned in Section 2.6. It is capable of revealing the most energetic transient signals. However, recommended OFBs from SK were rarely the same, making the spectrums difficult to compare.

Narrow-Band Filter Based on Manual Selection

Manually selecting the frequency band and was done by inspecting kurtograms. The frequency band with repeatedly high SK values in the kurtograms were chosen to bandpass filter the signal. This method is able to obtain highly energetic transient signals that are comparable since all are filtered the same way. The disadvantage is that the manual selection is cumbersome and time consuming.

After manually investigating the kurtograms, the frequency bands listed in Table 4.5 were selected. It was discovered that the frequency range with centre frequency at 9600 Hz and a bandwidth of 6400 Hz often had a SK value of 0.6 - 0.8 for all signals in all turbines. In many cases, it had the highest SK value. Thus, it was decided to investigate it for all selected signals from each WT.

Furthermore, the same narrow frequency band with high SK value in the kurtograms were inspected for each WT. This way, a comparison within each WT was possible. Because the selected narrow band across WTs were not the same, spectrums from different WTs was not.

Lastly, the two additional frequency bands for WT03 and WT04 were considered interesting and were included.

Table 4.5: Selected frequency bands for each WT.

Wind turbine	Centre frequency [Hz]	Bandwidth [Hz]
WT01	6425	50
	9600	6400
WT02	7500	50
	9600	6400
WT03	6125	50
	4500	1500
	9600	6400
WT04	6625	50
	8200	800
	9600	6400

Frequency filtering was done using SciPy's filtering techniques from *scipy.signal* (Virtanen et al., 2020). Note that the signals were filtered *before* resampling. This means that the filtering was executed in the frequency domain $[Hz]$, not order domain $[X]$. Resampling into order and taking the Fourier transform followed the same steps described in Section 4.2.3.

Analysing Envelope Order Spectrums

The analysis of envelope order spectrums were conducted similarly to order spectrums. All spectrums of the five selected signals from each WT had to be compared across WTs to identify characteristics which could indicate faults (answering RQ1). This was done to compensate for missing vibration expertise and CFs. In addition, the spectrums within each WT were compared to detect fault development (answering RQ2).

4.3 PART 2: Fault Development Analysis Using Clustering

The main goal of the data-driven clustering approach was to explore whether later signals could be separated (grouped) from the earlier signals, thereby indicating a change in state over time. Hundreds of signals from the same turbine were analysed together to find these patterns. The clustering was done using K-means.

In broad terms, the following degradation pattern analysis was carried out separately for each WT:

Step 1: Select vibrations signals above 1450 rpm (4.3.1).

Step 2: Extract a feature data set from the signals (4.3.2).

Step 3: Handle outliers and extreme values in the feature data set (4.3.3).

Step 4: Explore the feature data (4.3.4).

Step 5: Cluster the feature data set using different subsets of the extracted features (4.3.6).

Step 6: Inspect whether there exists a degradation pattern over time.

In step 2, common features for detecting faults were extracted from each of the four WTs based on the Literary Survey in Section 3.2. After extracting features, clustering was applied in step 5.

Clustering was selected because no prior information was needed regrading the state of the turbine components. Advantages of K-means over other clustering methods is its simplicity and documented success in fault detection. Disadvantages of K-means is that it is sensitive to outliers in the data set and poorly chosen features. Feature selection with limited domain knowledge also presented a challenge.

4.3.1 Selecting Vibrations Signals

Signals measured with an average shaft speed above 1450 rpm were selected, and features were extracted from these. This was to remove signals related to startups and shutdowns of the WTs. Table 4.6 shows how many signals each WT vibration data contained before and after selecting signals.

Table 4.6: Number of signals before and after filtering each turbine.

Wind turbine	Number of signals before filtering	Number of signals after filtering
WT01	410	250
WT02	419	264
WT03	415	262
WT04	424	269

4.3.2 Feature Extraction
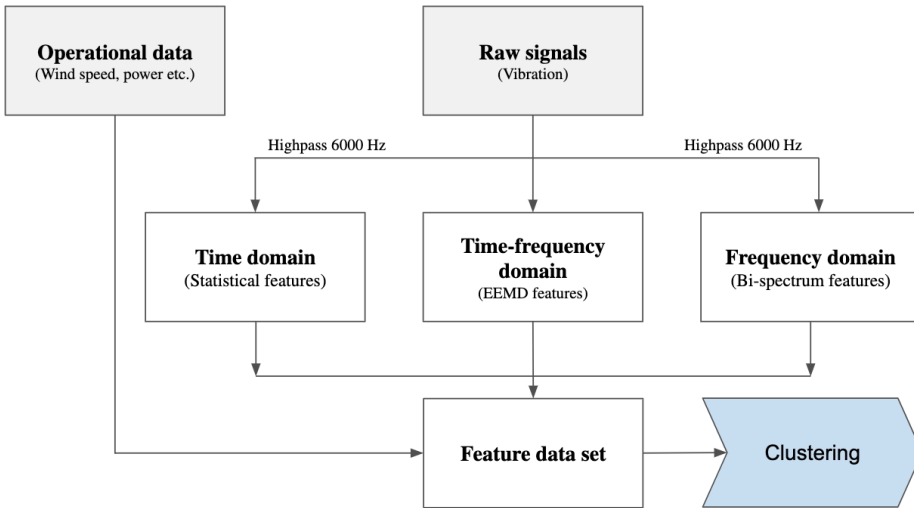
Figure 4.4: Schema showing the feature extraction process. A matrix consisting of N rows and S features, where each row represents one signal in a wind turbine, is returned for each WT. The raw input signals had an average shaft speed above 1450 rpm.

The proposed approach takes in operational data from a WT, e.g. wind speed data, as well as raw vibration signals from a single WT. A matrix (denoted feature data set) is returned, consisting of features to be analysed with a clustering method (Figure 4.4). One feature data set was extracted for each of the four WTs, and

features from the time domain, frequency domain and time-frequency domain were used. Each feature data set was analysed individually. Following is an explanation of the features in the data sets.

Operational Features

By including the four operational features shown in Table 4.7, machine learning methods such as K-means clustering are enabled to "connect" the running conditions of the signals with the corresponding vibration features presented below, since running condition will be related to the vibration response. This allowed for advanced pattern recognition.

Table 4.7: The operational features from the first 5 signals for WT 4.

Signal number	Average power [kW]	Active power [kW]	Wind speed [m/s]	Average rpm
0	2697.4	2332.1	9.1	1456.4
1	2606.1	2843.5	10.0	1468.5
2	2541.8	2694.1	10.5	1458.8
3	2853.3	3293.4	12.7	1460.6
4	2752.1	3040.3	9.7	1490.1

Time Domain: Statistical Features

The 11 time domain parameters in Table 4.8 were extracted from the raw signals high passed at 6000 Hz.

Table 4.8: Time domain features extracted from each signal x.

	Time domain features	
(1)	RMS	$\left(\frac{1}{N}\sum_{i=1}^{N} x^2\right)^{\frac{1}{2}}$
(2)	kurtosis	$\frac{1}{N}\sum_{i=1}^{N}\frac{(x_i-\bar{x})^4}{\rho^4}$
(3)	skewness	$\frac{1}{N}\sum_{i=1}^{N}\frac{(x_i-\bar{x})^3}{\rho^3}$
(4)	peak_to_peak	$x_{max} - x_{min}$
(5)	crest_factor	$\frac{x_{max}}{RMS}$
(6)	shape_factor	$\frac{RMS}{\frac{1}{N}\sum_{i=1}^{N}|x_i|}$
(7)	impulse_factor	$\frac{x_{max}}{\frac{1}{N}\sum_{i=1}^{N}|x_i|}$
(8)	margin_factor	$\frac{x_{max}}{\left(\frac{1}{N}\sum_{i=1}^{N}|x_i|\right)^2}$
(9)	signal_mean	$\bar{x} = \frac{1}{N}\sum_{i=1}^{N} x_i$
(10)	std	$\sigma = \left(\frac{1}{N}\sum_{i=1}^{N} x_i - mean\right)^{\frac{1}{2}}$
(11)	signal_energy	$\bar{x} = \sum_{i=1}^{N} x_i{}^2$

Frequency Domain: Bi-Spectrum

Since the bi-spectrum requires the input signal to be stationary, it is assumed that cutting each signal to only 0.1 s will cause the non-stationary signal to behave approximately stationary. Additionally, the 0.1 s signals were highpass filtered at 6 kHz using a butterworth filter (2.2.2). As presented in 2.3.2, weak resonance frequencies for rotating machinery are located in the higher ranges, which is why the input signals were HP-filtered before extracting bi-spectrum features.

Six features were extracted from the bi-spectrum, shown in Table 4.9. *Normalised bi-spectral squared entropy* was another feature often extracted in bi-spectral analysis for similar applications (Ben Ali et al., 2018; Saidi et al., 2015). It is defined as

$$B_5 = -\sum_{PD}^{n} q_n log(p_n) \tag{4.1}$$

where

$$q_n = \frac{|B(f_k, f_k)|^2}{\sum_{f_1,f_2 \in PD} |B(f_k, f_k)|^2} \tag{4.2}$$

However, because of small bi-spectrum values, Equation 4.1 often returned negative infinity. Consequently, the feature was not included in the feature data sets.

Table 4.9: The 6 extracted bi-spectrum features.

	Bi-spectrum features	
(1)	Sum of logarithmic amplitudes	$B_1 = \sum\limits_{f_1,f_2 \in PD} log(|B(f_1, f_2)|)$
(2)	Sum of logarithmic amplitudes of diagonal elements	$B_2 = \sum\limits_{f_k \in PD} log(|B(f_k, f_k)|)$
(3)	kth-order spectral moment of amplitudes of diagonal elements (k=1,k=2,k=3)	$B_3 = \sum\limits_{f_k \in PD} klog(|B(f_k, f_k)|)$
(4)	Normalised bi-spectral entropy	$B_4 = -\sum\limits_{PD}^{n} p_n log(p_n)$ where $p_n = \frac{|B(f_k, f_k)|}{\sum\limits_{f_1,f_2 \in PD} |B(f_k, f_k)|}$
(5)	First axe weighted center of bi-spectrum	$B_6 = \frac{\sum\limits_{PD} iB(i,j)}{\sum\limits_{PD} B(i,j)}$
(6)	Second axe weighted center of bi-spectrum	$B_7 = \frac{\sum\limits_{PD} jB(i,j)}{\sum\limits_{PD} B(i,j)}$

Time-Frequency Domain: EEMD

The IMF rate and IMF entropy features were calculated using the equations in Section 3.2.2. The kurtosis for each IMF was computed using the equation in Table 4.8.

For each sampled 10 s signal x, 15 features were extracted using the 5 first IMFs from the EEMD method. They were:

- 5 IMF energy rate features, one for each IMF:

$$[E_1/E, E_2/E, E_3/E, E_4/E, E_5/E] \tag{4.3}$$

  The energy in each IMF is $E_i = \sum\limits_{N} x_j^2$ over the data points in IMF i. E is the energy sum: $E = \sum_{i=1}^{5} E_i$.

- 5 IMF energy entropy features:

$$[-p_1 log(p_1), -p_2 log(p_2), -p_3 log(p_3), -p_4 log(p_4), -p_5 log(p_5)] \tag{4.4}$$

  where p_i is the energy rate $p_i = E_i/E$.

- 5 IMF kurtosis features: The kurtosis was calculated from each IMF using the equation in Table 4.8.

4.3.3 Handling Outliers and Extreme Values

The four extracted feature sets (one for each WT) consisted of 36 features in total: 4 operational features, 11 time domain features, 6 frequency domain features (bi-spectrum) and 15 time-frequency domain features (IMFs). Before continuing the data-driven analysis, outliers and extreme values were removed.

Box-plots were created for every feature in the extracted data set and studied to detect outliers. If a feature contained an extreme value, the whole row was omitted from the data set. Since K-means is sensitive to noise, it was essential that noisy samples were removed. This could be samples recorded by malfunctioning sensors. K-means uses every data sample to find cluster centroids. Consequently, noisy samples may cause the algorithm to find "wrong" clusters and thereby fail to detect any potential fault degradation patterns.

4.3.4 Feature Data set Exploration

Distribution of Samples Over Time
After removing outliers, the distribution of indexes in each feature data set was analysed to make sure the samples were spread out across the timeline. Especially for the later indices, it was important that there existed enough samples for the proposed K-means approach (Section 4.3.6) to be viable.

Single Feature Development Over Time
The N rows, equal to the number of signals in each WT, were grouped together by which month the signals were sampled. Furthermore, violin plots were created for every feature for every month in the data set.

The operational data features such as average wind speed and average power were inspected in these violin plots. For instance, these plots illustrated whether the turbines produced more power during the winter months. Knowledge like this is valuable when dealing with highly sensitive methods such as K-means, because features that change depending on the season may contaminate the partitions (clusters).

Grouped violin plots for the other features were also inspected. An increase in mean value over time of each monthly violin plot could indicate fault development by studying one feature at a time, since some features could theoretically indicate gearbox faults.

As mentioned in Section 2.7.5, a disadvantage of violin plots is that the distribution of data samples in different groups may look similar even though the number of samples differ. The number of samples in each violin plot was therefore presented below each plot.

Two-Feature Development Over Time
Scatter plots were created for the features to look for clustering tendencies (Jain and Dubes, 1988). Applying colour hues to the samples over time results in a human interpretable plot. Separate clusters consisting of samples from signals recorded at later times could indicate a change in state. Scatter plots allowed for analysis of two features at a time, combined with the Signal Index (time) to look for clusters. Furthermore, clustering with K-means allowed for an extension of this

scatter-analysis, since it is not restricted to comparing just two features at a time.

If *no* clustering patterns are visible in these plots for WT1-4, it is increasingly interesting to extend the study to n-dimensional feature space with K-means.

4.3.5 Feature Selection and Subsets

The Pearson correlation coefficient matrix (Section 2.7.4) was plotted for each data set for the four turbines. Highly linearly correlated (or linearly anti-correlated) features were handled by performing clustering on different subsets of the 36 features, where some subsets did not contain highly correlated features. The decision of splitting the complete feature sets into smaller subsets was done based on the challenges related to clustering high-dimensional data, mentioned in Section 2.7.4.

Feature Subsets

The 36 features were divided into 6 groups, shown in Table 4.3.5.

Table 4.10: The six feature groups and their features.

Subset name	Subset features
Operational (4 features)	[AvgPower, ActPower, WindSpeed, AvgSpeed]
Bi-spectrum (6 features)	[B1, B2, B3, B4, B6, B7]
Time (11 features)	[rms, kurt, skewness, peak_to_peak, crest_factor, shape_factor, impulse_factor, margin_factor, signal_mean, std, signal_energy]
IMF energy (10 features)	[imf_rate_1, imf_rate_2, imf_rate_3, imf_rate_4, imf_rate_5, imf_entropy_1, imf_entropy_2, imf_entropy_3, imf_entropy_4, imf_entropy_5]
IMF kurtosis (5 features)	[imf_kurtosis_1, imf_kurtosis_2, imf_kurtosis_3, imf_kurtosis_4, imf_kurtosis_5]
mixed features (4 features)	[imf_rate_5,imf_kurtosis_5,B1,B5]

Furthermore, the *Operational* features were combined with the other five groups to form the subsets to be clustered with K-means:

1. Operational and bi-spectrum
2. Operational and time
3. Operational and IMF energy
4. Operational and IMF kurtosis
5. Operational and mixed features

The *Operational* features were included in all sets to be clustered in order to capture patterns correlated to different running conditions. For instance, an increase load on the HSS caused by a higher average power may lead to a different vibration response.

4.3.6 K-Means Clustering

As mentioned in Section 2.7.2, the most crucial step when performing K-means clustering is the selection of how many clusters K the data is grouped into. This thesis presents a subjective approach to this challenge, and aims to find the K which best separates the most recent signals in the data, thus indicating some distinct fault vibration pattern towards the end of the recorded signals. Specifically, the most recent signal were defined as having index or signal number from 350 to approximately 400 (depending on the WT).

The subsets from each WT were clustered using K-means. The distance metric used was *Euclidean Distance*. N was the number of signals and S the number of features in a subset. The following strategy for selecting parameter K was used:

1. The elbow criterion method (Section 2.7.2) was used with K from 1 to 30 to gain an understanding of the range for K.

2. Using the plot produced by the elbow method, a range was defined for K: $Range_K = [1, ..., K_{max}]$. K_{max} denotes the K where the change in within-cluster variation is minimal (by visual inspection).

3. For every K_i in $Range_K$:

   (a) Obtain the K_i clusters through the K-means algorithm. The signals (rows) in the feature data set is separated into K_i clusters and returned in a *labels* array of length N. This array holds information about which signal index $[0, ..., N]$ was assigned which cluster.

   (b) Transform the *labels* array to a *key-value* pair dictionary where the *keys* are the cluster labels (integers) and *values* a list of signal indices within the cluster.

   (c) Pass the dictionary to Algorithm 1 to acquire the cluster number containing the maximum percentage of indices after index 350. An example of a result after this process is shown in Table 4.11.

   (d) Furthermore, the cluster with the maximum (highlighted in Table 4.11) percentage number of indexes above 350 is selected and appended to a new matrix $M_{maxPercentage}$.

4. Based on $M_{maxPercentage}$, shown in Table 4.12, the most fitting parameter K is determined by inspection. The max percentage number works as the *external criteria* for evaluating the clusters. It is ideal that this number is as close to 100 % as possible.

5. Finally, K-means was performed on the subsets and the results analysed.

Algorithm 1: GETCLUSTERSTATISTICS: Get statistics from clusters

Input: *clusterDictionary*: *Keys* (Int) represent cluster index.
　　　　Values (List) contains index of signals/intervals in cluster.
Output: *statsMatrix*: Matrix with statistics about the input
　　　　clusters

statsMatrix ← declare empty 2-dimensional matrix
for *cluster* **in** *clusterDictionary* **do**
　　mean ← calculate mean of indexes in *cluster*
　　count ← count the number of indexes *cluster*
　　percentage ←
　　percentage of indexes in *cluster* with value above 350

　　// Append row of variables to `statsMatrix`
　　statsMatrix.`appendRow`(*mean*, *count*, *percentage*)
return *statsMatrix*

Table 4.11: Example of clusters statistics from running Algorithm 1 (GETCLUSTERSTATISTICS) with $K = 7$.

Cluster label	Intervals in cluster	Average index value	Number of indices greater than index 350	Percentage of indices greater than 350
1	29	193.7	5	17.0
2	48	187.8	5	10.0
3	5	240.6	1	20.0
4	38	217.2	8	21.0
5	61	201.5	8	13.0
6	16	175.0	2	12.0
7	68	231.588	17	25.0

Table 4.12: The $M_{maxPercentage}$ matrix. The rows contain the clusters with the *percentage of cluster indexes* above 350 maximised, when K-means was executed with values K from $[2, ..., K_{max}]$. In this example, K=7 is selected because it maximeses the objective.

Iteration	K	Intervals in cluster	Max percentages
0	2	97	20.0
1	3	70	19.0
2	4	71	18.0
3	5	38	24.0
4	6	38	24.0
5	7	68	25.0

4.4 Hardware and Technical Implementation

The programming language Python v3.7.5 was used for data processing and analysis. The code is written in Jupyter Notebook, an open-source web application that supports mixing markdown sections and code. This results in code that can be easily reviewed. All the code written for this thesis is in the following repository: `https://github.com/stianismar/master-thesis/`.

Matlab v9.7.0.1190202 was utilised for Spectral Kurtosis (MATLAB, 2019). The Python library used for data processing was mainly Pandas v1.0.1. Also, Scipy v1.4.1 was used for signal processing and Scikit-learn v0.22.1 was used for implementing K-means. EEMD was implemented with with pyEMD developed by Laszuk (2017), and bi-spectrum analysis was conducted through the implmentation in Eulenfeld (2018).

With regards to hardware, the analysis were run on a MacBook Pro with 3.1 GHz Intel Core i5 processor and 8 GB RAM.

Chapter 5

Results and Analysis

This chapter first presents the results from the TVA (Section 5.1). Afterwards, the results from the clustering analysis (Section 5.2) is presented. Interpretations of the results is presented continuously.

5.1 PART I: Traditional Vibration Analysis

The following results presented in this section. First, a Fourier transformation of all signals is presented. Next, an example of a resampled signal and its Fourier transformation is presented and compared to the original. Lastly, the results regarding the two TVA methods are presented; order analysis and envelope order analysis. The results for every WT from a method is presented before advancing to the next method.

5.1.1 Fourier Transformation of all WTs

The Fourier transformation of every unfiltered GbxHssRr signal is plotted consecutively for each WT in Figure 5.1. Even though the signals were unfiltered, the figure still allowed for an initial comparison between the WTs.

WT01 and WT04 were similar, although WT04 had a higher RMS amplitude in the high frequency region. The plot also showed that WT02 and WT03 were similar. They had high spikes in RMS amplitude around 1800 Hz. These findings were interesting and are further discussed in Chapter 6.
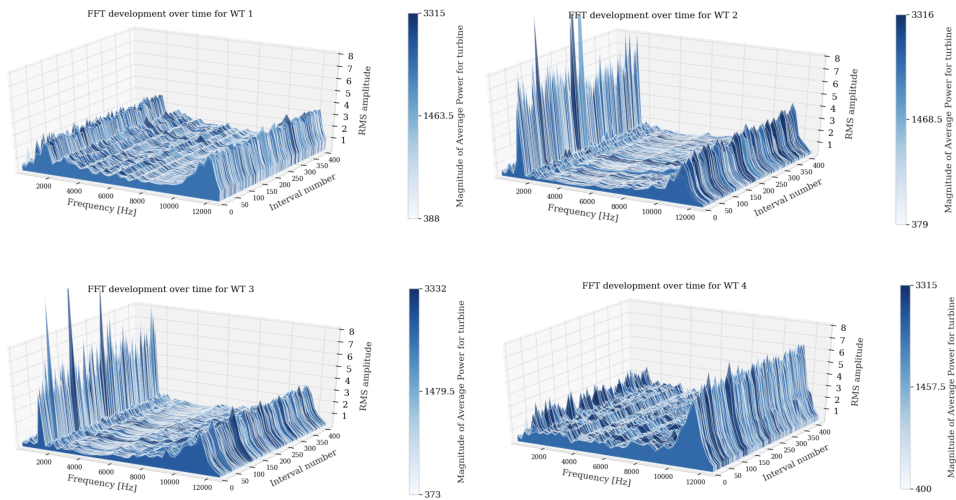
Figure 5.1: Fourier transform of all GbxHssRr signals for each turbine. The images were plotted with a RMS limit of 8 to capture the weaker frequency amplitudes of WT01 and WT04 in the lower frequency ranges.

5.1.2 Resampling Signal Validation

A resampled signal is shown in Figure 5.2 for validation. The vibration signals show the first two shaft revolutions. The Fourier transformation of the original- and the resampled signal is also provided for comparison.

The resampled signal was almost identical to the original, whilst the spectrums were very different. The signal had become cyclo-stationary, spectral smearing was reduced and spectral lines more clear. In addition, some amplitudes increased. This validated the resampling method.

5.1.3 Order Analysis

This section first presents the OA results regarding gear fault detection for the first 200 orders. Following are the results from the OA from the complete spectrum. These analysis were conducted on the five chosen signals for each WT. Lastly, the median values with the 5th and 95th percentile of all comparable signals is presented.

Gear Fault Development: First 200 Orders

Order spectrums showing the first 200 orders of each WT is shown in Figure 5.3 and 5.4. They were scaled such that spectrums were easily compared.

In regards to fault development , the spectrums from the first 200 orders indicated no fault development. Spectral lines were constant and no new harmonics or side-
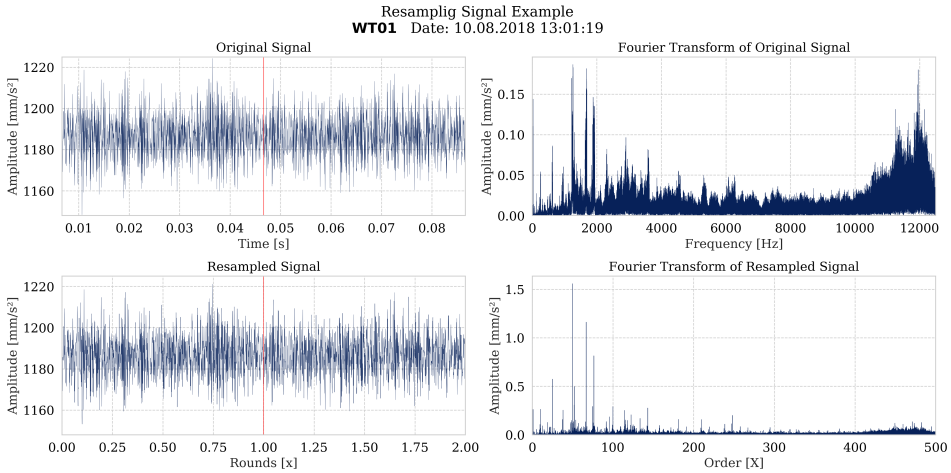
Figure 5.2: Validating the resampling method. Left: Vibration signal, before and after resampling. The red line indicates a new revolution. Right: Spectrums after Fourier Transformation. The resampled signal produced a clearer spectrum.

bands emerged during the time period.

The spectrum from the OA showed that WT01 and WT04 were similar and WT02 and WT03 were similar. Even though the CF of the parallel gear was unknown, the component could be identified based on the spectral lines and harmonics. A spectral line appeared at order 25 with clear harmonics at 50 and 75 in the spectrums from WT01 and WT04. This was most likely originating from a parallel gear with 25 teeth on the wheel connected to the high speed shaft. This is based on the Equation 2.2 and the fact that the parallel gear was the same shaft as the vibration sensor. The spectrums from WT02 and WT03 had a spectral line at 28 and a distinct 2nd harmonic at 56 as well as less clear harmonics at 84 and 112. This appeared to be a different parallel gear with 28 teeth.

It was discovered during conversations with WT operators and experts at TrønderEnergi that Vestas may use different components from different manufacturers when assembling their WTs. Consequently, the WTs may not be exactly the same. These findings suggests that the WTs were indeed assembled with different gearboxes. Unfortunately, it complicated the comparison across WTs. Still, it was possible to compare WTs with the assumed same gearbox. Comparing WT02 and WT03, there were no significant differences between them. Comparing WT01 and WT04, the 3rd harmonic was less clear in WT04 and there were more sidebands around each harmonic, which could indicate an early fault on the parallel gear as described in Section 2.5.4.

The level of noise was higher in WT04's spectrums than any of the other WTs'

spectrums. Different spectral lines appeared in the WT04 spectrums compared to WT01'. However, these lines could not be linked to any components since the CFs were unknown. The differences suggest that WT04 was more likely to have a fault than WT01 given that their gearboxes were the same.
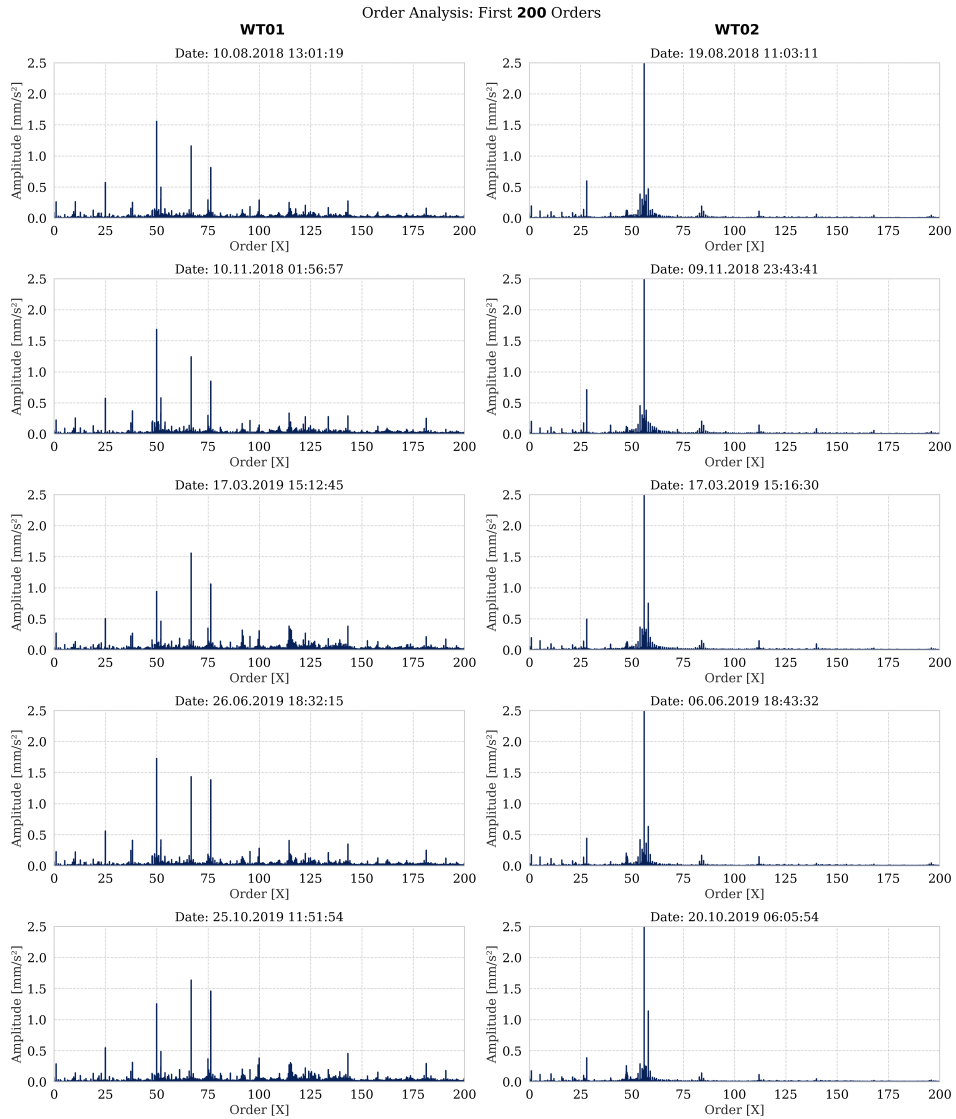

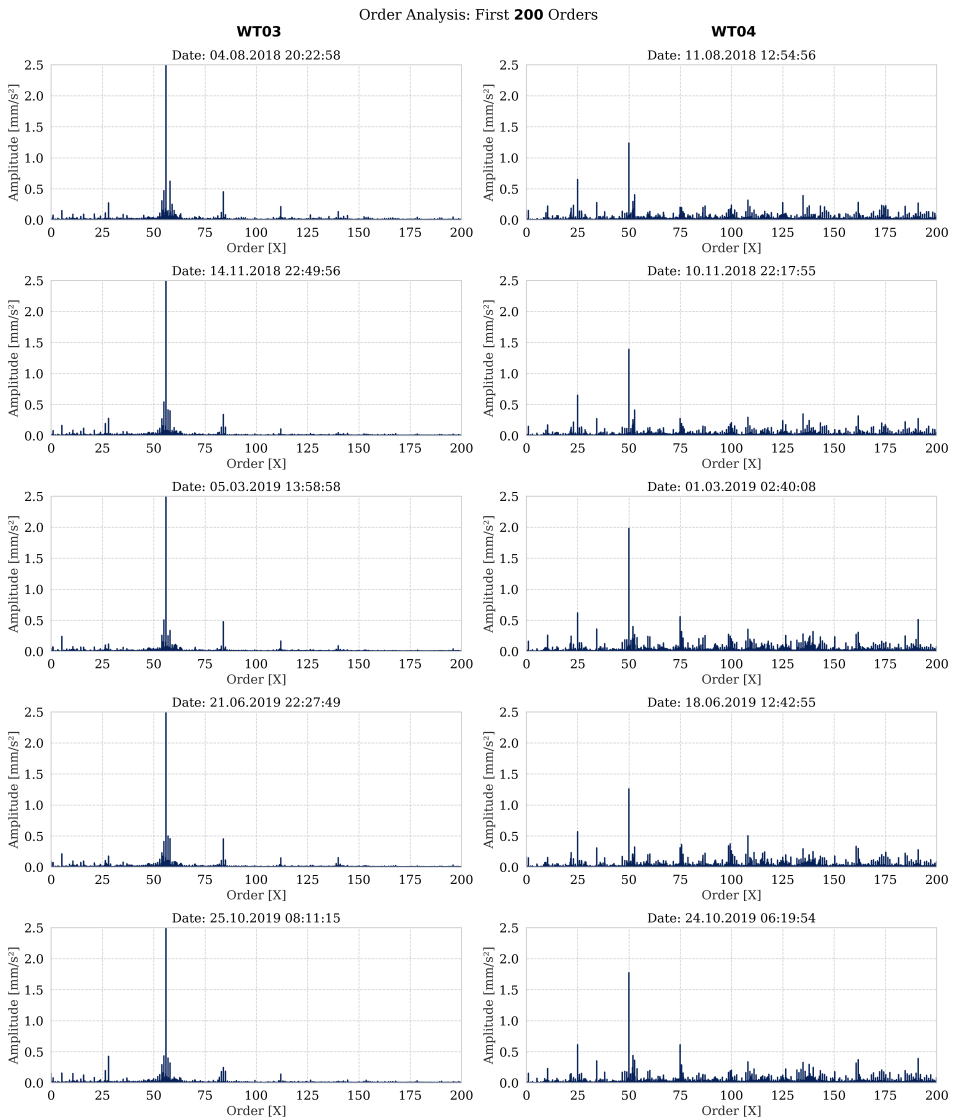**Figure 5.3:** Order analysis of the five selected signals from WT01 and WT02. The first 200 orders are displayed.

Figure 5.4: Order analysis of the five selected signals from WT03 and WT04. The first 200 orders are displayed.

Gear Fault Development: Complete Order Spectrums

Order spectrums showing all orders of each WT is shown in Figure 5.5 and 5.6.

In regards to fault development, the spectrums were similar throughout the time period, indicating no fault development. Some spectral lines appeared, disappeared and reappeared more frequently, but seemed to be independent of time. This makes them likely to be natural variation rather than fault development.

Regarding fault identification, none of the WTs were exactly the same. Compared to WT02, WT03 displayed slightly more vibration in the higher order region. Yet, the difference was minimal, meaning that no faults could be identified.

The difference between WT01 and WT04 was notable and varied more for higher orders than the previously inspected lower orders. Some notable spectral lines were observed in WT01 (up to 300 orders), while WT04's spectrums were chaotic with higher spectral lines appearing throughout the spectrum. It also showed high variation regarding the amplitudes of the spectral lines. These findings suggested that WT04 could indeed have an early fault.
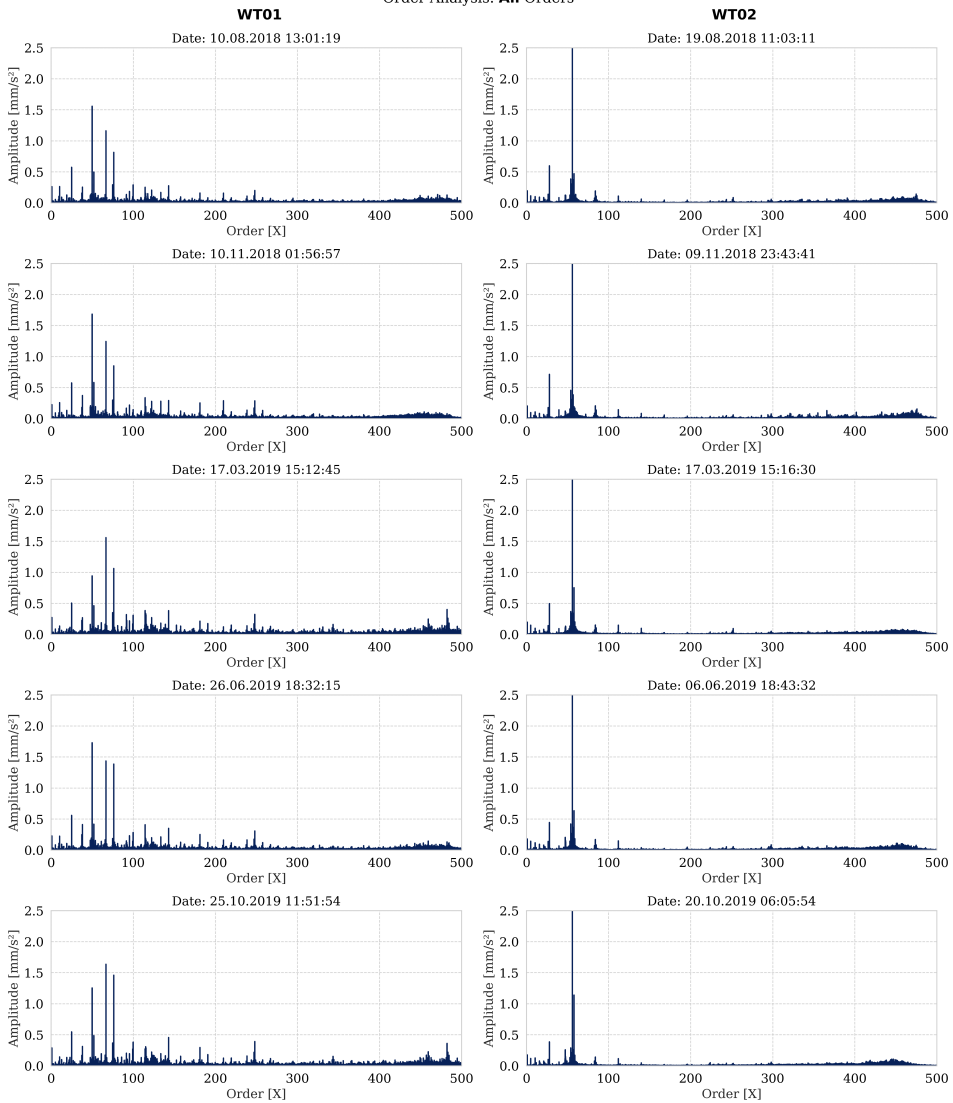
Figure 5.5: Order analysis of the five selected signals from WT01 and WT02. All orders are displayed.
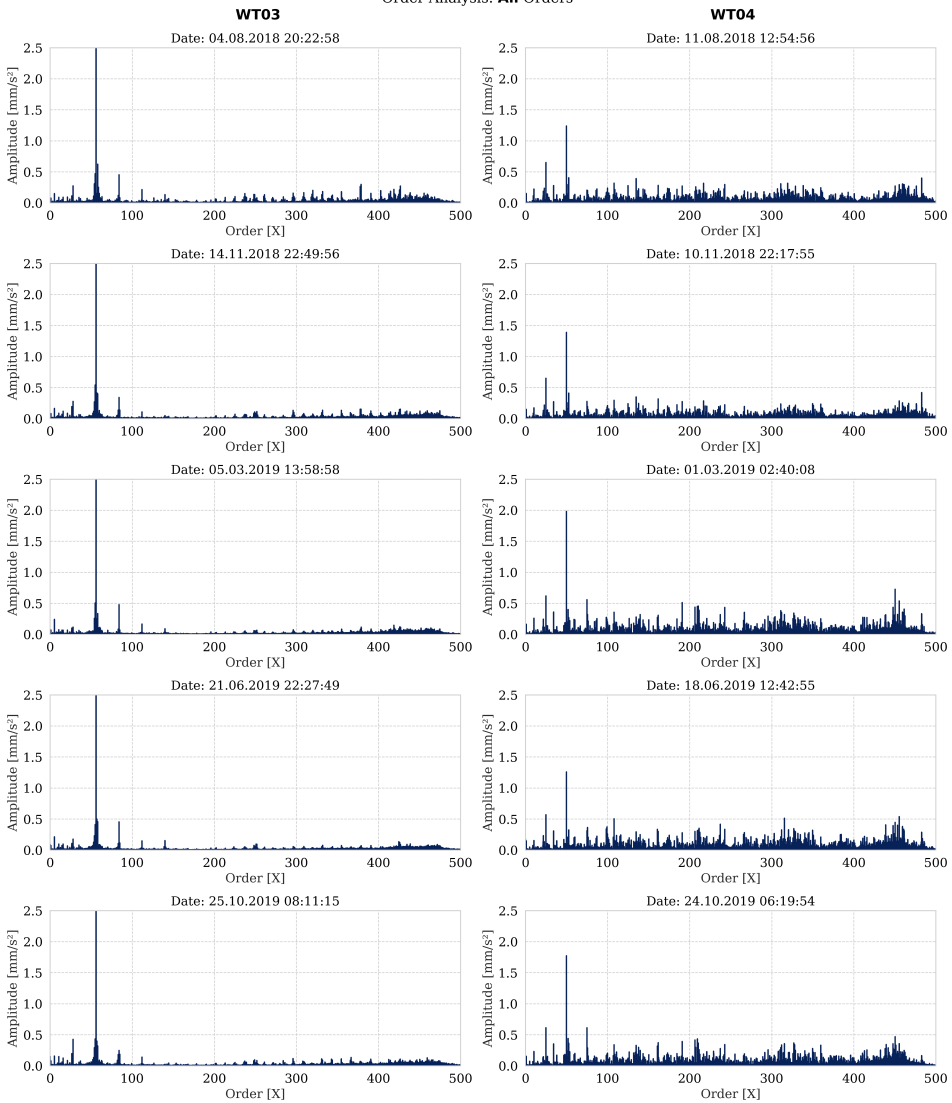
Figure 5.6: Order analysis of the five selected signals from WT03 and WT04. All orders are displayed.

Median, 5th and 95th Percentile of all Comparable Signals

Figure 5.7, 5.8, 5.9 and 5.10 show the the median RMS amplitudes for each order, together with the 5th and 95th percentile for for *all* comparable signals (more than 80% of nominal power output) for each turbine. The figures were equally scaled to simplify comparison. They give an indication of how much the spectrums varied.

Again, the spectrums of WT02 and WT03 were similar, especially up to 120 orders. Above 120, the median values were still similar, although WT03 had more variation shown by the 5th and 95th percentile.

WT01 and WT04 were similar in the lower order range, however, the variation in higher order range (above 120) were much higher in WT04. It strongly differed from the other WTs.
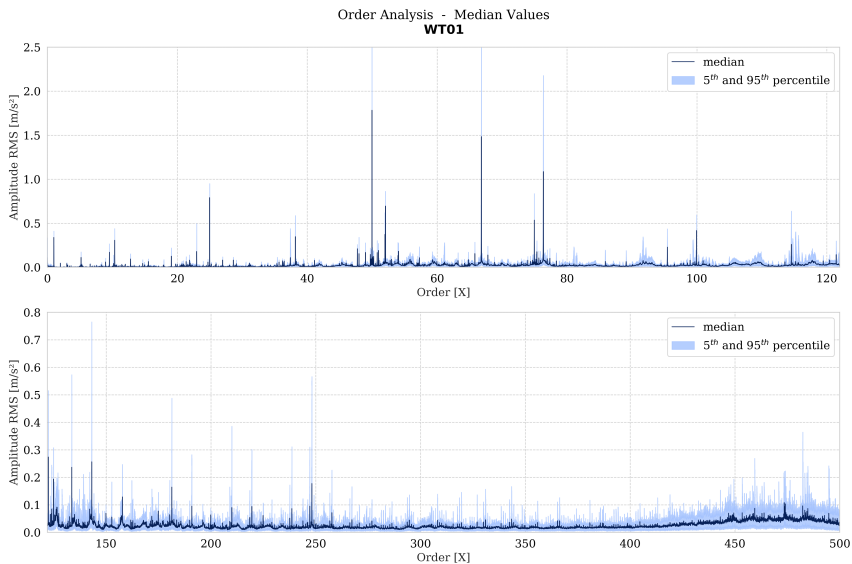
Figure 5.7: Median RMS values together with the 5th and 95th percentile of all comparable signals from WT01.
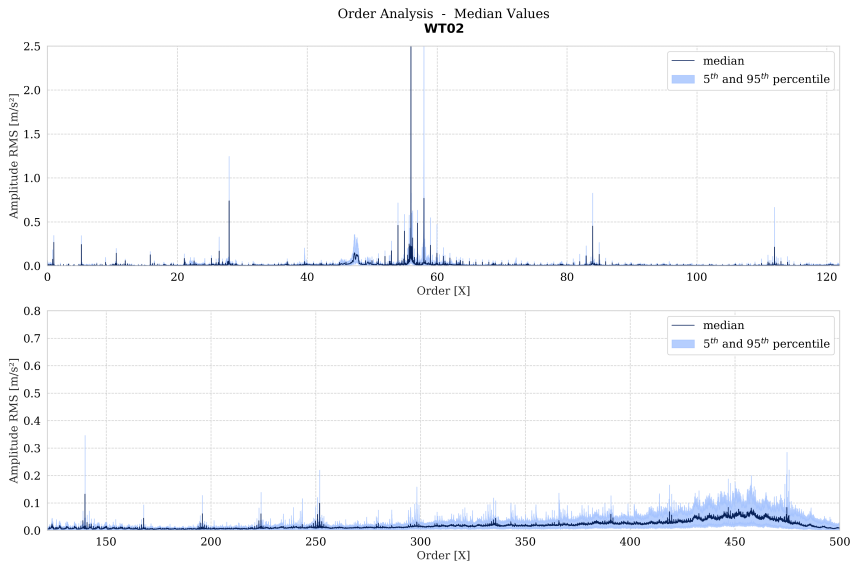
Figure 5.8: Median RMS values together with the 5th and 95th percentile of all comparable signals from WT02.
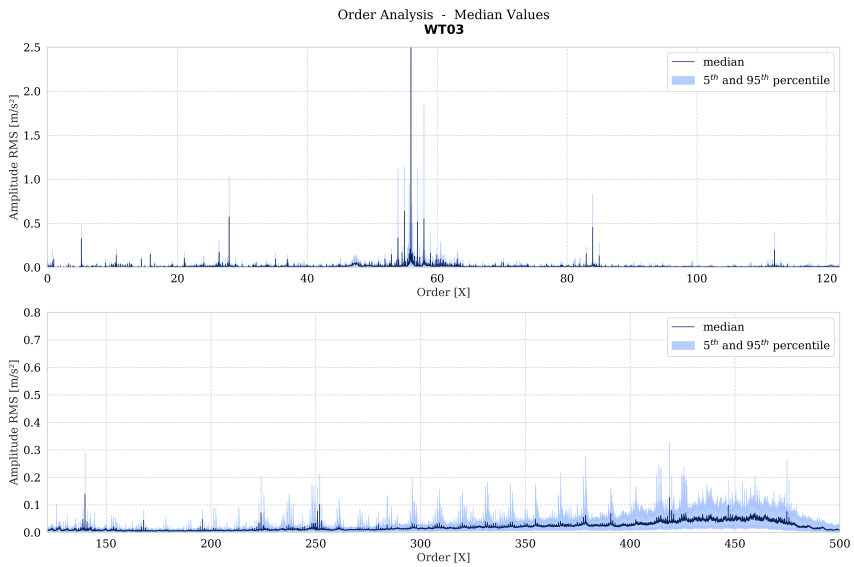
Figure 5.9: Median RMS values together with the 5th and 95th percentile of all comparable signals from WT03.
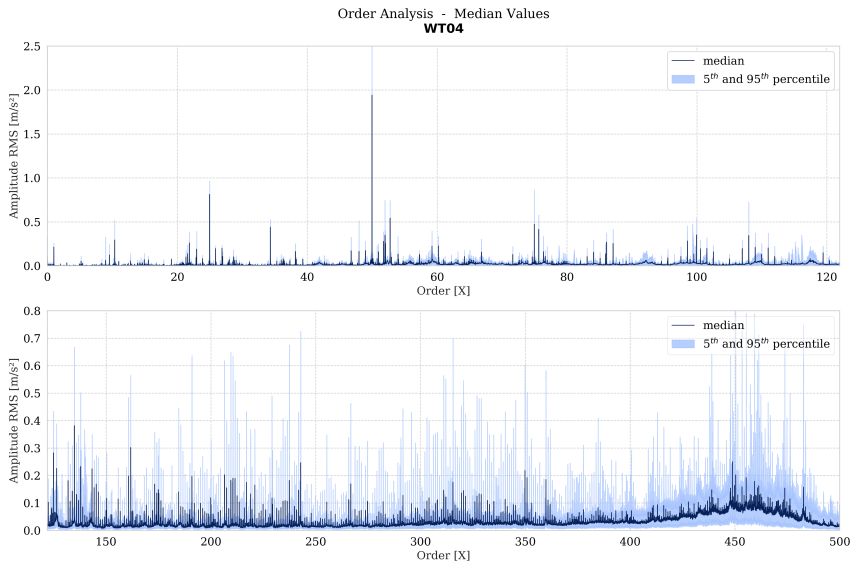
Figure 5.10: Median RMS values together with the 5th and 95th percentile of all comparable signals from WT04.

5.1.4 Envelope Order Analysis

The results of envelope order analysis is presented in this section. Distinguishable spectral lines are commented. A complete analysis of each spectrum is impossible without knowing the characteristic frequencies. However, some findings are presented. The EOA results based on the three different filtering approaches from Section 4.2.4.

Highpass Filtered: 2500 Hz

Figure 5.11 and 5.12 show the first 30 orders. The spectrums were equally scaled to easily compare.

Regarding fault development in the WTs, the spectrums varied slightly when compared within each WT. However, spectral lines appeared inconsistently, suggesting natural variation rather than degradation.

Regarding fault identification, the overall vibration level was slightly lower in WT02 than WT03. In addition WT02 had no evident spectral lines while interesting spectral lines appeared in WT01 at 10.96, 11.96, 12.96, 21.93, 22.93 and 23.93. They were likely related given their spacing. It was difficult to interpret whether the existence of these spectral lines were enough to indicate a fault or not. If they were related to REBs it is more likely to be a sign of early fault (as described in Section 2.5.6). However, one cannot be certain without knowing the CFs.

Comparing WT01 and WT04 some interesting spectral lines appeared in WT01 (especially around 10 and 20), while many more were present in WT04. WT04's spectrums were more chaotic and the general level of vibration was higher. As with WT03, it was difficult to interpret whether the existence of spectral lines in WT01 were enough to indicate fault. The higher spectrum amplitudes in WT04 could mean that it had a fault.
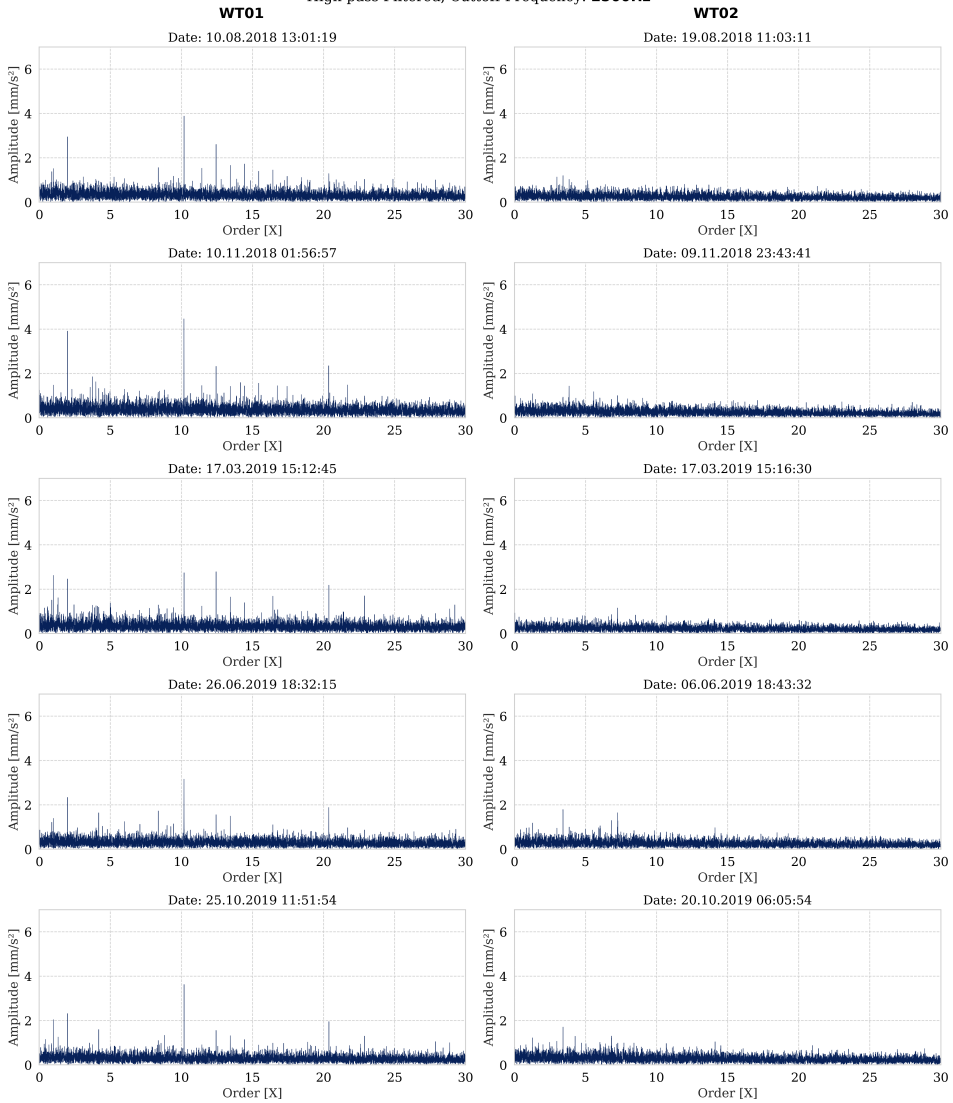
Figure 5.11: Envelope order spectrums of the five selected signals from WT01 and WT02. Filtered with cutoff frequency 2500Hz. First 30 orders shown.
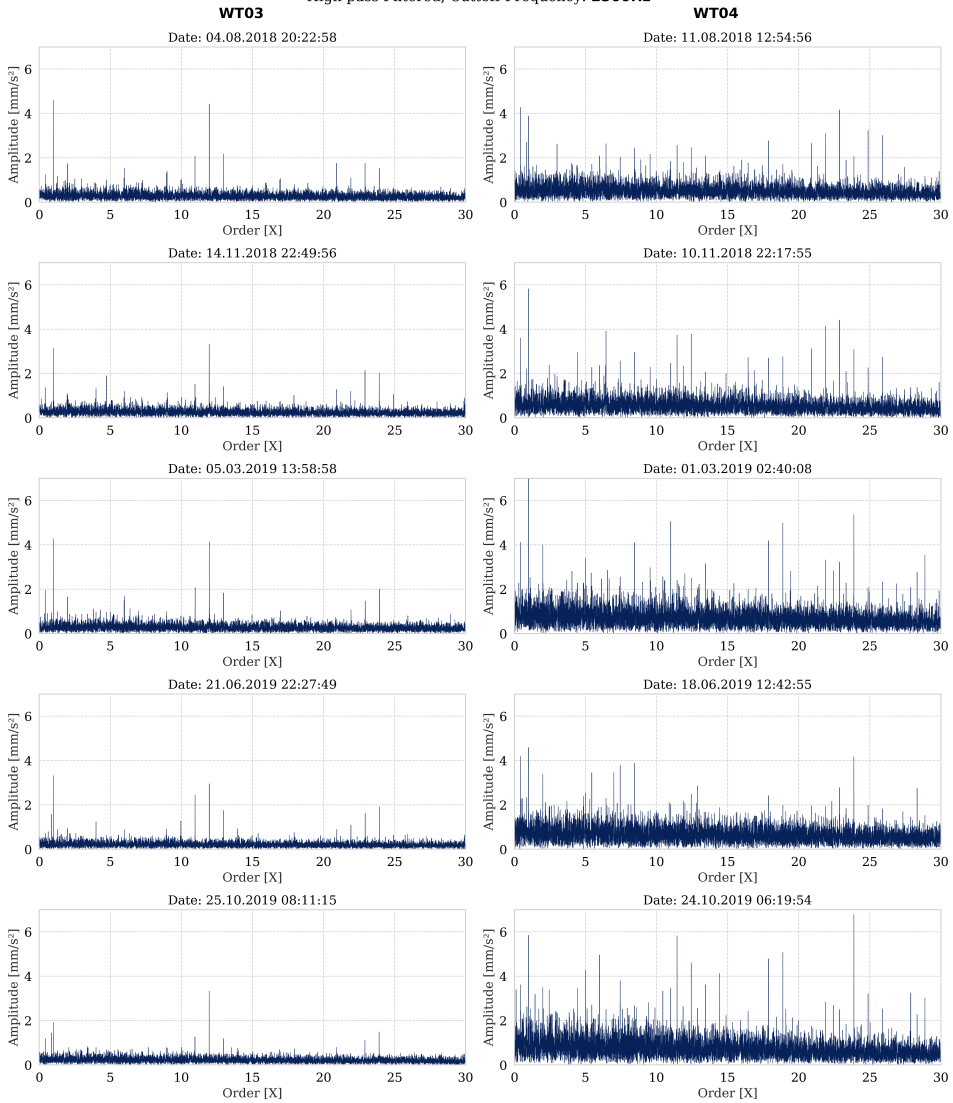
Figure 5.12: Envelope order spectrums of the five selected signals from WT03 and WT04. Filtered with cutoff frequency 2500Hz. First 30 orders shown.

Narrow-Band Filter Based on Optimal SK Values

Kurtograms

Kurtograms visualise the SK values in different frequency bands. A sample of kurtograms showing the first selected signal from each WT is provided in Figure 5.13, 5.14, 5.15 and 5.16. The rest of the selected signals' kurtograms are found in Appendix B.1. A SK value of 0 corresponds to a random, Gaussian distribution and is therefore uninteresting. Note that the kurtisis value is centered around 0 and not 3 in Matlab's implementation. Higher SK values indicate the presence of energetic, transient signals and are considered more interesting.

In general, the kurtograms differed from each other, both within a WT and across WTs. The kurtograms were especially different in the short frequency bands found at level 8 (521). However, there were some similarities. For instance, the frequency range with centre frequency at 9600 Hz and a bandwidth of 6400 Hz often had a SK value of 0.6 - 0.8 for all selected signals.

The kurtograms from WT01 and WT02 were the most similar, although WT01 sometimes had higher SK values in level 8. SK values from WT02 were consistently lower than the others. WT03 often highlighted other frequency bands and their kurtograms looked different from the others. WT04 often had the highest SK values.
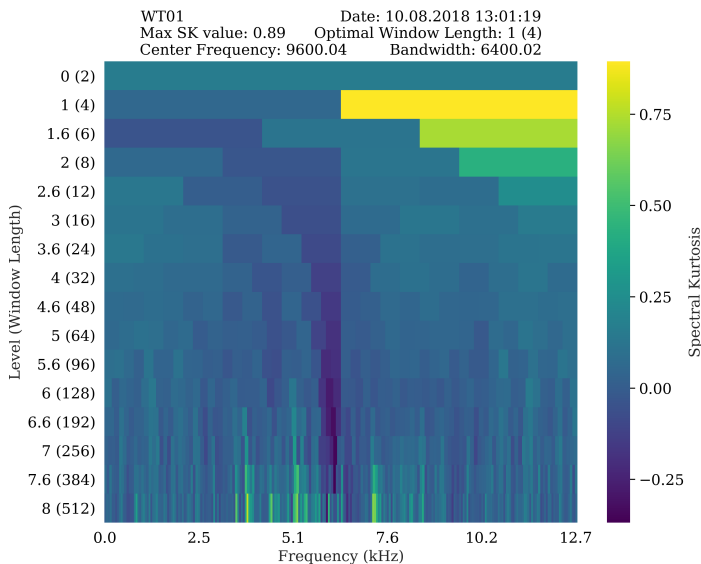

Figure 5.13: Kurtogram visualising SK-values in different frequency bands for the first chosen signal in WT01.
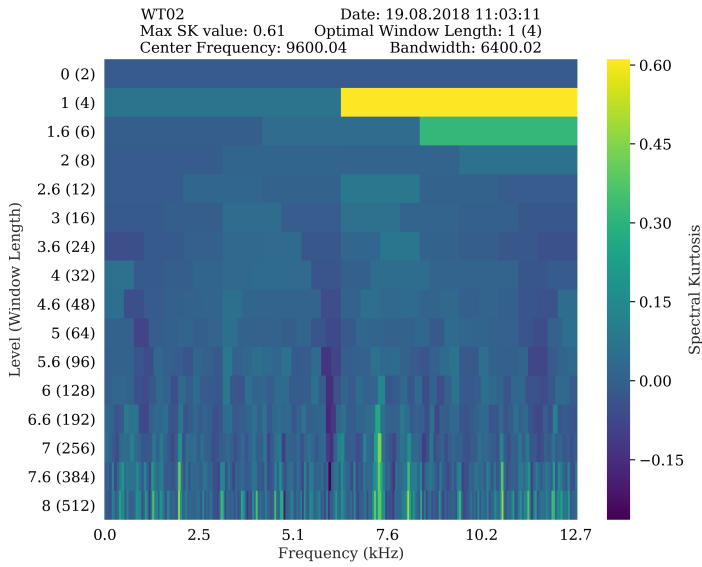
Figure 5.14: Kurtogram visualising SK-values in different frequency bands for the first chosen signal in WT02.
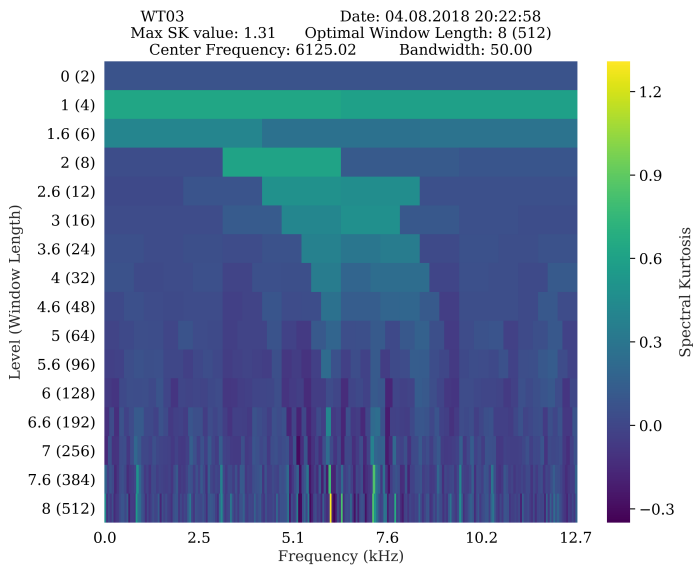

Figure 5.15: Kurtogram visualising SK-values in different frequency bands for the first chosen signal in WT03.
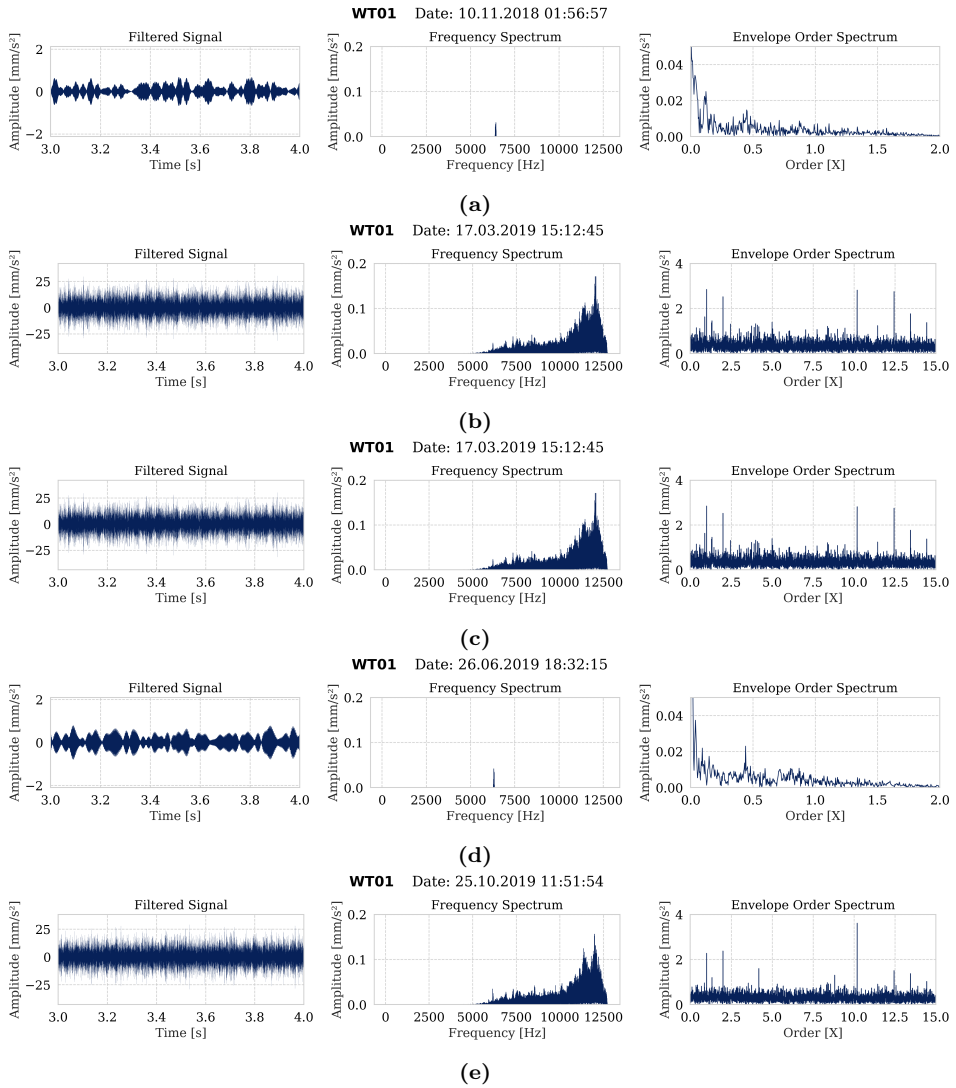
Figure 5.16: Kurtogram visualising SK-values in different frequency bands for the first chosen signal in WT04.

Envelope Order Based on Optimal SK Values

The results are given in Figure 5.17, 5.18, 5.19 and 5.20. The left figures show the signals after filtering with the recommended frequency band based on SK. The middle figures show the signals filtered with the optimal frequency band. Finally, the right figures show the envelope order spectrums. They display different orders based on how narrow their bandwidth were.

The spectrums would be more interesting to inspect if the characteristic frequencies were known. It is difficult to detect if any fault existed without them. Apart from WT02, the recommended OBF were often from different frequency regions. This made it hard to discover changes during the time period which could indicate fault development. Further interpretations was therefore considered pointless. Manually selecting these frequency bands attempted to deal with this challenge and is presented next.

Figure 5.17: Envelope order spectrums of the five selected signals from WT01, band-pass filtered based on SK recommendations. Left figures: Signal after narrow-band filtering. Middle figures: Frequency band chosen for filtering. Right figures: Envelope order spectrum of signal.
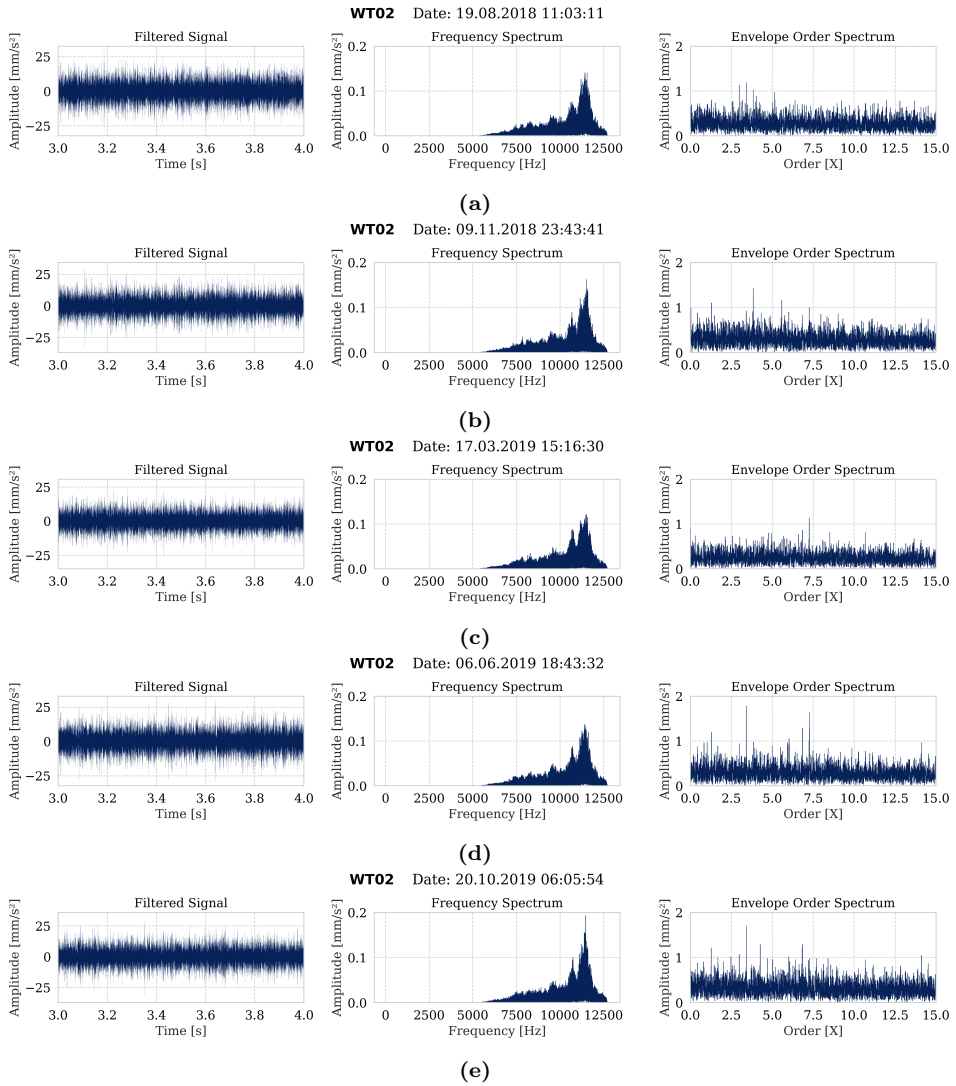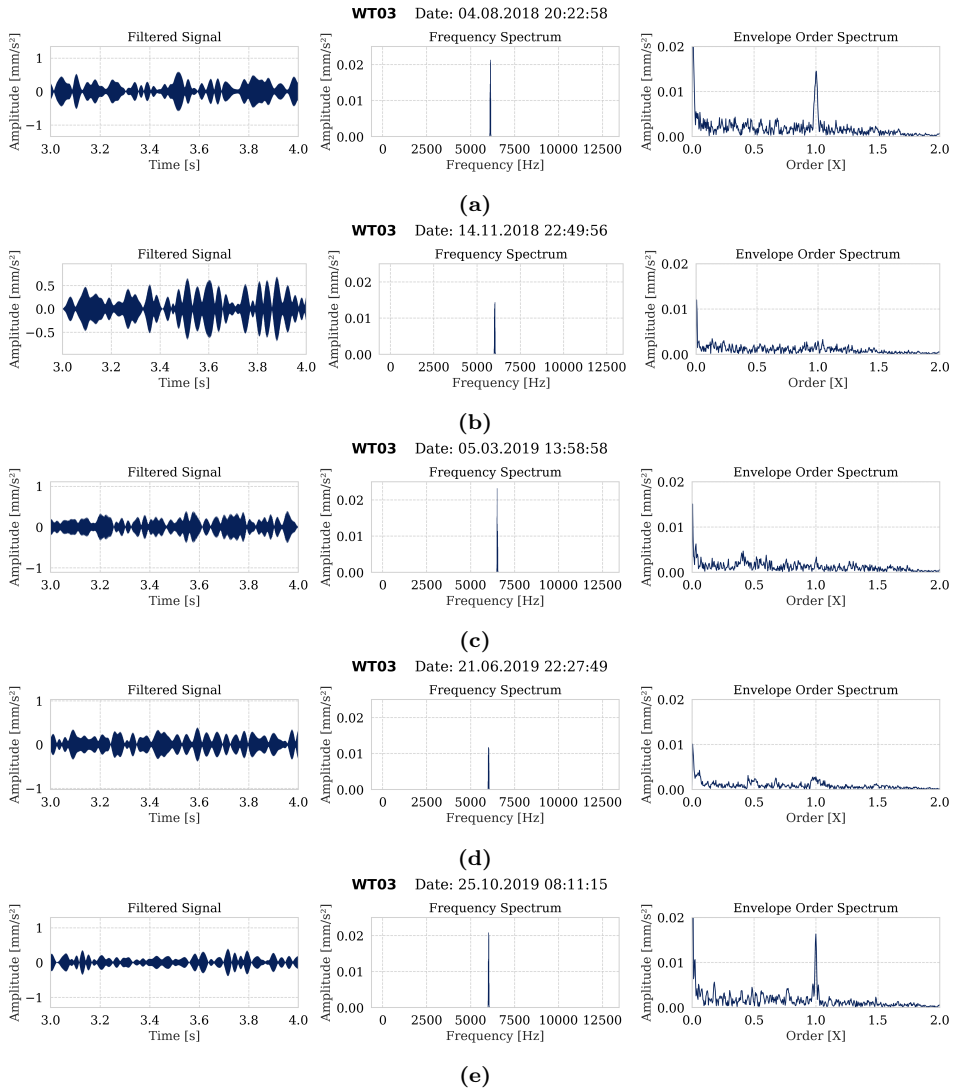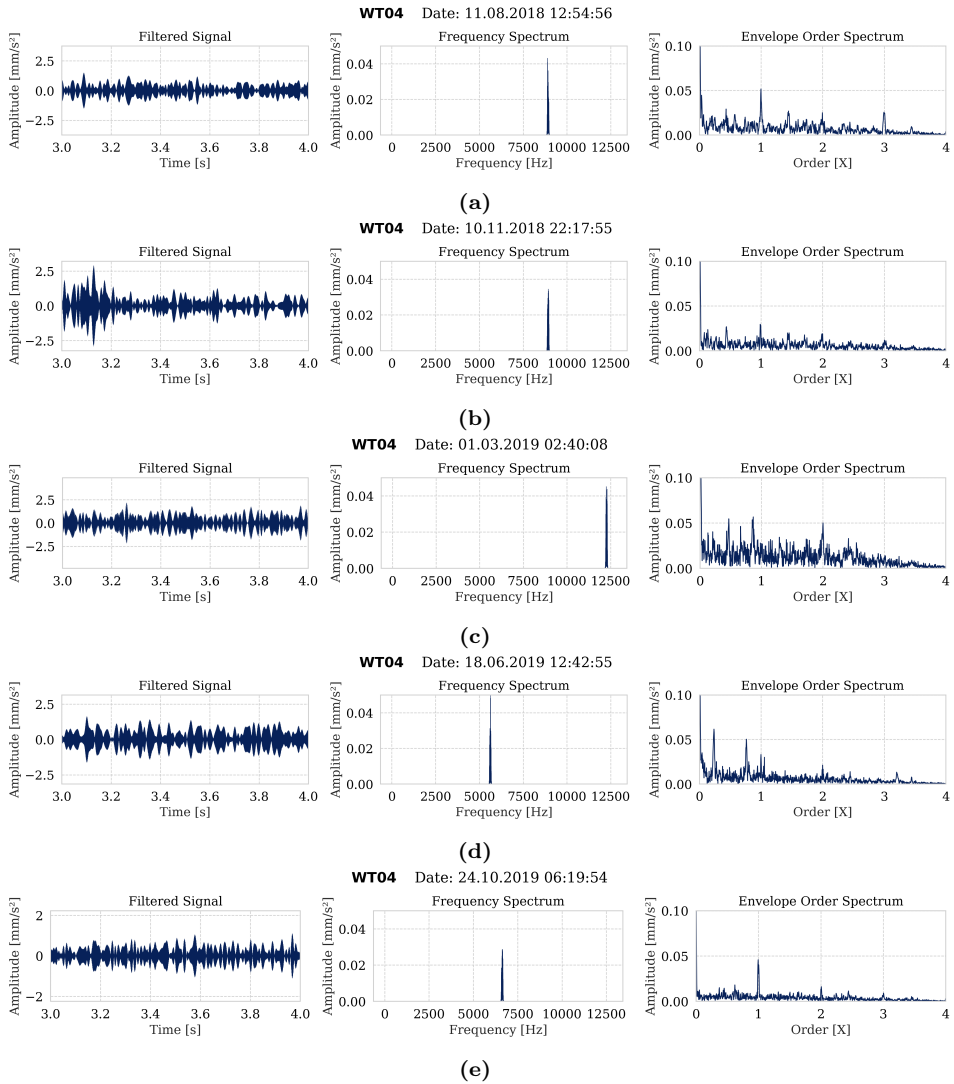
Figure 5.18: Envelope order spectrums of the five selected signals from WT02, band-pass filtered based on SK recommendations. Left figures: Signal after narrow-band filtering. Middle figures: Frequency band chosen for filtering. Right figures: Envelope order spectrum of signal.

Figure 5.19: Envelope order spectrums of the five selected signals from WT03, band-pass filtered based on SK recommendations. Left figures: Signal after narrow-band filtering. Middle figures: Frequency band chosen for filtering. Right figures: Envelope order spectrum of signal.

Figure 5.20: Envelope order spectrums of the five selected signals from WT04, band-pass filtered based on SK recommendations. Left figures: Signal after narrow-band filtering. Middle figures: Frequency band chosen for filtering. Right figures: Envelope order spectrum of signal.

Manually Selected Frequency Bands

The results from the manually selected frequency bands presented in Table 4.5 in Section 4.2.4 are found in this section.

Narrow-Band Filter with Bandwidth 6400 Hz
Figure 5.21 and 5.22 were produced using a band-pass filter with central frequency 9600 Hz and bandwidth 6400 Hz. The results strongly resembled those obtained by a high-pass filter (5.1.4) and similar observations could be made.

Narrow-Band Filter with Bandwidth 50 Hz
Figure 5.23 and 5.24 were produced by the 50 Hz, narrow-band filter. The centre frequency were different for each WT, thus the spectrums were not comparable across WTs. Note that the spectrum from WT04 is scaled differently than the others to show its higher amplitudes.

Regarding WT01, the spectral line at order 0.43 was present in three of the spectrums. Still, it was unknown which component this order corresponded to. The spectrums were chaotic and spectral lines in one spectrum was not necessarily found in the next. Overall, it was difficult to say if any fault development had occurred, since every spectrum was slightly different.

WT02 showed no obvious sign of fault development. The spectrums were chaotic with the most distinguishable spectral lines appearing in low orders (less than 0.1) and at 2.

Spectrums from WT03 were less chaotic than WT02. The spectral lines at 1 and sometimes at lower orders (around 0.004) were clear. However, no clear fault development could be observed through the time period.

Spectrums from WT04 had much higher vibration amplitudes. The spectral lines at 1, 2 and at lower orders (around 0.004) were clear. Other spectral lines appeared inconsistently. Thus, no fault development could be observed through the time period.

Narrow-Band Filter with Bandwidth of 800 Hz and 1500 Hz
Figure 5.25 shows envelope order spectrums filtered with centre frequency 4500 Hz and 8200 Hz, and bandwidth 1500 Hz and 800 Hz of WT03 and WT04 respectively. Note that only WT03 and WT04 were selected in this section due to their interesting spectrums. The spectrums from both WT03 and WT04 strongly resembled those obtained using highpass filter (Figure 5.12). However, the spectrums in Figure 5.25 displayed much clearer spectral lines. This indicates that CFs were better separated from noise.

In regards to WT03's spectrum, sharp spectral lines at order 1 and 2 were evident. In addition, an interesting pattern was revealed. What seems to be harmonics

with sidebands occurring between order 10 and 14, between 21 and 26 and again between 34 and 36. This was impossible to know for certain without knowing the CF. Even though the amplitudes varied, neither the number of sidebands nor the general level of vibration increased during the time period, making it unlikely that fault development had taken place.

In WT04's spectrums, clear spectral lines were visible along the whole order spectrum form 0 to 30. These were repeated almost every order. In some areas, spectral lines appeared every half order. Again, it was impossible to know which components they originated from. Regardless, it was an interesting pattern, unique for this turbine. Concerning fault development, the amplitudes in WT04 showed no increase over time. Still, it was difficult to determine whether the components' condition had a fault development during the time period, or if it was due to natural variation.
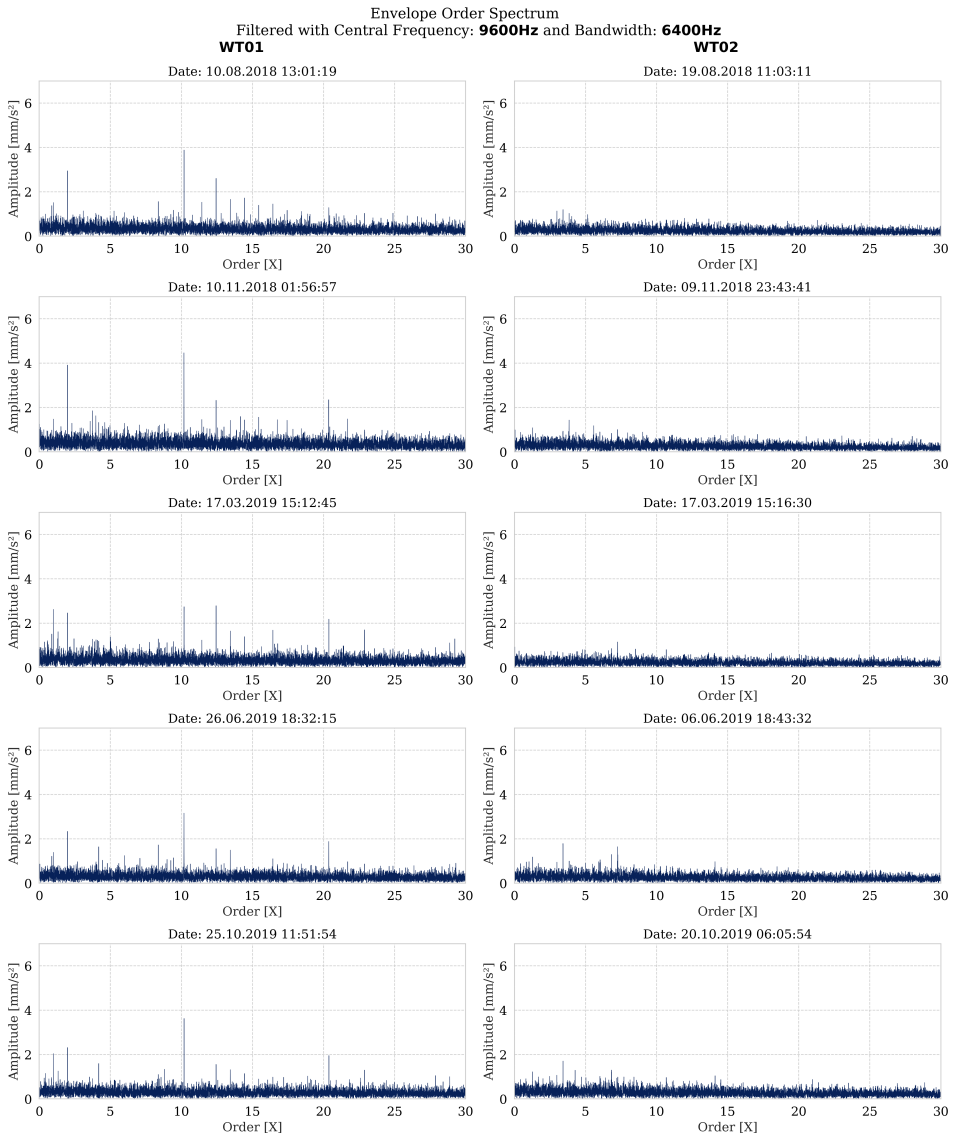
Figure 5.21: Envelope Order Spectrum of the five selected signals from WT01 and WT02.
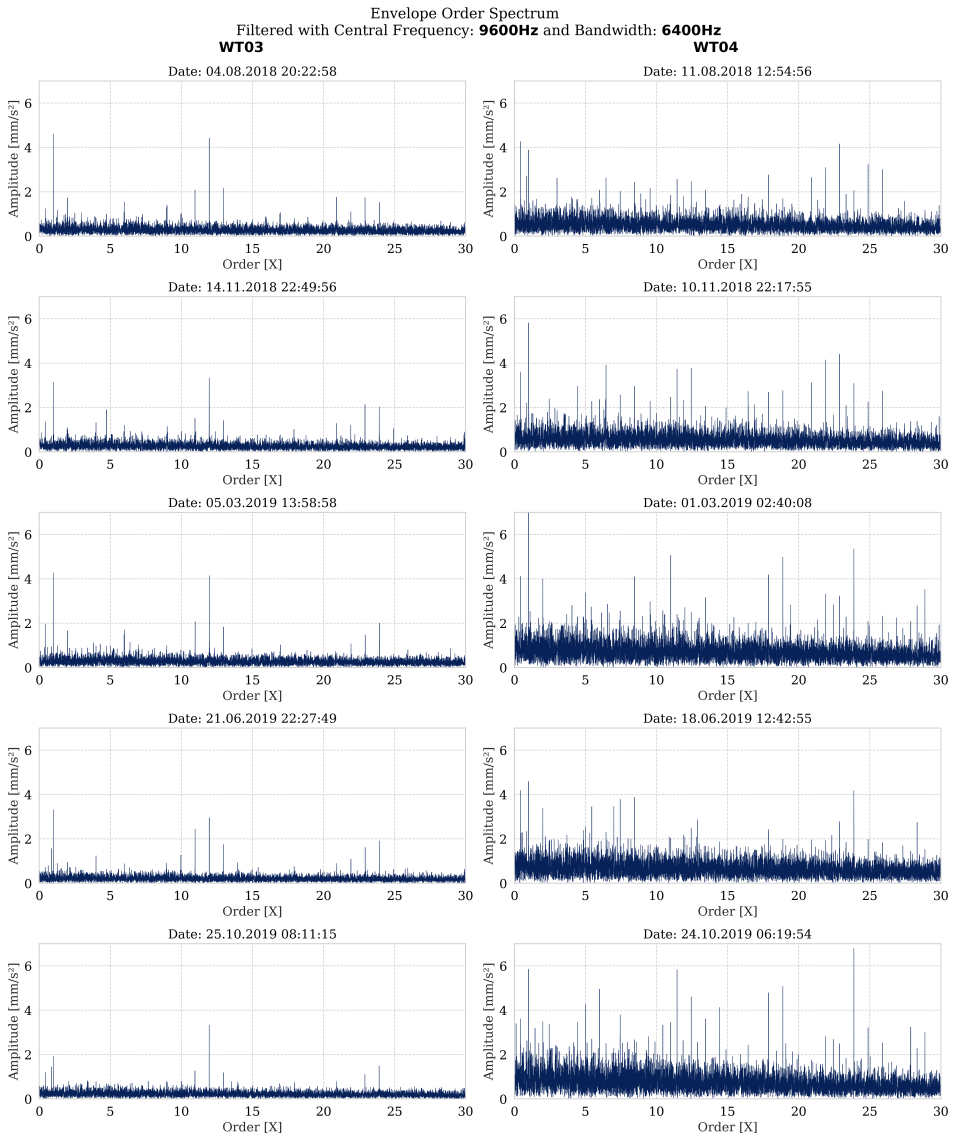
Figure 5.22: Envelope Order Spectrum of the five selected signals from WT03 and WT04.
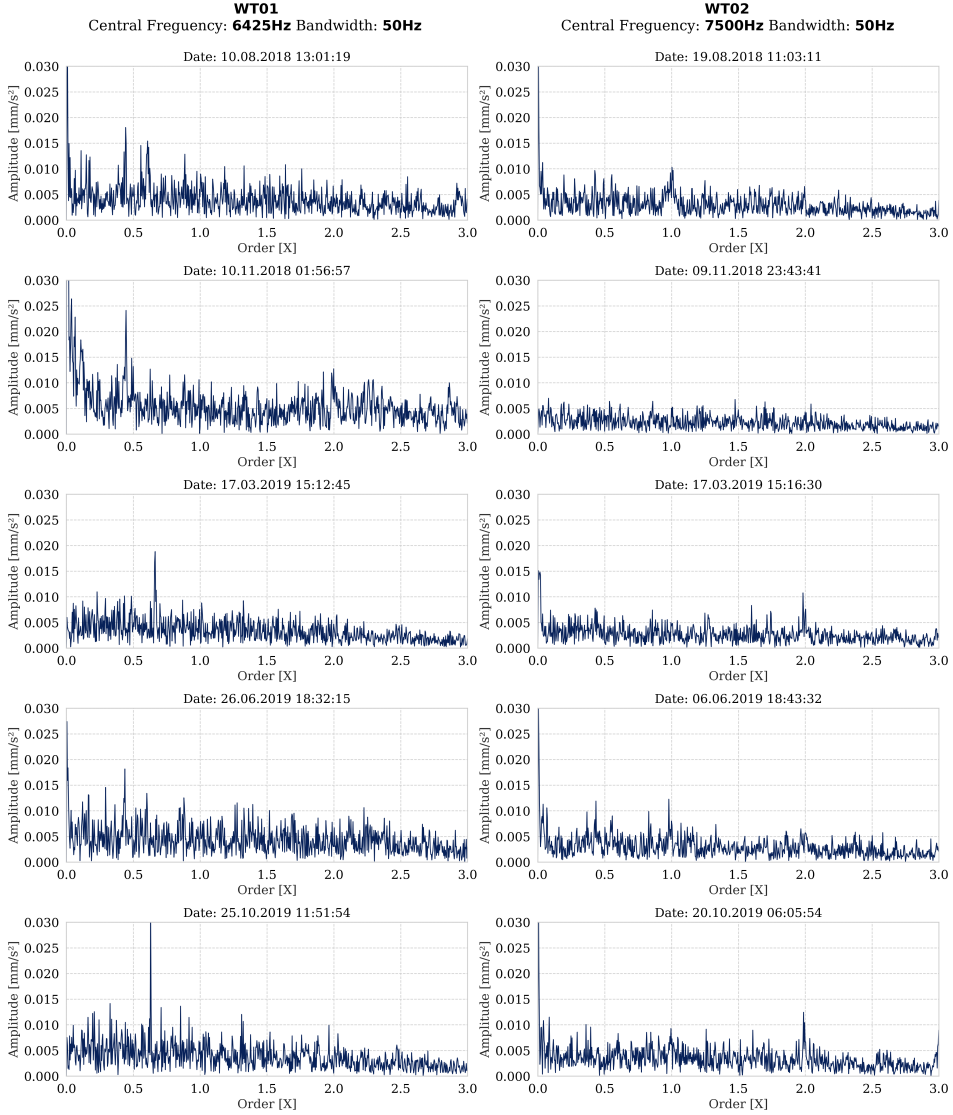
Figure 5.23: Envelope Order Spectrum of the five selected signals from WT01 and WT02.
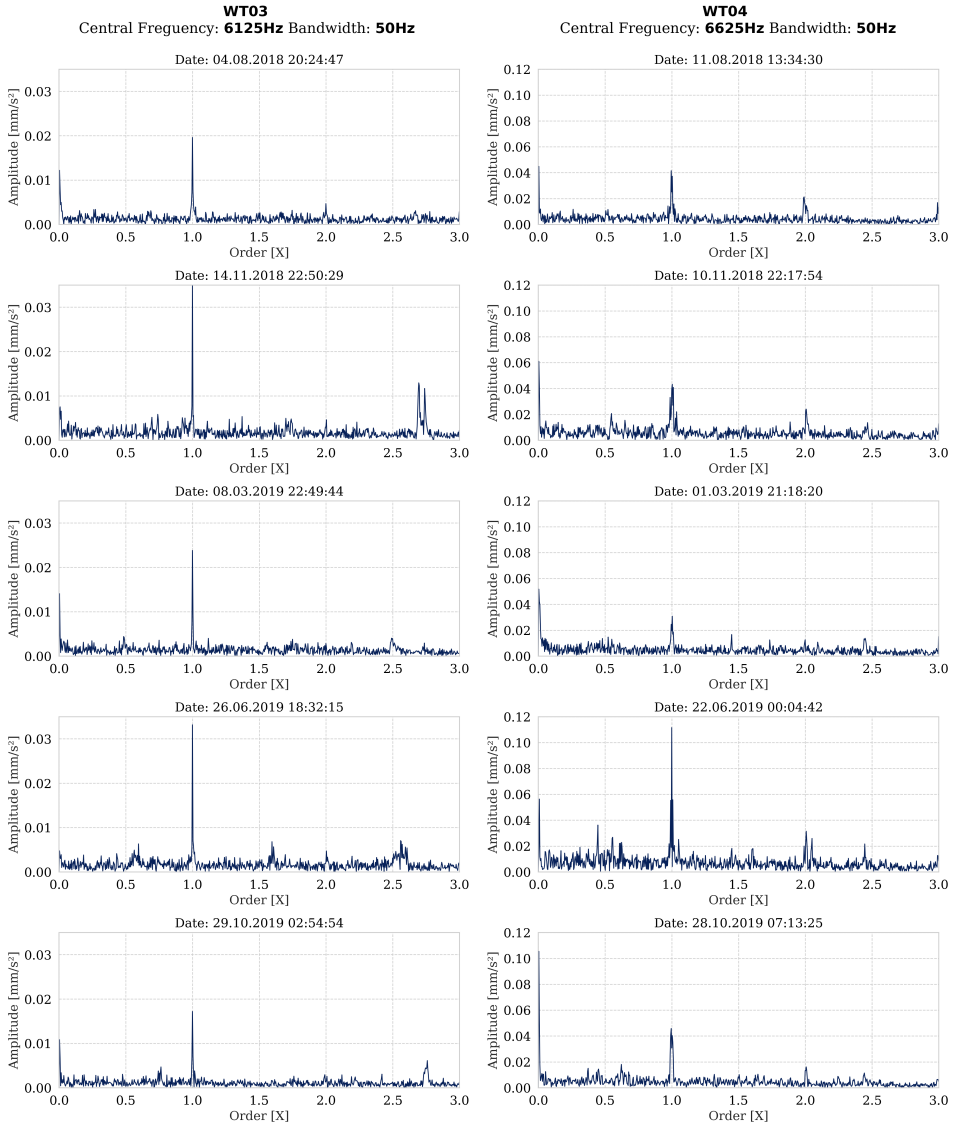
Figure 5.24: Envelope Order Spectrum of the five selected signals from WT03 and WT04.
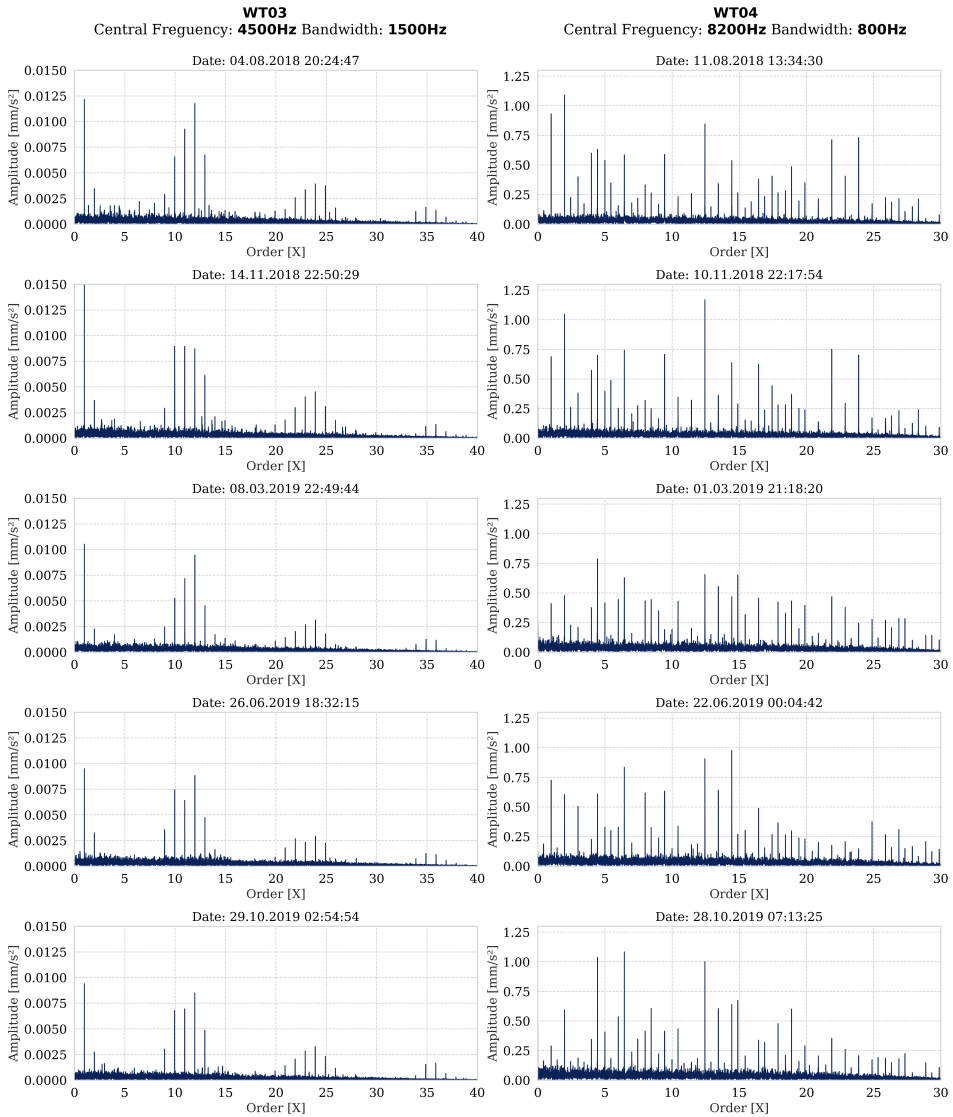
Figure 5.25: Envelope Order Spectrum of the five selected signals from WT03 and WT04.

5.2 PART 2: Fault Development Analysis Using Clustering

This section first presents the results from an initial exploratory study of the operational features in Section 5.2.1. Second, outlier handling and exploration of the extracted feature data sets is presented in Section 5.2.2. Third, the results from K-means clustering is presented in Section 5.2.6.

It is important to bear in mind that the clustering approach will always attempt to group the data, even though no patterns are present.

5.2.1 Exploration of Operational Features

WindSpeed, AvgPower and AvgSpeed are grouped by month of recording and visualised for WT01 in Figure 5.26. The features are grouped by month, and the colours resemble the seasons for easy interpretation. The figures indicated no particular seasonal trends. For instance, the wind speeds do not seem to increase around the winter months. As a consequence, K-means might not be affected by any variations in the operational features due to seasonality. The seasonal trends may not be visible because the signals were filtered, thereby ensuring similar operational conditions. WT02-4 showed similar results, and their plots are placed in Appendix B.2.
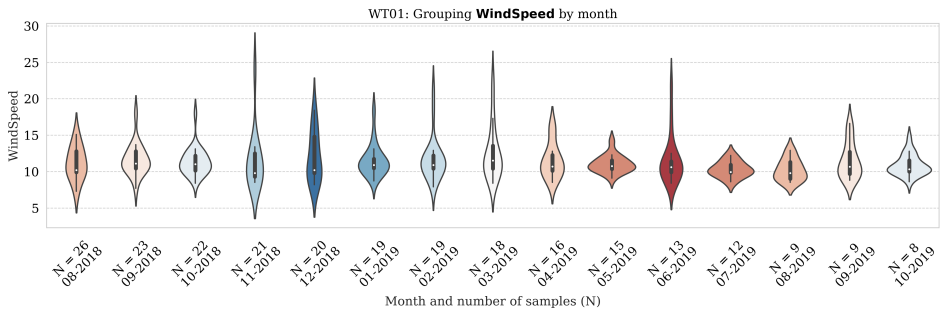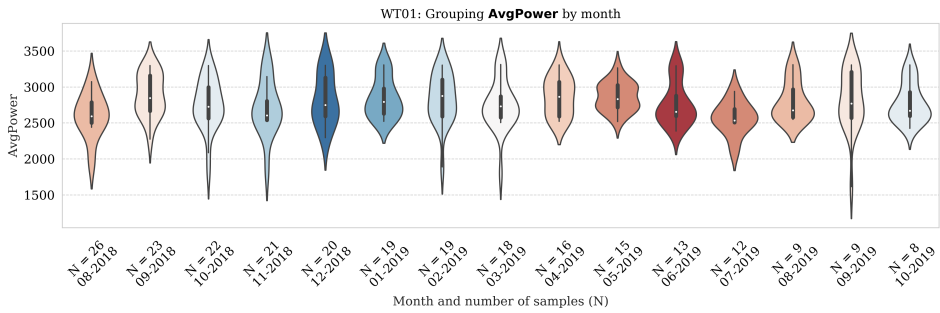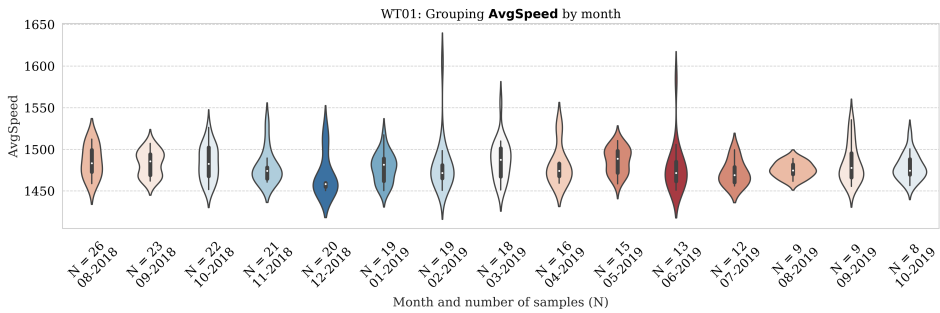
Figure 5.26: WT1: Wind speed, Average Power produced and Average Shaft speed (High Speed shaft) grouped by month. No seasonal trend is visible.

5.2.2   WT01: Outlier Handling and Exploration

Outlier Handling

The box-plot of the extracted features for WT01 in Appendix B.28, shows that there exists some outliers in the EEMD-features, namely the imf-rate and imf-kurtosis features. These values suggested that the EEMD implementation was unable to decompose some signals correctly. Therefore, the intervals with index

127, 158, 243, and 336 were removed altogether from the data set. Note that these indexes are in relation to the original index, where index 0 is the first recorded signal (04.08.2018) and index 409 being the most recently recorded signal (27.10.2019). The box-plot also reveals that there exist one interval with negative average wind speed recorded. This sample was removed from WT01 feature data set.

Data set Exploration

The distribution of samples after selecting signals with shaft speed above 1450 rpm (Section 4.3.1) is seen in Figure 5.27. The distribution is approximately even across the timeline.
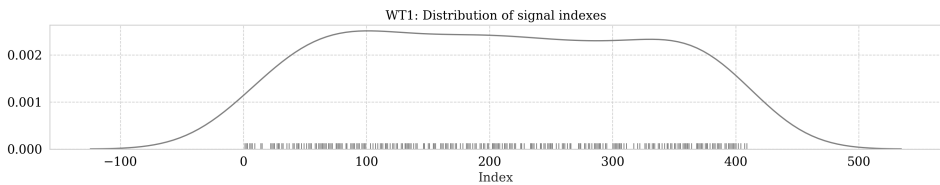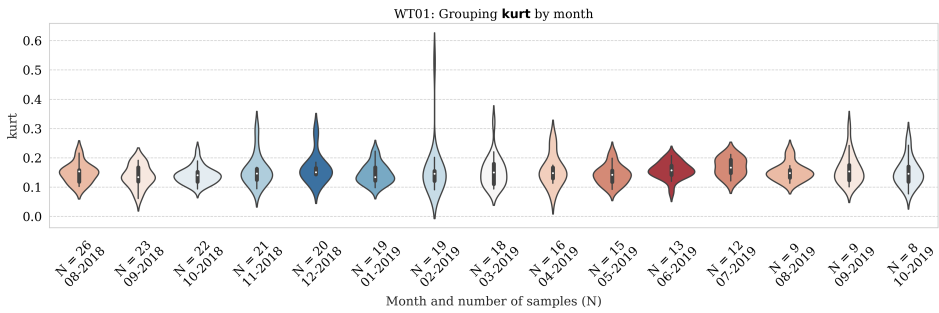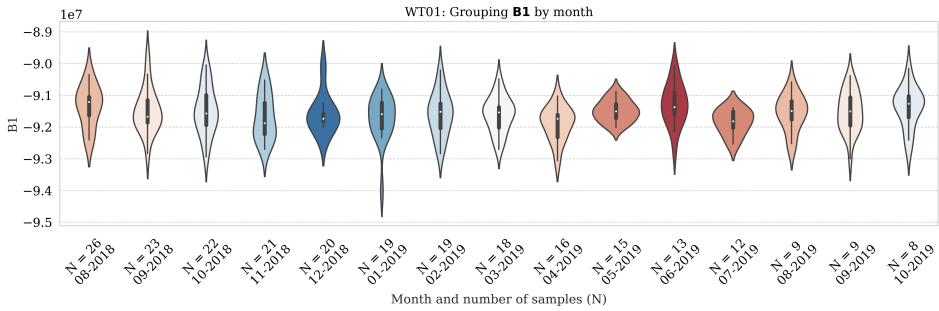

Figure 5.27: WT01: Distribution of the signals represented in the complete extracted feature data set.
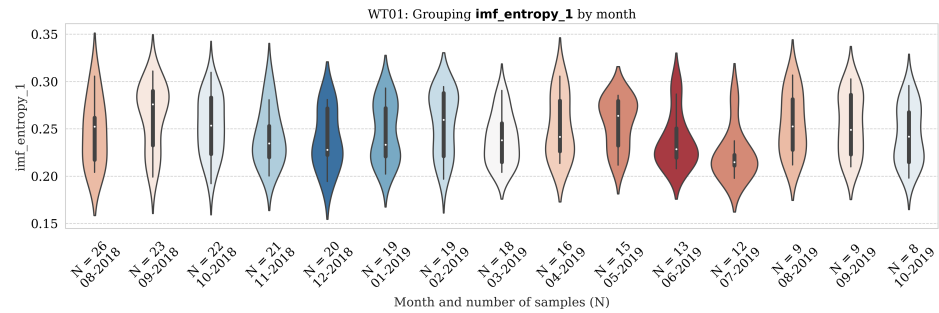
The violin plots for features kurtosis, B1 and imf_entropy_1 grouped over time are shown in Figure 5.28. The plots show no indication of deterioration over time. The other features were inspected as well, and provided no significant findings.

(a)

(b)

(c)

Figure 5.28: WT01: Kurtosis, B1 (1st bi-spectrum features) and imf_entropy_1 grouped by month.

Two-Feature Development Over Time

A collection of scatter plots is shown in the pairplot in Figure 5.29. No distinctive clusters were visible. Therefore, further clustering in n-dimensions was interesting.
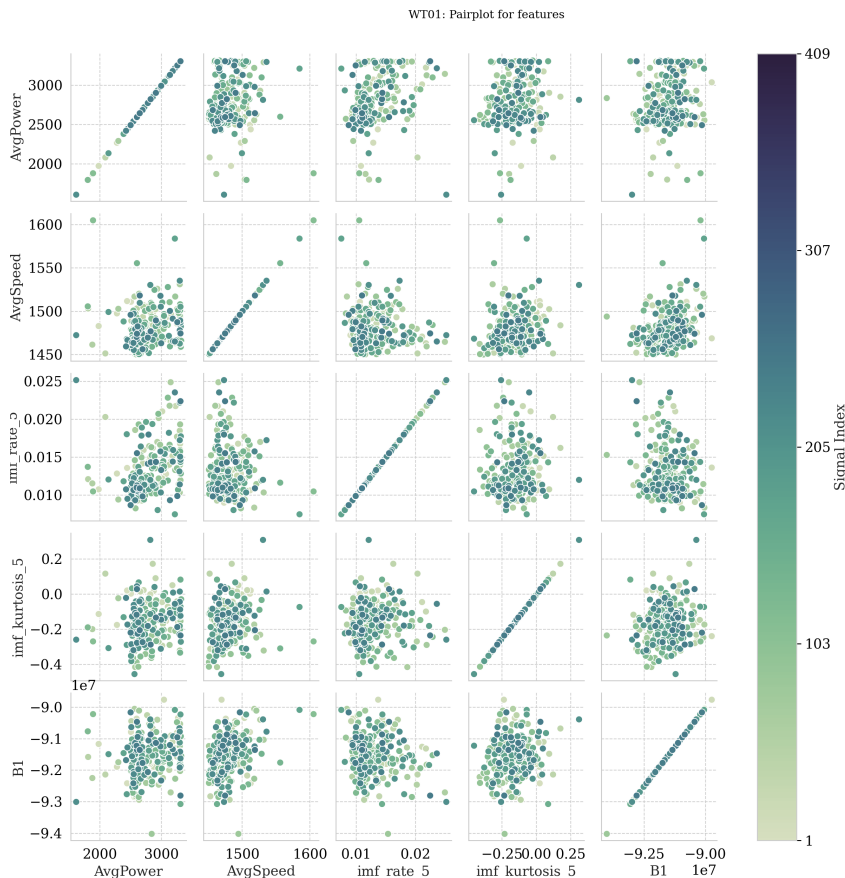
Figure 5.29: WT01: Pairplot of five selected features. Darker colour indicates later signal number.

5.2.3   WT02: Outlier Handling and Exploration

Outlier Handling

From inspection of the box-plot of the WT02 feature data set in Appendix B.4, samples with index 92, 169, 230 and 291 were removed. These signals had imf_kurtosis values larger than 500, which suggested an incomplete decomposition by EEMD.

Data set Exploration

Figure 5.30 shows the distribution of samples after selecting signals with shaft speed above 1450 rpm. The distribution is relatively even.
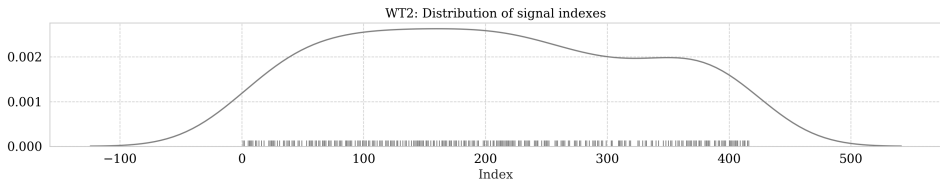
Figure 5.30: WT02: Distribution of the signals represented in the complete extracted feature data set.

Single Feature Development Over Time

The grouped violin plots for WT02 of features kurtosis, B1 and imf_entropy_1 show no conspicuous patterns indicating degradation. The remaining features were also inspected and showed similar patterns.
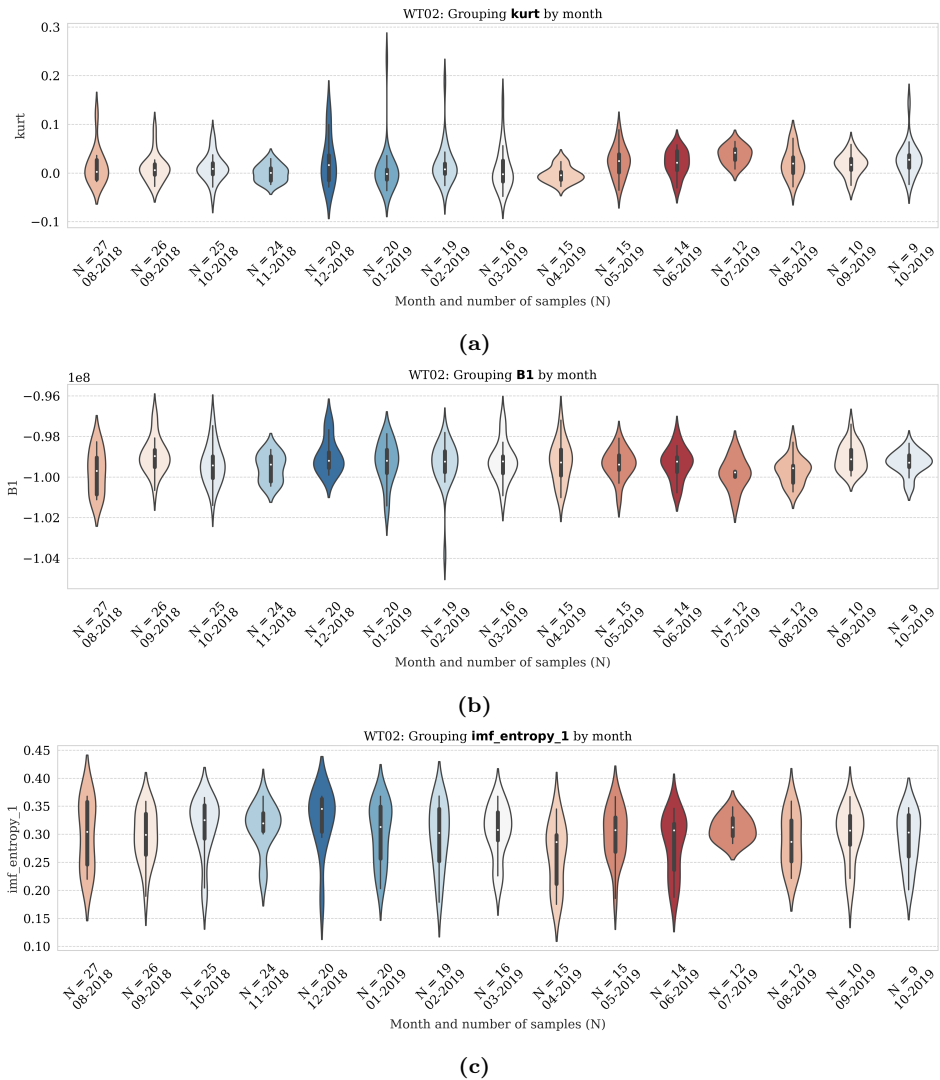
(a)

(b)

(c)

Figure 5.31: WT02: *kurtosis*, *B1* and *imf_ entropy_ 1* plotted. The colours represent the four seasons. Red is summer, blue is winter.

Two-Feature Development Over Time

A collection of scatter plots is shown in the pairplot in Figure 5.32. No apparent clustering are visible. Further analysis in n-dimensions was therefore relevant using *K*-means.
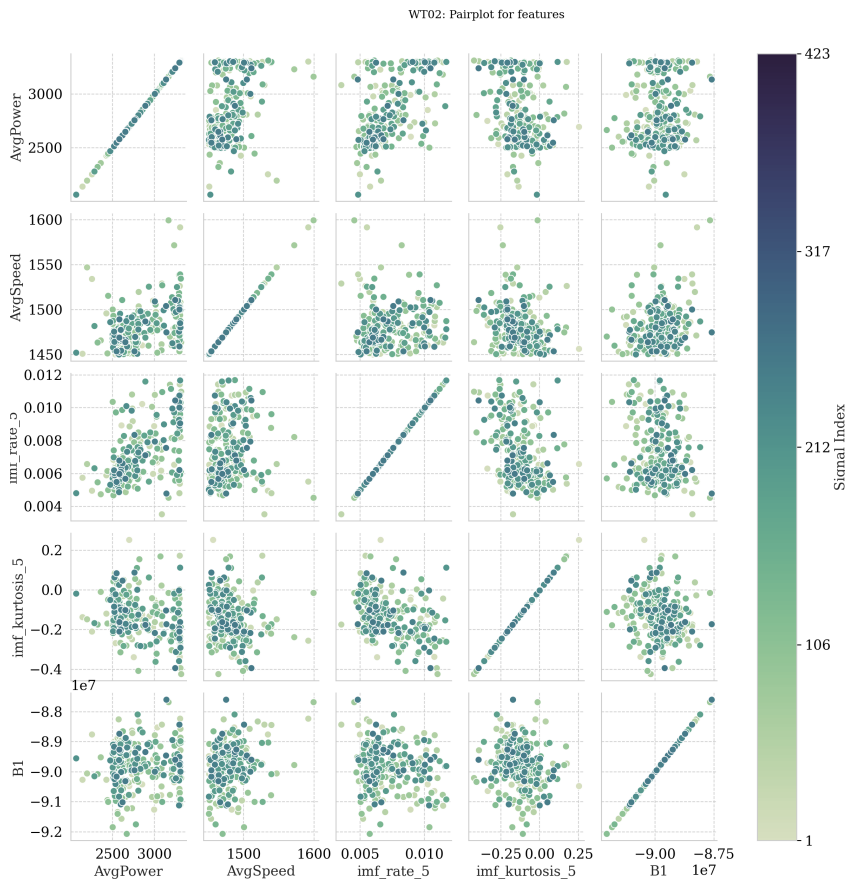
Figure 5.32: WT02: Pairplot of five features. Darker colour indicates later signal number.

5.2.4   WT03: Outlier Handling and Exploration

Outlier Handling

Outliers visible in the box-plot in Figure B.30 in the Appendix were removed from the data set for WT03. This was samples with index 39, 58, 141, 204, 210 and 269, which were removed by filtering the data set on feature imf_kurtosis_5 < 5. Additionally, the box-plot revealed two other outliers in the kurtosis feature. These samples, index 189 and 214, were therefore omitted from the data set.

Data set Exploration

The distribution of data samples for WT03 after selecting signals with average shaft speed above 1450 rpm is displayed in Figure 5.33. The distribution was even.
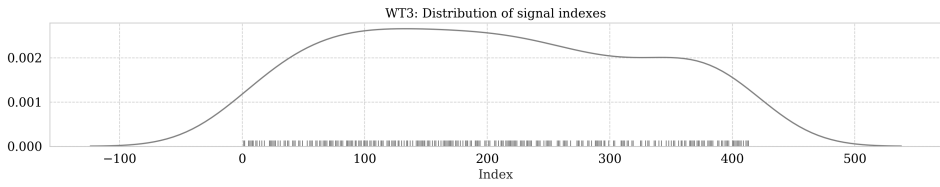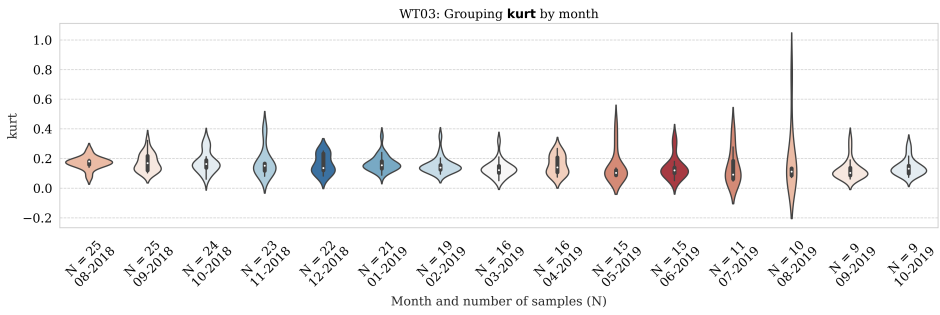
Figure 5.33: WT03: Distribution of the signals represented in the complete extracted feature data set.

Single Feature Development Over Time

The following three plots in Figure 5.34 show no significant change over time for either of the features kurtosis, B1 or imf_entropy_1. The rest of the features were also inspected over time, but did not change over time.

(a)
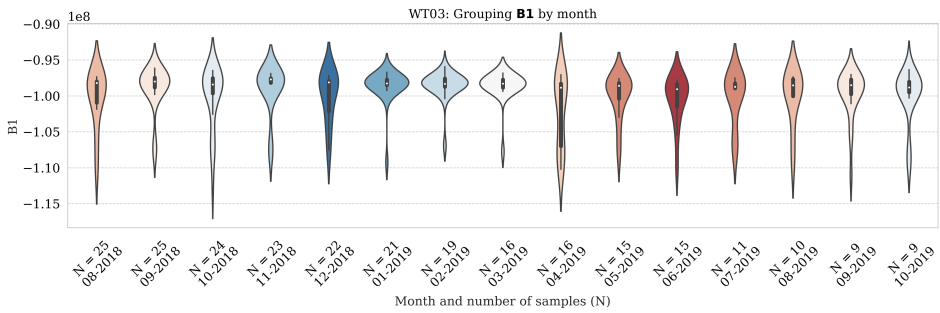
(b)

(c)

Figure 5.34: WT03: Kurtosis, B1 (1st bi-spectrum features) and imf_entropy_1 grouped by month.

Two-Feature Development Over Time

Figure 5.35 reveals no clustering trends of *later* samples. An extended analysis into n-dimensions using K-means was therefore relevant.
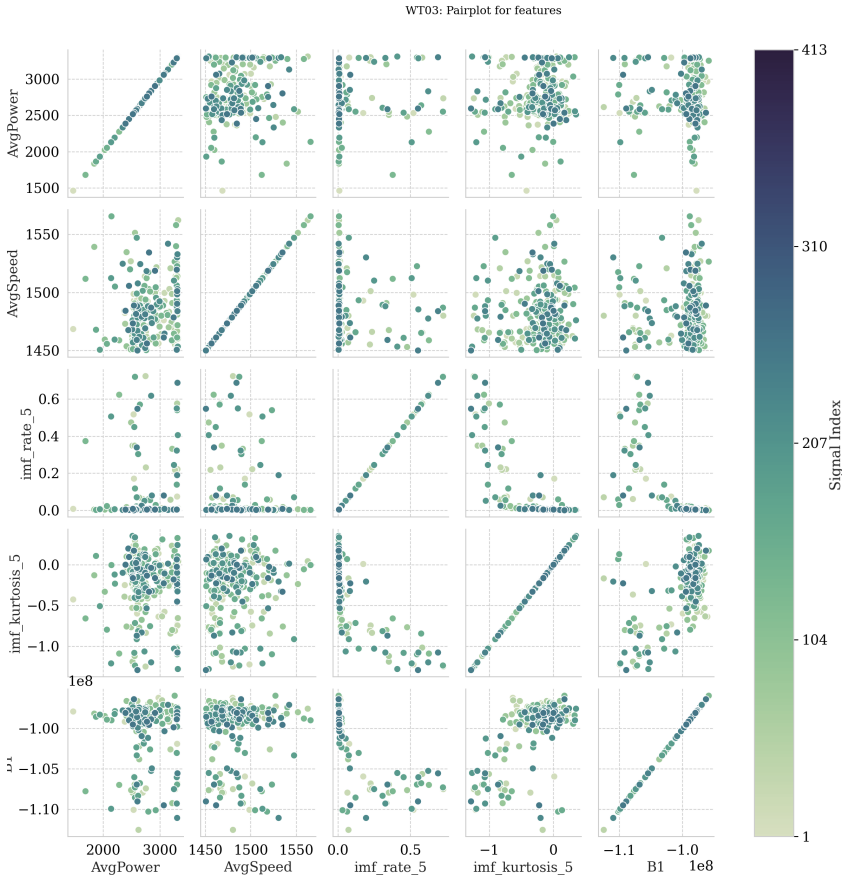
Figure 5.35: WT03: Pairplot of five selected features. Darker colour indicates later signal number.

5.2.5 WT04: Outlier Handling and Exploration

Outlier Handling

The box-plot for the extracted WT04 features can be seen in B.31. It shows that there exist a number of noisy data points for the imf_kurtosis variables. These values suggested that the signals were not decomposed properly using the EEMD method. Consequently, signal number 67, 85, 227, and 238 were removed from the data set.

The box plot showed that the WindSpeed feature also contained some measurements faults. Five samples (rows) where the wind speed was negative was removed altogether from the data set.

Data set Exploration

The distribution of samples after selecting signals with average shaft speed above 1450 rpm is shown in Figure 5.36. The distribution was approximately even.
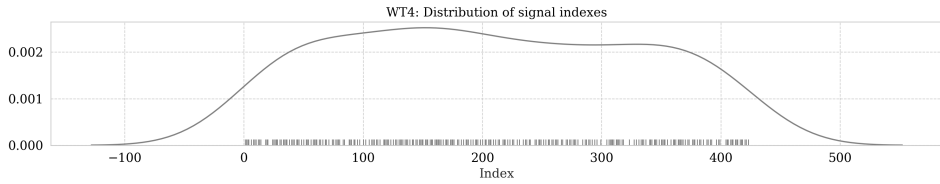

Figure 5.36: WT04: Distribution of the signals represented in the complete extracted feature data set.
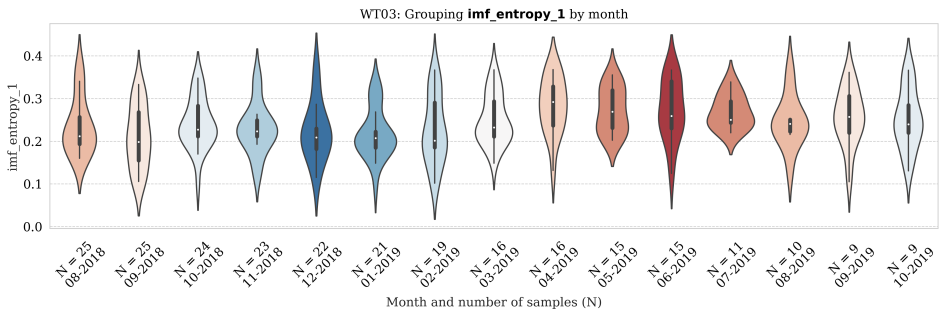
Single Feature Development Over Time

Some other features were plotted over time using violin plots in figure 5.37, grouped by month. However, the feature development over time yielded no patterns regarding degradation for WT04. This could have been because of the varying running conditions for the turbine. With clustering, these variations are taken into account through the operational features.

(a)

(b)

(c)
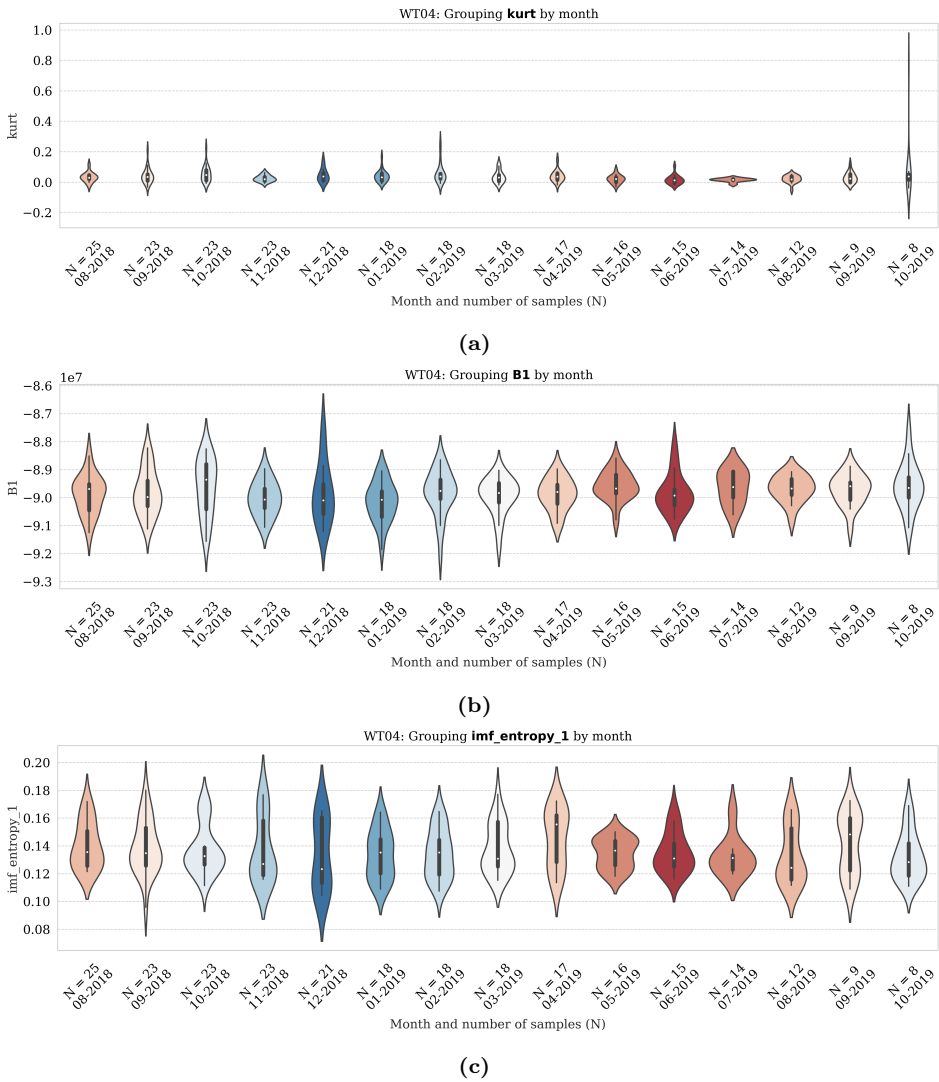
Figure 5.37: WT04: Kurtosis, B1 (1st bi-spectrum features) and imf_entropy_1 grouped by month.

Two-Feature Development Over Time

The features were also studied in two dimensions using scatter plots. Plotting the features in two dimensions shows that there are no apparent relations between later signals and fault characteristics, i.e. in Figure 5.38, no accumulations of later signals were visible. This suggested that it was relevant to extend the analysis to n-dimensions with K-means.
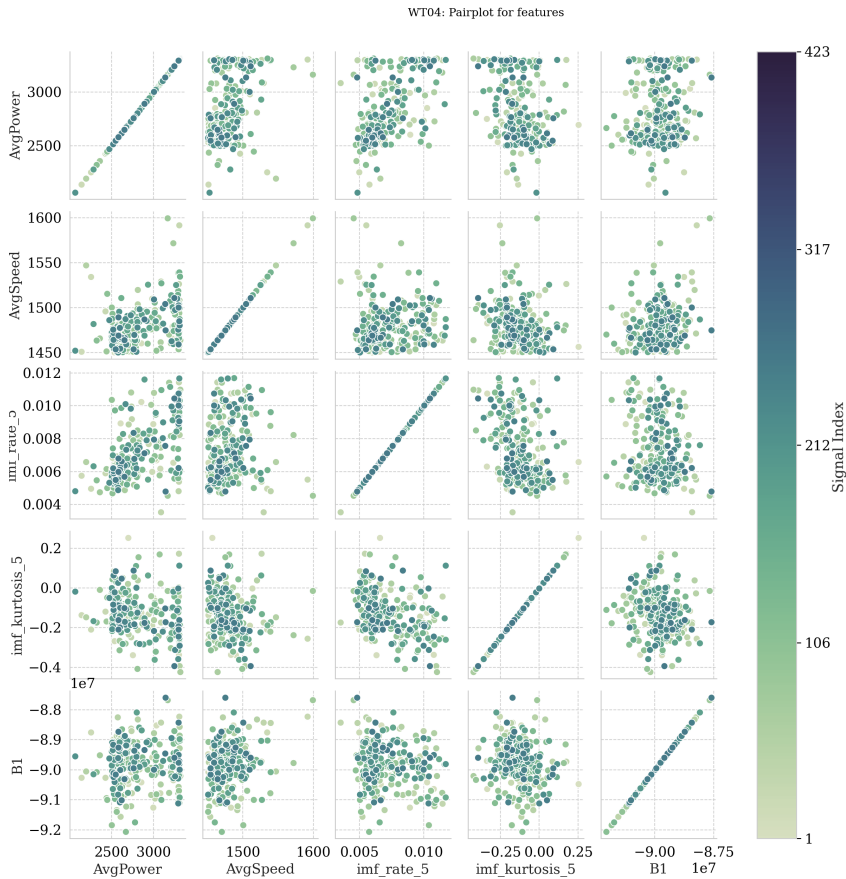
Figure 5.38: WT04: Pairplot of five selected features. Darker colour indicates later signal number.

5.2.6 Clustering Results

As stated in the Method, Section (4.3.5), K-means was run for every WT with different feature data sets:

1. Complete data set (36 features)

2. Operational and bi-spectrum features only

3. Operational and time features only

4. Operational and IMF energy features only

5. Operational and IMF kurtosis features only

6. Operational and mixed features

The results of the clustering process for each wind turbine for all subsets is presented in the following section.

WT01

The correlation plot for WT01 is shown in Figure B.24. The coefficients range from -1.0 to 0.2. The imf_rate_1 feature shows a strong anti-correlation between some of the other IMF-features. Clustering on all of the IMF features could therefore be redundant.

Table 5.1: WT01: Subsets and the selected selected K for the four other subsets of the features data set.

Subset	Selected K	Max percentage of samples above index 350 in cluster	Samples in max cluster
Complete Data set	17	37 %	27
Operational and bi-spectrum	17	26 %	23
Operational and time	12	36 %	11
Operational and IMF kurtosis	18	40 %	15
Operational and IMF energy	17	43 %	14
Mixed features	17	31 %	13

The results in Table 5.1 shows that the subset *Operational and IMF energy* best separates the signals recorded after index 350 (2019-08-30 07:01:59) from the rest of the signals. The distribution of the points in the max cluster is shown in Figure 5.39. In spite of the separation percentage being at 43 %, it is still too low to conclude that there is any fault development in WT01.

Figure 5.39: WT01: Which samples are assigned which cluster with **K=17** using the *Operational and IMF energy feature* subset. Cluster number 1 was most interesting based on the objective of separating the later samples (highlighted here).

WT02

The correlation plot for the extracted features from the WT02 vibration signals is placed in Figure B.25. It shows that there exists an anti-correlation of about -1 between the IMF rate and IMF entropy features.

Table 5.2: WT02: Subsets and the selected selected K for the four other subsets of the features data set.

Subset	Selected K	Max percentage of samples above index 350 in cluster	Samples in max cluster
Complete Data set	18	36 %	11
Operational and bi-spectrum	11	39 %	18
Operational and time	15	45 %	11
Operational and IMF kurtosis	14	36 %	14
Operational and IMF energy	18	50 %	10
Mixed features	7	37 %	27

The results in Table 5.2 show to which degree the *later* data samples in WT02 were separated from the rest using K-means clustering. *Operational and IMF kurtosis* separated the data best, with 50 % of the samples in one cluster coming from signals recorded after index 350 (2019-08-18). However, since there were 45 samples in the filtered data set recorded after index 350, and only 5 samples (50 % of the samples in the selected cluster highlighted) were detected, no implications of bearing and gearbox deterioration is present.

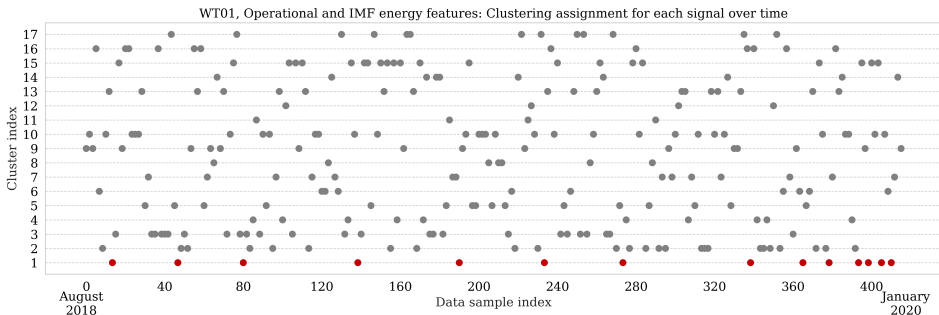Clustering the *Operational and IMF energy* subset with K=18 yielded the grouping of signals in Figure 5.40.

Figure 5.40: WT02: Which samples are assigned which cluster with **K=18** using the *Operational and IMF kurtosis* feature subset. Cluster number 18 was most interesting based on the objective of separating the later samples.

WT03

The correlation plot for the extracted features from WT03 ranges from -1.0 to 0.2, shown in Figure B.26. It shows a strong anti-correlation between margin_factor and the bi-spectrum features (B1-3), as well as the signal_energy and SD features.

Table 5.3: WT03: Feature subsets and the results using K-means.

Subset	Selected K	Max percentage of samples above index 350 in cluster	Samples in max cluster
Complete Data set	7	25 %	68
Operational and bi-spectrum	12	38 %	8
Operational and time	17	42 %	12
Operational and IMF kurtosis	18	42 %	12
Operational and IMF energy	10	38 %	26
Mixed features	13	40 %	15

Based on Table 5.3, running K-means on the subset *Operational and IMF kurtosis* best separated the signals recorded after index 350 (2019-08-28). The percentage of samples in the cluster maximising the objective of isolating the later signal features was 42 %. However, as seen in Table 5.3, this particular cluster only contained 12 signal indexes in total. Therefore, no indication of fault development is detectable.
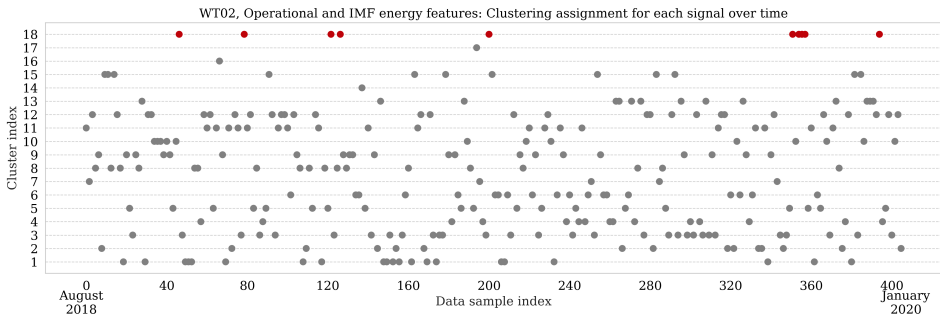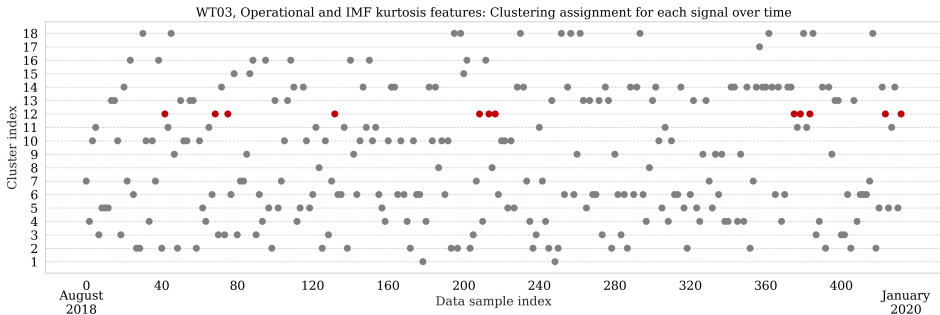

Figure 5.41: WT03: Which samples are assigned which cluster with **K=18** using the Operational and IMF kurtosis feature subset. Cluster number 12 was most interesting based on the objective of separating the later samples.

WT04

The correlation plot between the extracted features for WT04 is placed in Figure B.27. The correlation coefficients range from -1.0 to 0.2. The 10 energy-entropy and energy-rate features extracted using the EEMD method are strongly anti-correlated. Using them all when finding the clusters can be considered redundant. The correlation matrix does not indicate any other highly correlated features.

The results from clustering the data set extracted from WT04 vibration is shown in Table 5.4.

Table 5.4: WT04: Subsets and the selected selected K for the four other subsets of the features data set.

Subset	Selected K	Max percentage of samples above index 350 in cluster	Samples in max cluster
Complete Data set	14	41 %	27
Operational and bi-spectrum	14	32 %	19
Operational and time	8	26 %	54
Operational and IMF kurtosis	13	26 %	34
Operational and IMF energy	14	43 %	21
Mixed features	13	33 %	15

The results show features extracted from vibration signals recorded after index 350 (2019-08-15 20:10:25) are separated from the rest. Clustering the data in *Operational and IMF energy* yielded the best result. 43 % of the data points in cluster number 8 were from samples with index $>= 350$. However, with 57 % of the points coming from earlier signals, these result did not imply any fault degradation over time. The distribution of points with K=14 for the subset *Operational and IMF energy* is shown in Figure 5.42.

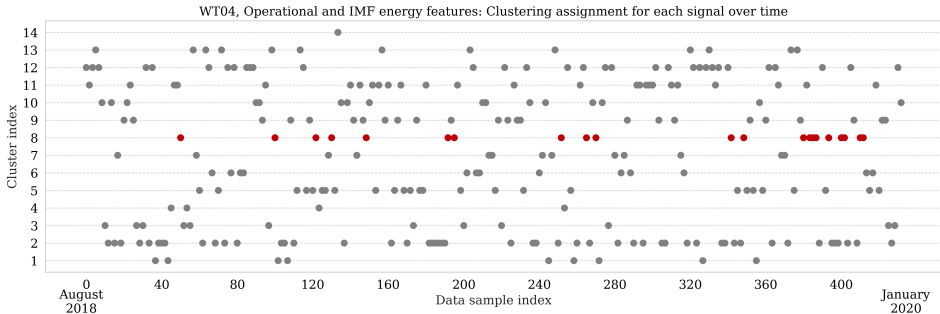

Figure 5.42: WT04: Which samples are assigned which cluster with **K=14** using the Operational and IMF energy feature subset. Cluster number 8 was most interesting based on the objective of separating the later samples.

Chapter 6

Discussion

This thesis demonstrated an exploratory analysis aimed to answer three research questions (RQ) concerning gear and bearing faults based *solely* on vibration and operational data. Similar studies rely on knowing the dimensions of the components to properly identify and track them. Additionally, knowledge of a component's state is often used to confirm that an indicated fault came from an actual fault. These two factors separates this thesis from other research, and answers the following research questions: (1) Is there any indication of faults present? (2) Is there any indication of fault development? (3) Is there a relation between a large number of start-stop cycles and the indication of faults?

This chapter discusses how the results from the TVA and clustering analysis answered the three research questions. Limitations and how they impacted the results is also presented.

6.1 Traditional Vibration Analysis

TVA was applied to explore all three research questions. There were two main findings; the fault detection results showed that the WT04 spectrums were different from the others, which could indicate an early fault. However, there were no signs of fault development during the time period for any of the WTs, including WT04. The results regarding each research question is discussed consecutively.

RQ1
For RQ1, it is important to bear in mind that the spectrums were compared across the different WTs to compensate for the lack of information regarding CFs. The presented discussion is based on the results showing that WT01 and WT04 most likely contained similar gearboxes. Similarly, WT02 and WT03 were assumed to have the same gearbox.

The results of the order analysis showed that WT02 and WT03 had similar order spectrums. However, with no healthy spectrum as reference it was difficult to determine the gears' health for WT02 and WT03. This is further discussed in Section 6.1.1. The order analysis indicated that WT04 had greater amplitudes in the higher order range compared to WT01. Additionally, WT04 demonstrated notably more sidebands than WT01, indicating that WT04 might be in a deteriorated condition.

Results of the EOA showed comparably greater vibration amplitudes for WT04. The EOA results also showed that spectral lines appeared in WT01's and WT03's spectrums. Spectral lines from an EOA could be an indication of early REB faults. No significant spectral lines was detected in WT02 which suggests non-faulty REB.

The kurtograms from the five WT04 signals indicated that some kurtosis values were around 1.5. This may indicate an early fault, as described in Section 3.1. No notable kurtosis values were detected in the other three WTs.

RQ2
In regards to RQ2, the results from the order analysis and EOA showed no signs of fault development during the time period for any of the WTs. No new spectral lines or sidebands consistently reoccurred over time or increased in magnitude. Based on these results, there are two possible scenarios; (i) there is no fault development in the gearbox or HSS bearings, or (ii) there exist some development, but the TVA methods were unable to detect it.

If scenario (i) is true the results suggested that WT04 could either contain an early stage fault which is *unchanging*, or not contain any faults altogether. However, the former is more probable, reflecting the findings above. However, if scenario (ii) is true, this suggests that the TVA methods are incapable of detecting change over time. As pointed out by Ben Ali et al. (2018), fault detection for TVA methods depend on the experience of the vibration analysts. An expert might have been able to detect fault development in the spectrums in Section 5.1.3.

RQ3
Regarding RQ3, the results indicated that there could indeed be a relationship between frequent start-stop cycles and degradation. WT04 had the highest start-stop cycles while WT02, showing no signs of degradation, had the least.

6.1.1 Limitations

Fault development could have been more evident in other signals, since only five were chosen for manual inspection. Selecting the optimal five signals is a challenging task, as shown by the variation in the frequency median plots (for example Figure 5.10). Additionally, deterioration in early stage faults could develop slowly and therefore be unnoticed by TVA.

The TVA methods answer the proposed research questions, but there is significant uncertainty related to the conclusiveness of the results. Although spikes in the spectrums were clearly visible, only the CFs of the parallel gear could be identified. Therefore, the TVA shows that it is highly beneficial to know the dimensions of the relevant components in order to compute and track CFs.

As mentioned, WT01 was compared to WT04, and WT02 to WT03. If all four turbines were equipped with exactly the same set of components, the analysis proposed would have been easier to carry out, even without component dimensions. If they had been the same, and a healthy reference had been obtained as well, the results would have been easier to interpret.

6.2   Fault Development Analysis Using Clustering

The clustering approach is only capable of detecting change, hence, only RQ2 is answered through this approach. As seen in the results, no sign of mechanical fault development for either of the four WTs was visible. These results indicate two possible scenarios; (i) there are no fault development patterns present in the vibration signals, or (ii) there exist degradation patterns, but the proposed clustering approach was unable to detect it.

If scenario (i) is true, the clustering approach would obviously not detect similarities between later points related to any fault degradation. In this scenario, there could either exists a fault which is not developing over time or there could exist no fault at all.

If scenario (ii) is true, fault development is present in the signals, but the extracted features and clustering failed to detect it. If the faults are at an early stage, it is possible that the degradation process is so slow that changes in the later signals are undetectable by the selected features. Another alternative is that K-means is unable to detect any faults because of the sensitive nature of the method (Section 2.7.2). K-means is, as mentioned in Section 4.3, highly reliant on the input features. Thus, a poor feature choice or feature combination could prevent the detection of interesting fault developments.

Since no fault detecting was apparent, due to the poor "separation" of later sampled signals, no further cluster analysis was applied. There was no reason to look into *why* certain samples had been grouped together.

6.2.1   Limitations

The "no free lunch" theorem states that there is no universally best model to every ML problem (Wolpert, 1996). A limiting factor of this clustering approach is therefore that other clustering methods should also have been explored to strengthen the analysis and potentially detect fault development. There exist a range of clustering

techniques, some of which are presented in future work, Section 6.4.

Jain and Dubes (1988) presented nine challenges associated with clustering (Appendix A.2). Here, a selection of the challenges will be discussed in relation to the results:

1. *What features should be used when clustering?*

   Selecting the optimal features for detecting fault development is an important but challenging task. When clustering data in more than three dimensions, humans cannot inspect and verify any clustering tendencies. Therefore, one should be critical towards every included feature. The relevance of some of the extracted features could be questionable. For instance, *wind speed* is not as relevant for capturing the different running conditions as for example average power, which captures the load of the HSS. The information provided by wind speed could therefore be redundant and contaminate the clusters. In such circumstances, expert knowledge could be of use (Jain, 2010).

2. *Should the data be normalised?* Since the features in this proposed approach are normalised, they are equally important through the "eyes" of K-means. However, it is debatable whether the wind speed feature is as important as for example the bi-spectrum features.

3. *Are there any outliers (extreme values) in the data?* Outliers in the data set were removed manually through an inspection of the feature distributions. However, it can be hard to determine the filtering threshold for outliers. Here, statistical approaches can be used more actively to remove samples. Other approaches include interpolating values suspected to be outliers, instead of removing the whole data points altogether.

4. *Are the discovered clusters valid?* Jain and Dubes (1988) state that the validity of clusters can be challenging to asses. The measure used in this approach was an external criteria; the percentage of samples originating from signal index 350 or later. This is an objective measurement evaluating whether the proposed approach answered RQ2. It is important to have a measure, since clustering methods will group the data even if there are no interesting patterns.

It is difficult to know if the method *actually* pickedup fault development. An interesting approach could have been to assess it using simulated data. This is discussed in Recommendations and Future Work, Section 6.4.

6.3   Traditional Vibration Analysis vs. Data-Driven Approach

As discussed, the TVA method encapsulates all three RQs. Spectral lines can be tracked closely to determine faults and deterioration over time. Only RQ2 is discussed using the clustering approach. This is because the clustering approach is

only capable of detecting change.

The TVA results are interpretable to human vibration analysts, making them trustworthy in decision making processes. This is useful when planning maintenance, and is one of the reasons why they are implemented in commercial online CM systems (Barszcz and Randall, 2009). The clustering results, on the other hand, are less interpretable to humans, especially with multi-dimensional data. This make them less suitable in situations where the consequence of a poor decision is dreadful or costly, for example when deciding whether a gearbox is faulty or if maintenance is needed.

The TVA results require manual inspection, and may be less suited for detecting fault degradation over time. K-means, however, is capable of finding complex patterns in hundreds of vibration signals under various running conditions. This makes clustering more applicable in automated degradation analysis than TVA.

Clustering requires no a priori knowledge of vibration signals. Contrarily, the results show that TVA is highly dependant on prior knowledge, such as component dimensions.

6.4 Recommendations and Future Work

This section presents future work related to the TVA methods, clustering approach, and other sensor data.

6.4.1 Traditional Vibration Analysis

Potential for EEMD to Isolate REB Signal

Extracting the OBF to use with EOA is the main challenge in regards to this method. An alternative approach to SK using EEMD to isolate the faulty bearing signal was proposed by Zhao et al. (2014). They found that EEMD outperformed other methods when used on complex vibration signals from multiple components. EEMD was more resilient to noise and was better at separating the faulty vibration signals. It would be interesting to investigate if this method would yield different results.

6.4.2 Clustering Approach

The K-means clustering method could have been validated on similar or simulated data sets with known fault development. It would be wise to test the method prior to running it on real world data. This would increase the viability of the method.

Some of the features extracted in the clustering approach could also have been studied further. The bi-spectrum and EEMD contain interesting information regarding the state of various WT components. A bi-spectrum analysis could have

been used in isolation to look for fault indications, in research question 1 (Saidi et al., 2015; Wang et al., 2018). EEMD could have been combined with further signal analysis to detect and diagnose machinery (Saidi et al., 2014). However, both of these methods would require known dimensions in order to locate faults.

Various improvements could have been implemented in the clustering procedure. Firstly, other clustering approaches could have been applied to strengthen the research. Secondly, different subsets of features could have been mixed. Outliers could have been handled using statistics, instead of completely removing the sample.

Jain and Dubes (1988) stated that a challenge related to clustering is knowning which clustering method to use. K-means assigns a cluster to every data sample, and is therefore sensitive to noisy data samples (Section 2.7.2). Density-based clustering approaches such as DBSCAN omits samples in low-density regions and classifies them as noise (Frigui, 2008). It is therefore not as sensitive to noise as K-means. DBSCAN could be an interesting clustering method to apply to the feature data in this thesis.

6.5 Other Data-Driven Methods

Autoencoders is a type of neural network used to detect anomalies in data (Alla and Adari, 2019). Autoencoders takes a feature data set as input, and attempts to reconstruct the input in the output. If a new measurement, e.g. vibration measurement from a CM system, is recorded, it can be run through the already trained autoencoder. The method then returns a *reconstruction* error, stating how well the input data was reconstructed. A high error indicates anomalies, which can be used to indicate fault development. This method works well with high volumes of data and more than five features (Alla and Adari, 2019).

6.6 Other Sensor Data

Vibration measured in the GbxHssRr sensor was studied in this thesis because of the failure rates of gearbox components and HSS bearings. However, faults could have appeared in other places and other sensor measurements, e.g. GbxHssFr, could have been interesting to explore. Additionally, oil analysis could have been studied to gain a further understanding of the WTs' states.

Chapter 7

Conclusion

Condition monitoring of WT components could provide useful knowledge of their state. Particularly, components with high failure rates, such as gearboxes and HSS, are valuable to monitor. In this thesis, traditional analysis methods and a clustering approach was applied to detect faults ($RQ1$), fault development ($RQ2$) and reveal any relationship between the number of start-stop cycles and faults ($RQ3$). Contrary to similar studies which rely heavily on geometric dimensions and component's state to validate their results, this thesis aims to demonstrate the potential for exploratory analysis using only vibration and operational data.

The examined data was streamed from four WTs located in Trøndelag, Norway, covering a time period from August 2018 to January 2020. The data consisted of 10-second vibration signals and operational data such as power production. The vibration signals were sampled at 25.6 kHz and were measured on the HSS. WT04 had logged approximately twice as many start-stop cycles (1805) as the other three.

The traditional vibration analysis (TVA) methods studied five selected signals from each turbine, and aimed to answer all three research questions. TVA consisted of an order analysis directed towards detecting gear faults and an envelope order analysis used to detect bearing faults (REB). The proposed clustering approach used the K-means algorithm and was aimed at detecting fault development patterns (changes) in the signals, and therefore answered RQ2. The clustering method was not directed towards identifying any specific faults. Instead, it was capable of detecting transient signals and non-linearities, often associated with mechanical faults.

A traditional analysis and a data-driven approach was selected for detecting fault development due to their different properties. The TVA methods are advantageous over the data-driven approach because they are interpretable by technicians. However, the TVA methods rely on manual inspection, which is cumbersome when

looking for fault development. The clustering approach is powerful in the way it handles hundreds of signals at once, with no need for a priori knowledge. Data-driven approaches are therefore applicable in automated CM systems.

In order to answer the research questions using TVA, spectrum comparison was applied to compensate for the lack of information regarding the CFs. WT01 was compared to WT04, and WT02 was compared to WT03. These pairs were assumed to contain the same gearbox components, due to similarities in the frequency responses. To answer $RQ1$, the results from the OA indicated that the parallel gears of WT04 were more degraded than WT01. None of the other three WTs showed any noticeable gear fault characteristics. The EOA results demonstrated more vibration noise in WT04 compared to WT01. This could potentially indicate REB faults in WT04. The location of the faulty bearings were not determined. In regards to $RQ2$, no fault development was detected through either the order analysis or the EOA analysis. Concerning $RQ3$, the detected WT04 degradation implied that there could be a relationship between a relatively high number of start-stop cycles and faults.

The clustering approach grouped extracted features from the time domain, frequency domain and the time-frequency domain. K-means was run with different subsets of the extracted features to strengthen the analysis. The measurable objective of the clustering approach was assessed with an external criteria; how many indexes after 350 could be separated from the rest. This would indicate a change, potentially related to fault developments. In respect to $RQ2$, the clusters showed no sign of mechanical fault development for either of the four WTs. The *best* separation of indexes after 350 was approximately half of the samples of a relatively small cluster. Therefore, the K-means clusters were unable to indicate any fault degradation.

The TVA and the clustering approach produced similar fault development results, indicating no degradation over the time period for any of the WTs. This could either mean that no fault development existed in the signals, or that the fault development was undetected by the TVA and clustering. Validating the TVA and clustering method on other data with known faults would have been valuable in order to test the viability of the methods. Furthermore, findings from the TVA suggested that the parallel gears and bearings in WT04 were degraded.

This thesis demonstrated the potential of an exploratory analysis based only on vibration and operational signals, when component dimensions are unavailable from the manufacturer. Although, the research questions were answered, it is evident that the lack of information and domain knowledge limited the conclusiveness of the results. This study would greatly benefit from knowing component dimensions, and it is recommended that efforts are made to obtain such information in future projects.

Bibliography

Abu-Mostafa, Y.S., Magdon-Ismail, M., Lin, H.T., 2012. Learning From Data: A short Course , 215.

Alla, S., Adari, S.K., 2019. Beginning Anomaly Detection Using Python-Based Deep Learning. doi:`10.1007/978-1-4842-5177-5`.

Antoni, J., Randall, R.B., 2006. The spectral kurtosis: Application to the vibratory surveillance and diagnostics of rotating machines. Mechanical Systems and Signal Processing 20, 308–331. doi:`10.1016/j.ymssp.2004.09.002`.

Arthur, D., Vassilvitskii, S., 2007. k-means++: the advantages of careful seeding, in: Bansal, N., Pruhs, K., Stein, C. (Eds.), SODA. SIAM, p. 1027–1035. URL: `http://dblp.uni-trier.de/db/conf/soda/soda2007.html#ArthurV07`.

Barszcz, T., 2019. Vibration- Based Condition Monitoring of Wind Turbines. Springer International Publishing.

Barszcz, T., Randall, R.B., 2009. Application of spectral kurtosis for detection of a tooth crack in the planetary gear of a wind turbine. Mechanical Systems and Signal Processing 23, 1352–1365. doi:`10.1016/j.ymssp.2008.07.019`.

Bartnes, G., Amundsen, J.S., Holm, I.B., 2018. Kraftmarkedsanalyse 2018-2030 Mer vindkraft bidrar til økt nordisk kraftoverskudd. 84. URL: `http://publikasjoner.nve.no/rapport/2018/rapport2018_84.pdf`.

Basics, B.T.O., 2009. Part 1 : Maintenance Strategy Overview 29, 0–5.

Ben Ali, J., Saidi, L., Harrath, S., Bechhoefer, E., Benbouzid, M., 2018. Online automatic diagnosis of wind turbine bearings progressive degradations under real experimental conditions based on unsupervised machine learning. Applied Acoustics 132, 167–181. doi:`10.1016/j.apacoust.2017.11.021`.

Ben Ali, J., Sayadi, M., Fnaiech, F., Morello, B., Zerhouni, N., 2013. Importance of the fourth and fifth intrinsic mode functions for bearing fault diagnosis. 14th

International Conference on Sciences and Techniques of Automatic Control and Computer Engineering, STA 2013 , 259–264doi:10.1109/STA.2013.6783140.

Benesty, J., Chen, J., Huang, Y., Cohen, I., 2009. Pearson Correlation Co-efficient. volume 2. URL: http://www.springerlink.com/index/10.1007/978-3-642-00296-0, doi:10.1007/978-3-642-00296-0.

Berkhin, P., 2002. Clustering survey Bherkin. Technical Report, Accrue Software , 1–56doi:10.1007/3-540-28349-8{_}2.

Boutsidis, C., Mahoney, M.W., Drineas, P., 2009. Unsupervised feature selection for the k-means clustering problem. Advances in Neural Information Processing Systems 22 - Proceedings of the 2009 Conference , 153–161.

Caesarendra, W., Tjahjowidodo, T., 2017. A review of feature extraction methods in vibration-based condition monitoring and its application for degradation trend estimation of low-speed slew bearing. Machines 5. doi:10.3390/machines5040021.

Chang, K.M., 2010. Ensemble empirical mode decomposition: A Noise-Assited. Biomedizinische Technik 55, 193–201. doi:10.1515/BMT.2010.030.

Chen, H., Chen, P., Chen, W., Wu, C., Li, J., Wu, J., 2017. Wind turbine gearbox fault diagnosis based on improved EEMD and Hilbert square demodulation. Applied Sciences (Switzerland) 7. doi:10.3390/app7020128.

Commission, I.E., 2019. INTERNATIONAL STANDARD , 1–15.

Coultate, D.J., Hornemann, M., 2018. Why wind-turbine gearboxes fail to hit the 20-year mark. Windpower Engineering & Development , 24–26URL: https://www.windpowerengineering.com/wind-turbine-gearboxes-fail-hit-20-year-mark/.

Drago, R.J., 2007. The effect of start-up load conditions on gearbox performance and life - Failure analysis and case study. American Gear Manufacturers Association - Fall Technical Meeting of the American Gear Manufacturers Association 2007, AGMA , 125–138.

Drineas, P., Frieze, A., Kannan, R., Vempala, S., Vinay, V., 2004. Clustering large graphs via the Singular Value Decomposition. Machine Learning 56, 9–33. doi:10.1023/B:MACH.0000033113.59016.96.

Elkan, C., 2003. Using the Triangle Inequality to Accelerate k-Means. Proceedings, Twentieth International Conference on Machine Learning 1, 147–153.

Eulenfeld, T., 2018. Polycoherence: Calculate bicoherence, bispectrum, polycoherence and polyspectrum. URL: https://github.com/trichter/polycoherence.

Fackrell, J.W., White, P.R., Hammond, J.K., Pinnington, R.J., Parsons, A.T., 1995a. The interpretation of the bispectra of vibration signalsI. theory. Mechanical Systems and Signal Processing 9, 257–266. doi:10.1006/mssp.1995.0021.

Fackrell, J.W., White, P.R., Hammond, J.K., Pinnington, R.J., Parsons, A.T., 1995b. The interpretation of the bispectra of vibration signals—II. Experimental results and applications. Mechanical Systems and Signal Processing 9, 267–274. doi:`10.1006/mssp.1994.0022`.

Frigui, H., 2008. Clustering: Algorithms and applications. 2008 1st International Workshops on Image Processing Theory, Tools and Applications, IPTA 2008 doi:`10.1109/IPTA.2008.4743793`.

Gaci, S., 2016. A New Ensemble Empirical Mode Decomposition (EEMD) Denoising Method for Seismic Signals. Energy Procedia 97, 84–91. URL: `http://dx.doi.org/10.1016/j.egypro.2016.10.026`, doi:`10.1016/j.egypro.2016.10.026`.

Guo, W., Tse, P.W., Djordjevich, A., 2012a. Faulty bearing signal recovery from large noise using a hybrid method based on spectral kurtosis and ensemble empirical mode decomposition. Measurement: Journal of the International Measurement Confederation 45, 1308–1322. URL: `http://dx.doi.org/10.1016/j.measurement.2012.01.001`, doi:`10.1016/j.measurement.2012.01.001`.

Guo, Y., Liu, T.W., Na, J., Fung, R.F., 2012b. Envelope order tracking for fault detection in rolling element bearings. Journal of Sound and Vibration 331, 5644–5654. URL: `http://dx.doi.org/10.1016/j.jsv.2012.07.026`, doi:`10.1016/j.jsv.2012.07.026`.

Guyon, I., Elisseeff, A., 2003. An Introduction to Variable and Feature Selection. Journal of Machine Learning Research , 1157–1182doi:`10.1016/j.aca.2011.07.027`.

Guyon, I., Gunn, S., Ben Hur, A., Dror, G., 2005. Result analysis of the NIPS 2003 feature selection challenge. Advances in Neural Information Processing Systems .

Hinich, M.J., Wilson, G.R., 1990. Detection of Non-Gaussian Signals in Non-Gaussian Noise Using the Bispectrum. IEEE Transactions on Acoustics, Speech, and Signal Processing 38, 1126–1131. doi:`10.1109/29.57541`.

Hintze, J.L., Nelson, R.D., 1998. Violin Plots: A Box Plot-Density Trace Synergism Statistical Computing and Graphics Violin Plots: A Box Plot-Density Trace Synergism. Source: The American Statistician 52, 181–184. URL: `http://www.jstor.org/stable/2685478%5Cnhttp://www.jstor.org/%5Cnhttp://www.jstor.org/action/showPublisher?publisherCode=astata.%5Cnhttp://www.jstor.org`.

Huang, K.G.M.C.K.M.H., 2017. Anomaly Algorithms Principles and Detection.

Huitao, C., Shuangxi, J., Xianhui, W., Zhiyang, W., 2018. Fault diagnosis of wind turbine gearbox based on wavelet neural network. Journal of Low Frequency Noise Vibration and Active Control 37, 977–986. doi:`10.1177/1461348418795376`.

Jackson, L.B., 2002. Digital Filters and Signal Processing. URL: `http://dx.doi.org/10.1016/j.tws.2012.02.007`, doi:`10.1017/CBO9781107415324.004`.

Jain, A.K., 2010. Data clustering: 50 years beyond K-means. Pattern Recognition Letters 31, 651–666. URL: `http://dx.doi.org/10.1016/j.patrec.2009.09.011`, doi:`10.1016/j.patrec.2009.09.011`.

Jain, A.K., Dubes, R.C., 1988. Algorithms for Clustering Data.

James, G., Witten, D., Hastie, T., Tibshirani, R., 2013. An Introduction to Statistical Learning. volume 64. 1st ed. doi:`10.1016/j.peva.2007.06.006`.

Laszuk, D., 2017. Python implementation of Empirical Mode Decomposition algorithm. URL: `https://github.com/laszukdawid/PyEMD`.

Lee, J., Zhao, F., 2020. GWEC Global Wind Report. Wind energy technology , 78URL: `www.gwec.net`.

Li, H., Zheng, H., Tang, L., 2009. Gear fault diagnosis based on order tracking and Hilbert-Huang transform. 6th International Conference on Fuzzy Systems and Knowledge Discovery, FSKD 2009 4, 468–472. doi:`10.1109/FSKD.2009.220`.

Liu, C.S., 2005. Fault Detection Of Rolling Element Bearings.

Liu, X., Xu, X., Jiang, Z., Wu, G., Zuo, Y., 2016. Application of the state deterioration evolution based on bi-spectrum entropy and HMM in wind turbine. Chaos, Solitons and Fractals 89, 160–168. doi:`10.1016/j.chaos.2015.10.018`.

Lloyd, S.P., 1982. Least Squares Quantization in PCM. IEEE Transactions on Information Theory 28, 129–137. doi:`10.1109/TIT.1982.1056489`.

MATLAB, 2019. version 9.7.0.1190292 (R2019b). The MathWorks Inc., Natick, Massachusetts.

McFadden, P.D., 1989. Interpolation techniques for time domain averaging of gear vibration. Mechanical Systems and Signal Processing 3, 87–97. doi:`10.1016/0888-3270(89)90024-1`.

Mendel, J.M., 1991. Tutorial on Higher-Order Statistics (Spectra) in Signal Processing and System Theory: Theoretical Results and Some Applications. Proceedings of the IEEE 79, 278–305. doi:`10.1109/5.75086`.

Murphy, K.P., 2012. Machine Learning: A Probabilistic Perspective. The MIT press. doi:`10.1007/978-94-011-3532-0{\_}2`.

Musial, W., Butterfield, S., Mcniff, B., 2007. Improving wind turbine gearbox reliability. European Wind Energy Conference and Exhibition 2007, EWEC 2007 3, 1770–1779.

Nikias, C.L., Mendel, J.M., 1993. Statistics and Spectra of a Signal Can Be Defined in Terms. IEEE Signal Processing Magazine doi:`10.1210/jc.2010-2239`.

Randall, R.B., 2011. Vibration-Based Condition Monitoring.

Ribeiro, M.T., Singh, S., Guestrin, C., 2016. "Why should i trust you?" Explaining the predictions of any classifier. Proceedings of the ACM SIGKDD International Conference on Knowledge Discovery and Data Mining 13-17-Augu, 1135–1144. doi:`10.1145/2939672.2939778`.

Rivola, A., White, P.R., 1999. Detecting system non-linearities by means of higher order statistics. Revue Francaise De Mecanique 2, 129–136.

Saidi, L., Ali, J.B., Fnaiech, F., 2014. Bi-spectrum based-EMD applied to the non-stationary vibration signals for bearing faults diagnosis. ISA Transactions 53, 1650–1660. doi:`10.1016/j.isatra.2014.06.002`.

Saidi, L., Ben Ali, J., Fnaiech, F., 2015. Application of higher order spectral features and support vector machines for bearing faults classification. ISA Transactions 54, 193–206. doi:`10.1016/j.isatra.2014.08.007`.

Sanger, D., 2017. Reactive, preventive and predictive maintenance. URL: `https://ivctechnologies.com/2017/08/29/reactive-preventive-predictive-maintenance/`.

Statkraft, . Wind power briefly explained.

Stetco, A., Dinmohammadi, F., Zhao, X., Robu, V., Flynn, D., Barnes, M., Keane, J., Nenadic, G., 2019. Machine learning methods for wind turbine condition monitoring: A review. doi:`10.1016/j.renene.2018.10.047`.

Tchakoua, P., Wamkeue, R., Ouhrouche, M., Slaoui-Hasnaoui, F., Tameghe, T.A., Ekemb, G., 2014. Wind turbine condition monitoring: State-of-the-art review, new trends, and future challenges. Energies 7, 2595–2630. doi:`10.3390/en7042595`.

The International Renewable Energy Agency (IRENA), 2012. Wind Power. doi:`10.1007/978-3-642-20951-2{\_}8`.

TrønderEnergi, . Skomakerfjellet vindkraft. URL: `https://tronderenergi.no/produksjon/kraftverk/bessakerfjellet2`.

Uhrmann, H., Kolm, R., Zimmermann, H., 2014. Analog Filters. Springer Series in Advanced Microelectronics 45, 3–11. doi:`10.1007/978-3-642-38013-6{\_}2`.

Van Der Walt, S., Colbert, S.C., Varoquaux, G., 2011. The NumPy array: A structure for efficient numerical computation. Computing in Science and Engineering 13, 22–30. doi:`10.1109/MCSE.2011.37`.

Verbruggen, T., 2003. Wind turbine operation and maintenance based on condition monitoring WT-. Technical Report,ECN-C–03-047, .

Virtanen, P., Gommers, R., Oliphant, T.E., Haberland, M., Reddy, T., Courna-peau, D., Burovski, E., Peterson, P., Weckesser, W., Bright, J., van der Walt, S.J., Brett, M., Wilson, J., Millman, K.J., Mayorov, N., Nelson, A.R., Jones, E., Kern, R., Larson, E., Carey, C.J., Polat, , Feng, Y., Moore, E.W., Vander-Plas, J., Laxalde, D., Perktold, J., Cimrman, R., Henriksen, I., Quintero, E.A., Harris, C.R., Archibald, A.M., Ribeiro, A.H., Pedregosa, F., van Mulbregt, P., Vijaykumar, A., Bardelli, A.P., Rothberg, A., Hilboll, A., Kloeckner, A., Sco-patz, A., Lee, A., Rokem, A., Woods, C.N., Fulton, C., Masson, C., Häggström, C., Fitzgerald, C., Nicholson, D.A., Hagen, D.R., Pasechnik, D.V., Olivetti, E., Martin, E., Wieser, E., Silva, F., Lenders, F., Wilhelm, F., Young, G., Price, G.A., Ingold, G.L., Allen, G.E., Lee, G.R., Audren, H., Probst, I., Dietrich, J.P., Silterra, J., Webber, J.T., Slavič, J., Nothman, J., Buchner, J., Kulick, J., Schön-berger, J.L., de Miranda Cardoso, J.V., Reimer, J., Harrington, J., Rodríguez, J.L.C., Nunez-Iglesias, J., Kuczynski, J., Tritz, K., Thoma, M., Newville, M., Kümmerer, M., Bolingbroke, M., Tartre, M., Pak, M., Smith, N.J., Nowaczyk, N., Shebanov, N., Pavlyk, O., Brodtkorb, P.A., Lee, P., McGibbon, R.T., Feld-bauer, R., Lewis, S., Tygier, S., Sievert, S., Vigna, S., Peterson, S., More, S., Pud-lik, T., Oshima, T., Pingel, T.J., Robitaille, T.P., Spura, T., Jones, T.R., Cera, T., Leslie, T., Zito, T., Krauss, T., Upadhyay, U., Halchenko, Y.O., Vázquez-Baeza, Y., 2020. SciPy 1.0: fundamental algorithms for scientific computing in Python. Nature Methods 17, 261–272. doi:10.1038/s41592-019-0686-2.

Viseth, E.S., 2018. TrønderEnergi satser stort på vind - tredobler porteføljen. URL: https://www.tu.no/artikler/tronderenergi-satser-stort-pa-vind/449760.

Wang, G., Gu, F., Rehab, I., Ball, A., Li, L., 2018. A Sparse Modulation Signal Bis-pectrum Analysis Method for Rolling Element Bearing Diagnosis. Mathematical Problems in Engineering 2018. doi:10.1155/2018/2954094.

Wei, Y., Li, Y., Xu, M., Huang, W., 2019. A review of early fault diagnosis approaches and their applications in rotating machinery. Entropy 21, 1–26. doi:10.3390/e21040409.

Wolpert, D.H., 1996. The Lack of a Priori Distinctions between Learning Algorithms. Neural Computation 8, 1341–1390. doi:10.1162/neco.1996.8.7.1341.

Yiakopoulos, C.T., Gryllias, K.C., Antoniadis, I.A., 2011. Rolling element bearing fault detection in industrial environments based on a K-means clustering approach. Expert Systems with Applications 38, 2888–2911. URL: http://dx.doi.org/10.1016/j.eswa.2010.08.083, doi:10.1016/j.eswa.2010.08.083.

Yu, Y., YuDejie, Junsheng, C., 2006. A roller bearing fault diagnosis method based on EMD energy entropy and ANN. Journal of Sound and Vibration 294, 269–277. doi:10.1016/j.jsv.2005.11.002.

Zhao, M., Lin, J., Xu, X., Lei, Y., 2013. Tacholess envelope order analysis and its application to fault detection of rolling element bearings with varying speeds. Sensors (Switzerland) 13, 10856–10875. doi:10.3390/s130810856.

Zhao, M., Lin, J., Xu, X., Li, X., 2014. Multi-Fault detection of rolling element bearings under harsh working condition using imf-based adaptive envelope order analysis. Sensors (Switzerland) 14, 20320–20346. doi:10.3390/s141120320.

Appendix A

Supplementary Theory

A.1 Spectral Kurtosis Definition

The mathematical definition of Spectral Kurtosis is as follows (Barszcz, 2019). A system with input $x(t)$, an output $y(t)$ and a time varying impulse response $h(t, s)$, can be described as:

$$y(t) = \int_{-\infty}^{+\infty} e^{j2\pi} H(t, f) dX(f) \tag{A.1}$$

where $H(t, f)$ is the time varying transfer function. It can also be described as the complex envelope of the signal $y(t)$ at frequency f. Given that H is stationary and H and X are independent, the process y is considered conditionally non-stationary and the fourth order spectral cumulant of the process can be calculated. Its definition is show in equation A.2:

$$C_{4Y}(f) = S_{4Y}(f) - 2S_{4Y}^2(f) \tag{A.2}$$

where $S_{2nY}(t, f)$ is the 2nd-order instantaneous moment, interpreted as the measure of energy of the complex envelope. It is defined as:

$$S_{2nY}(t, f) = \frac{E\{|H(t, f)dX(f)|^{2n}\omega\}}{df} = |H(t, f)|^{2n} S_{2nX} \tag{A.3}$$

At last, Spectral Kurtosis is defined as the energy normalised cumulant and given in equation A.4

$$K_Y(f) = \frac{C_{4Y}(f)}{S_{2Y}^2(f)} = \frac{S_{4Y}(f)}{S_{2Y}^2(f)} - 2 \tag{A.4}$$

A.2   Challenges with Clustering

List of challenges associated with clustering by Jain and Dubes (1988):

1. What is a cluster?

2. What features should be used?

3. Should the data be normalized?

4. Are there any outliers (extreme values) in the data?

5. How do we define the pair-wise similarity?

6. How many clusters are present in the data?

7. What clustering method should be used?

8. Does the data have any clustering tendency?

9. Are the discovered clusters valid?

Appendix B

Data Plots

B.1 Kurtograms - Spectral Kurtosis

Figure B.1: WT01: Kurtogram of the first of five selected signals.
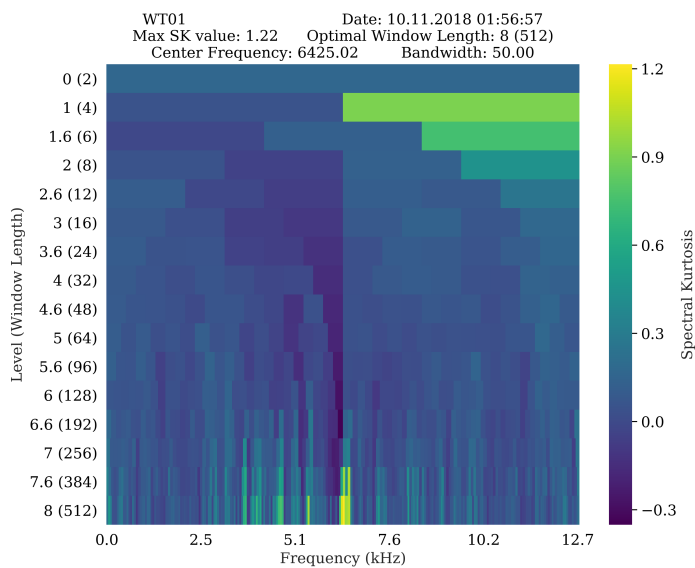
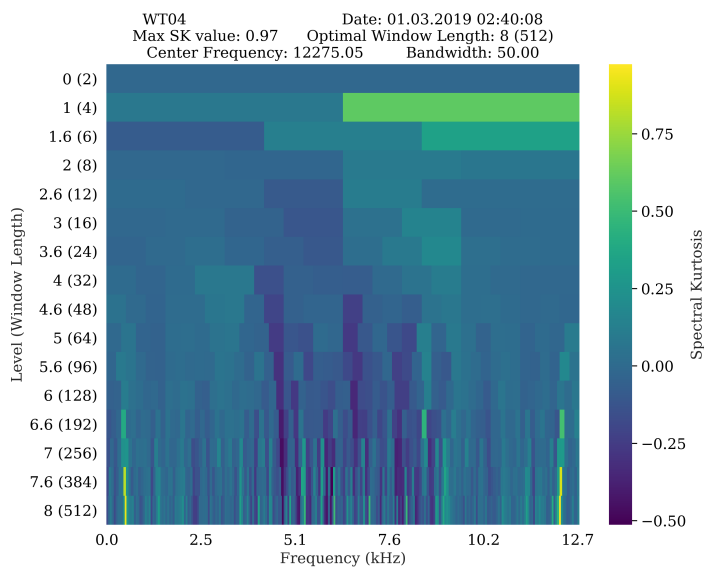**Figure B.2:** WT01: Kurtogram of the second of five selected signals.
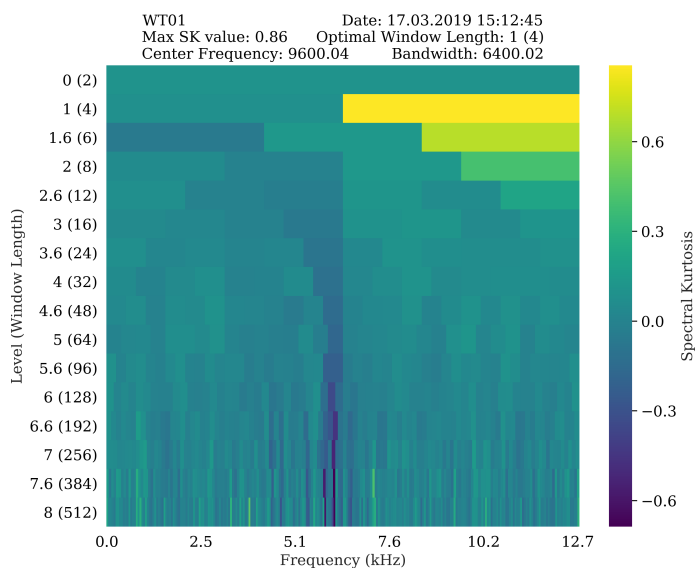
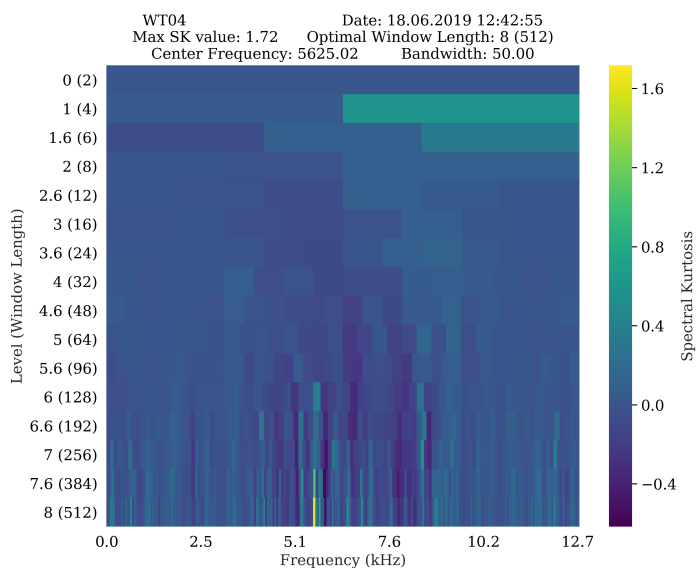**Figure B.3:** WT01: Kurtogram of the third of five selected signals.
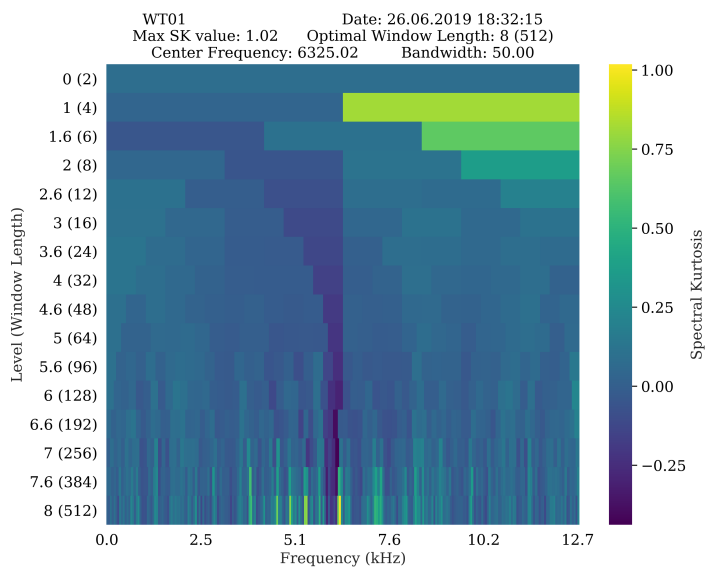
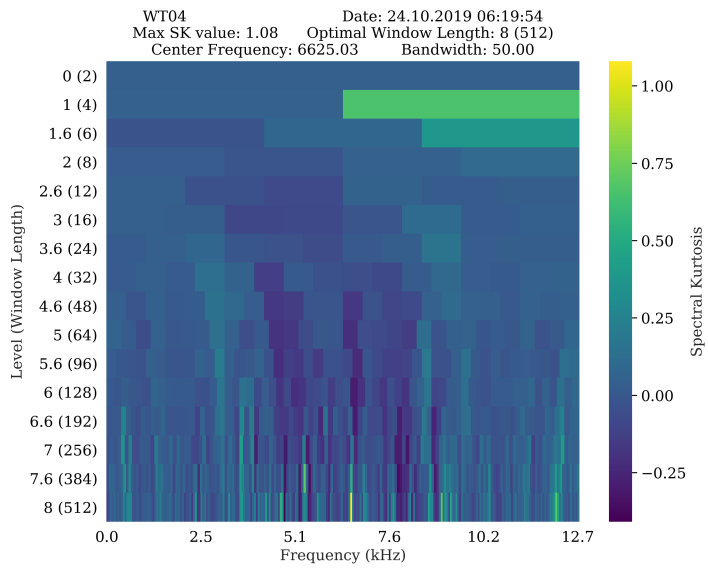**Figure B.4:** WT01: Kurtogram of the fourth of five selected signals.
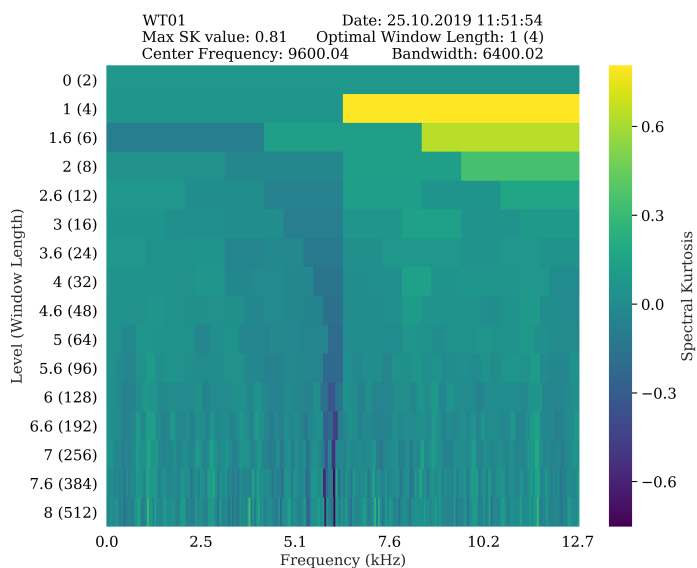
Figure B.5: WT01: Kurtogram of the fifth of five selected signals.
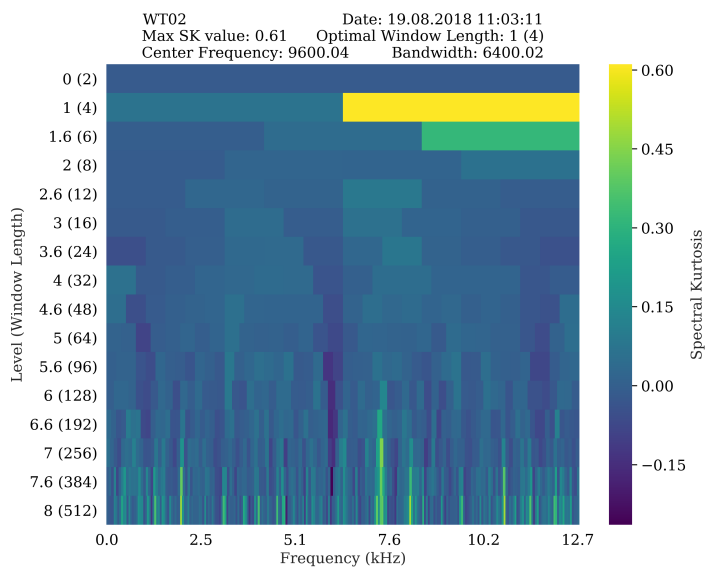
Figure B.6: WT02: Kurtogram of the first of five selected signals.
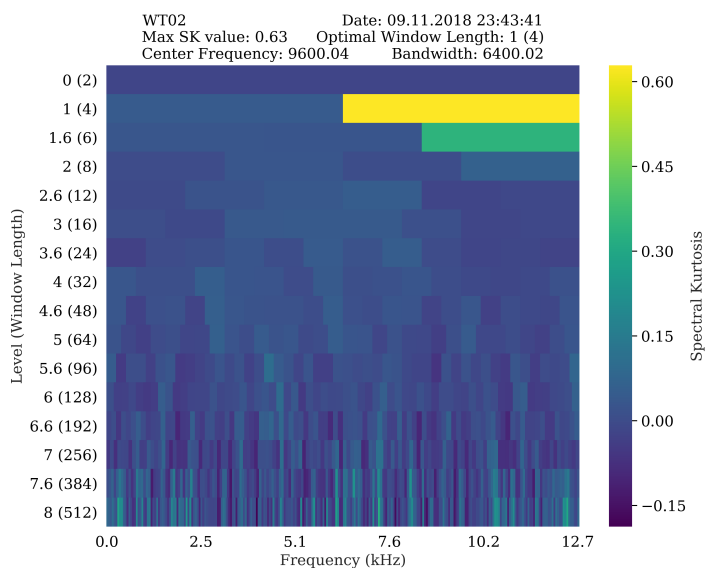
Figure B.7: WT02: Kurtogram of the second of five selected signals.
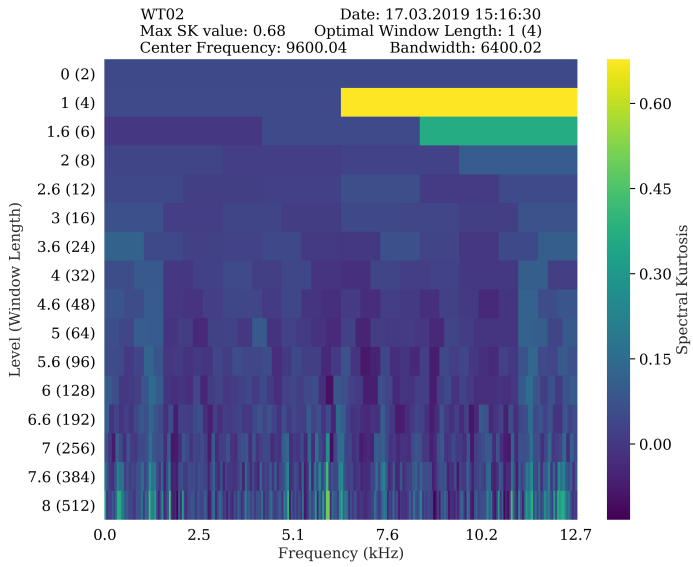
Figure B.8: WT02: Kurtogram of the third of five selected signals.
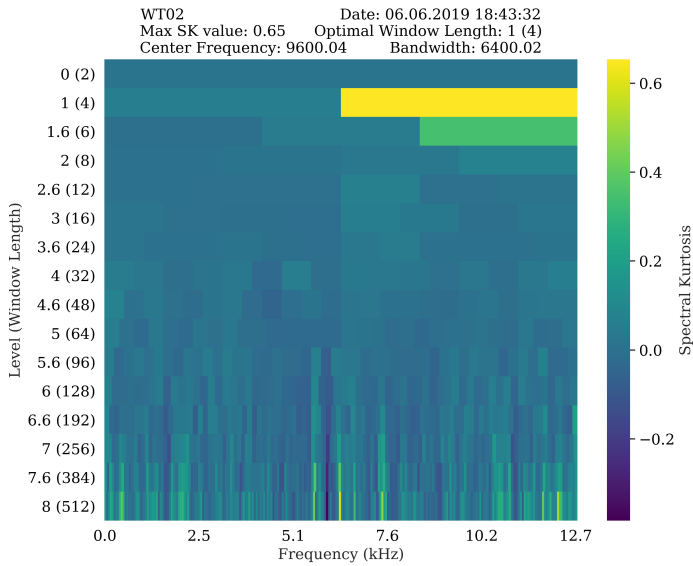
Figure B.9: WT02: Kurtogram of the fourth of five selected signals.
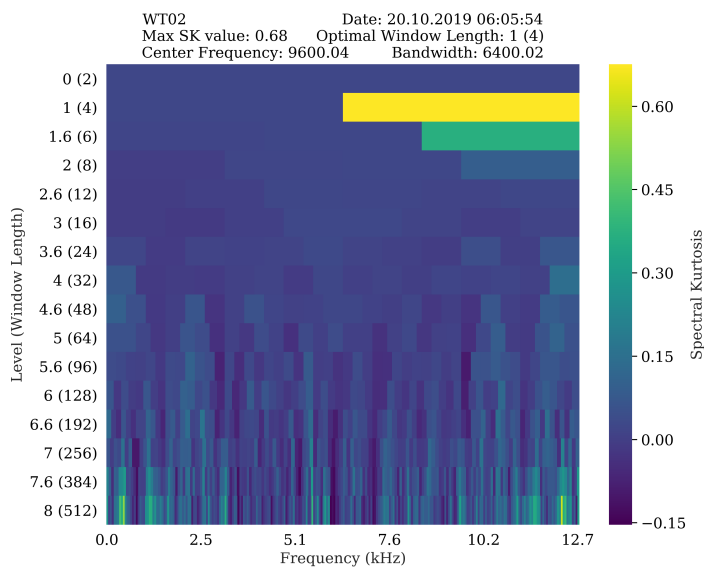
Figure B.10: WT02: Kurtogram of the fifth of five selected signals.
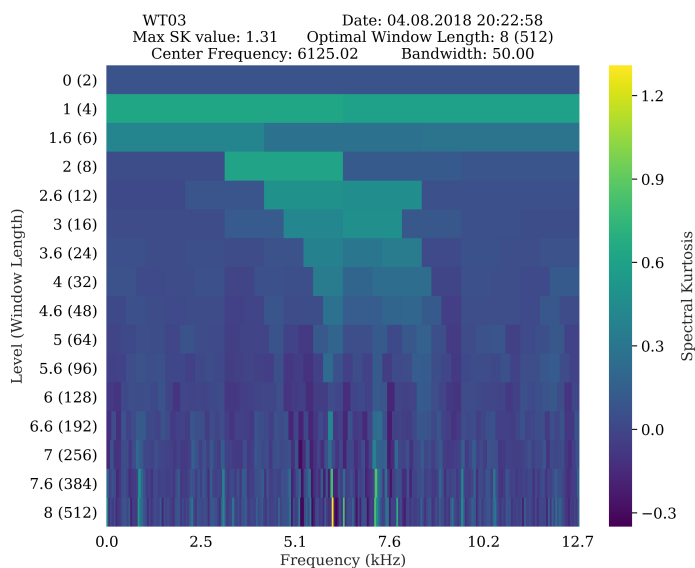
Figure B.11: WT03: Kurtogram of the first of five selected signals.
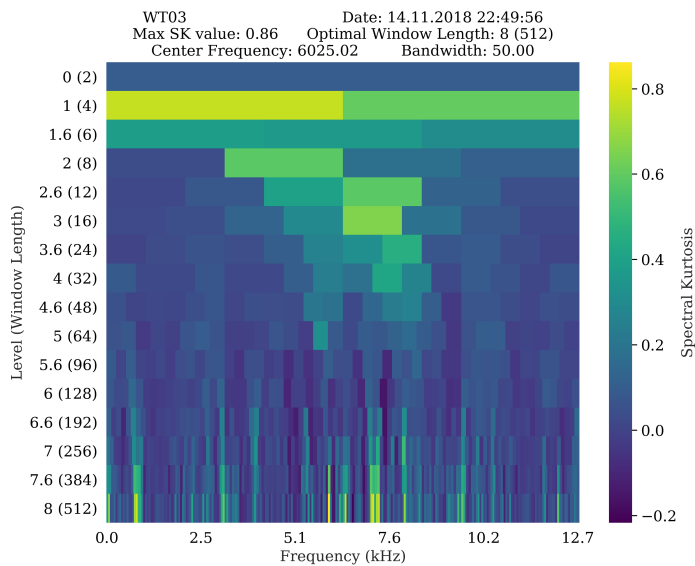
Figure B.12: WT03: Kurtogram of the second of five selected signals.
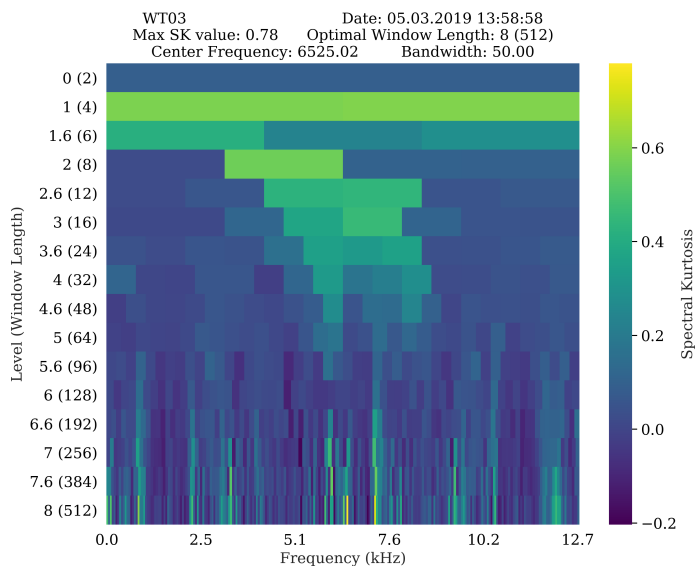
Figure B.13: WT03: Kurtogram of the third of five selected signals.
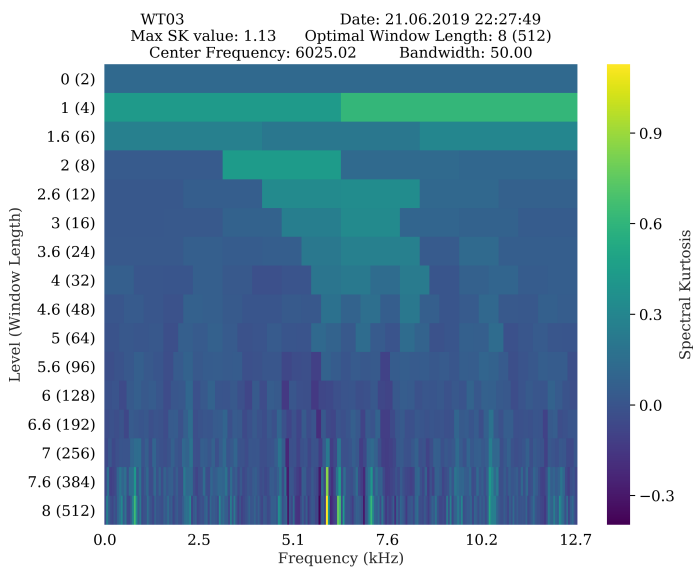
Figure B.14: WT03: Kurtogram of the fourth of five selected signals.
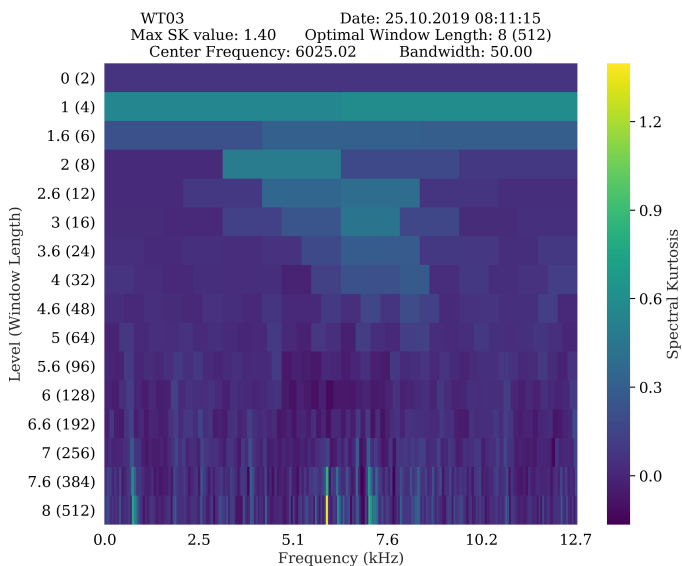
Figure B.15: WT03: Kurtogram of the fifth of five selected signals.
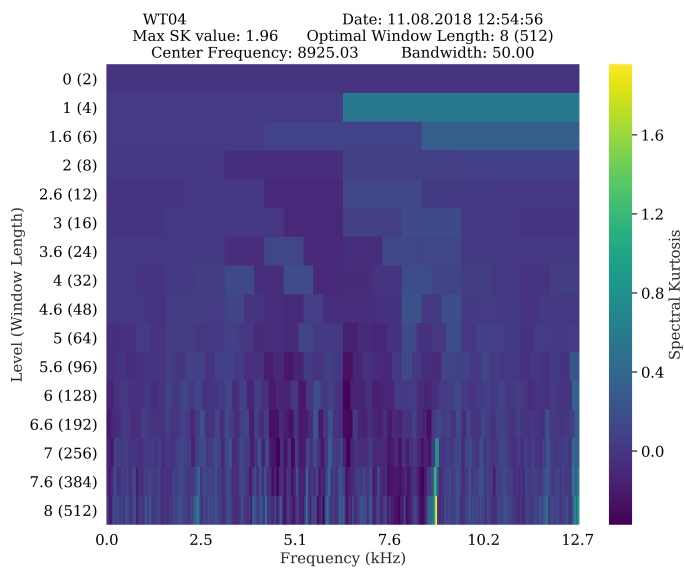
Figure B.16: WT04: Kurtogram of the first of five selected signals.
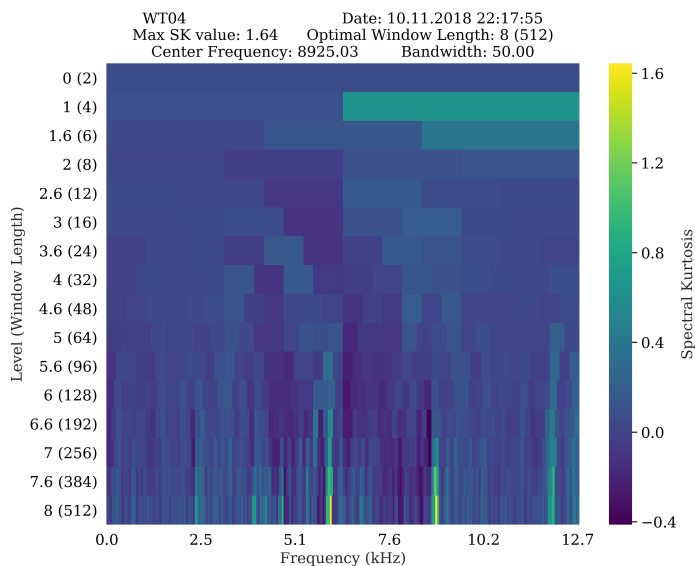
Figure B.17: WT04: Kurtogram of the second of five selected signals.

Figure B.18: WT04: Kurtogram of the third of five selected signals.

Figure B.19: WT04: Kurtogram of the fourth of five selected signals.

Figure B.20: WT04: Kurtogram of the fifth of five selected signals.

B.2 Feature Exploration Plots

B.2.1 WT02
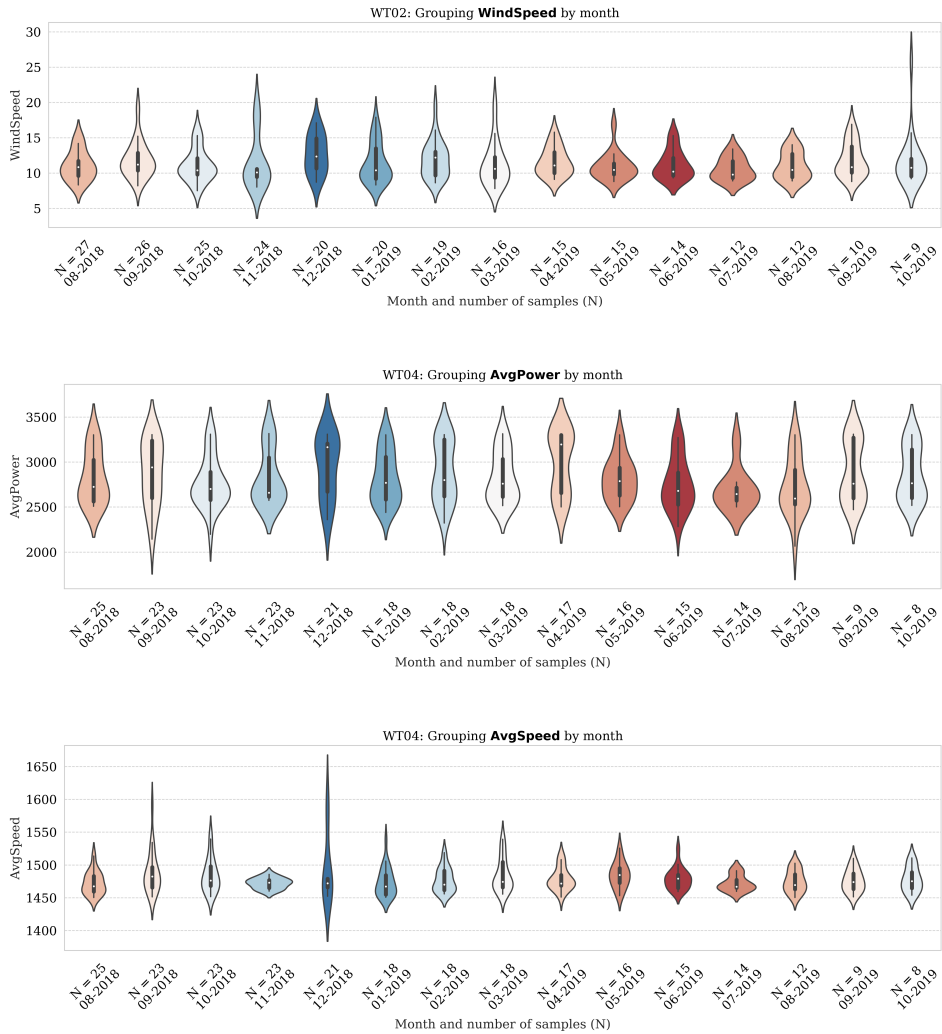
Figure B.21: WT02: Wind speed, Average Power produced and Average Shaft speed (High Speed shaft) grouped by month.

B.2.2 WT03
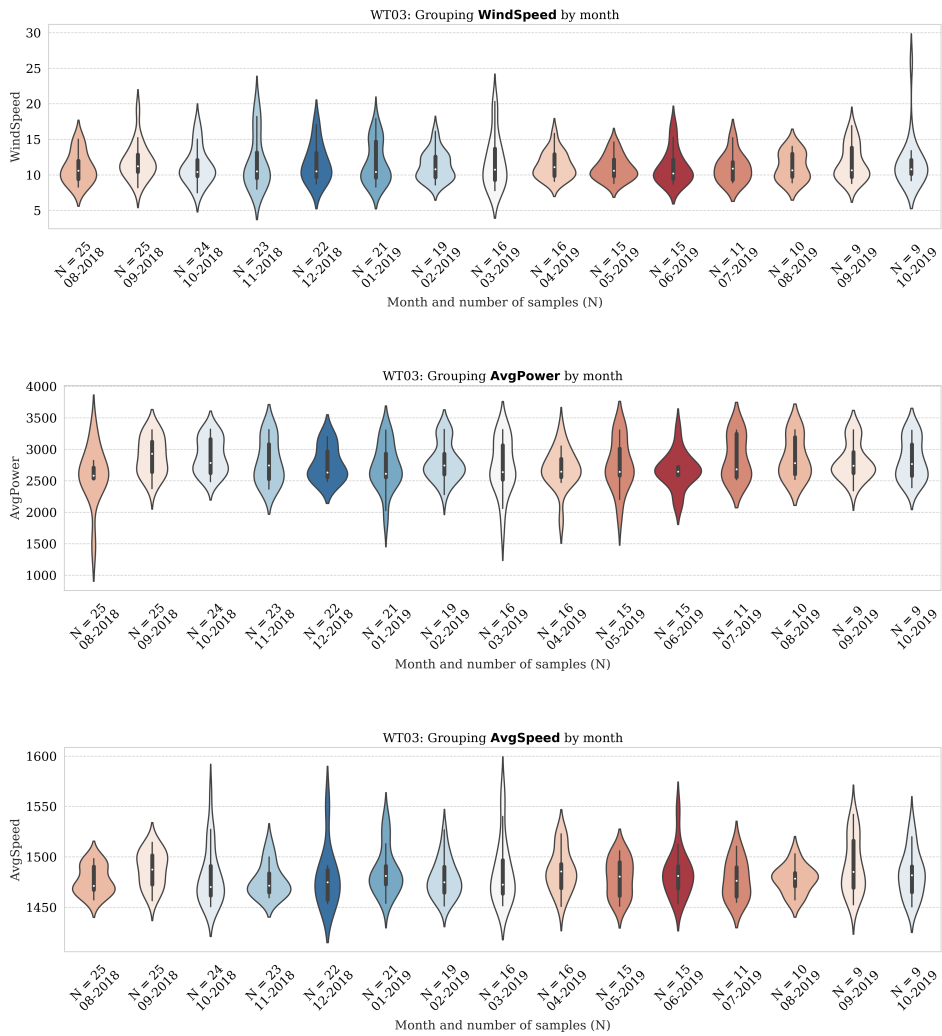
Figure B.22: WT03: Wind speed, Average Power produced and Average Shaft speed (High Speed shaft) grouped by month.

B.2.3 WT04
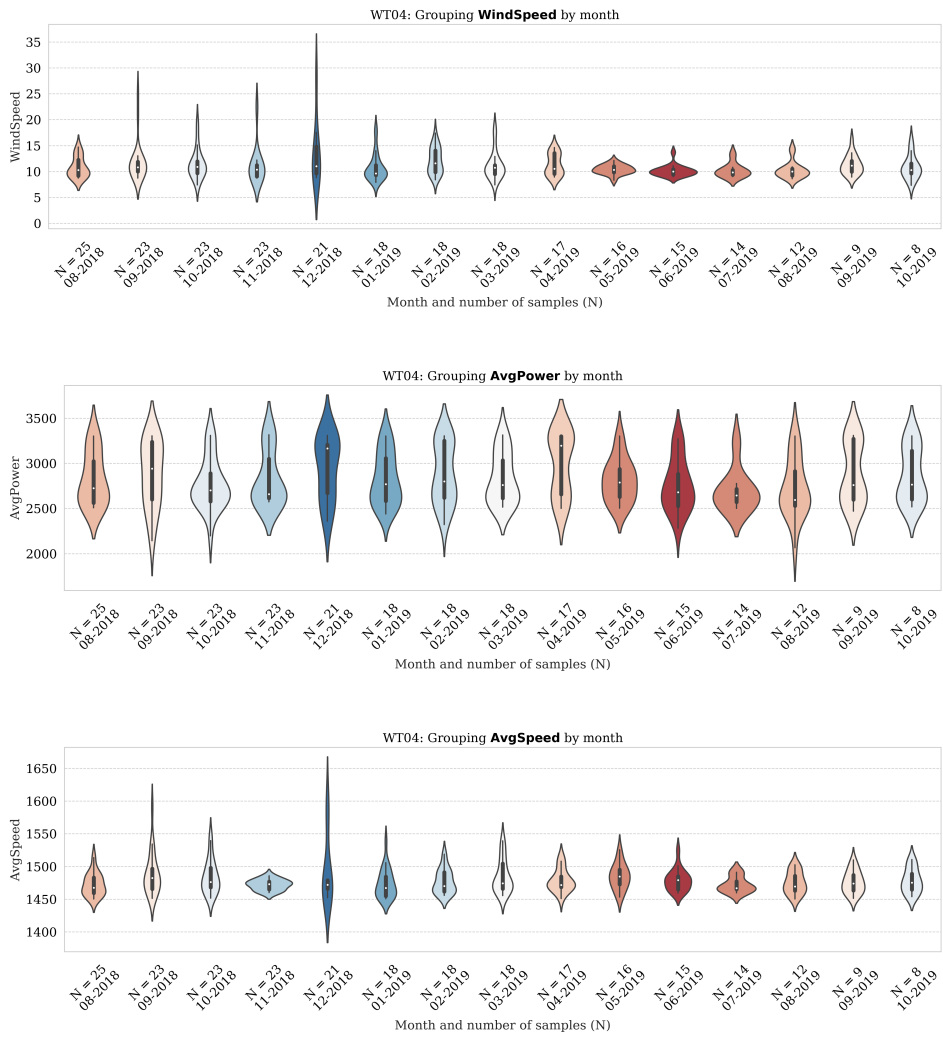
Figure B.23: WT04: Wind speed, Average Power produced and Average Shaft speed (High Speed shaft) grouped by month.

B.3 Correlation Plots for Data Sets
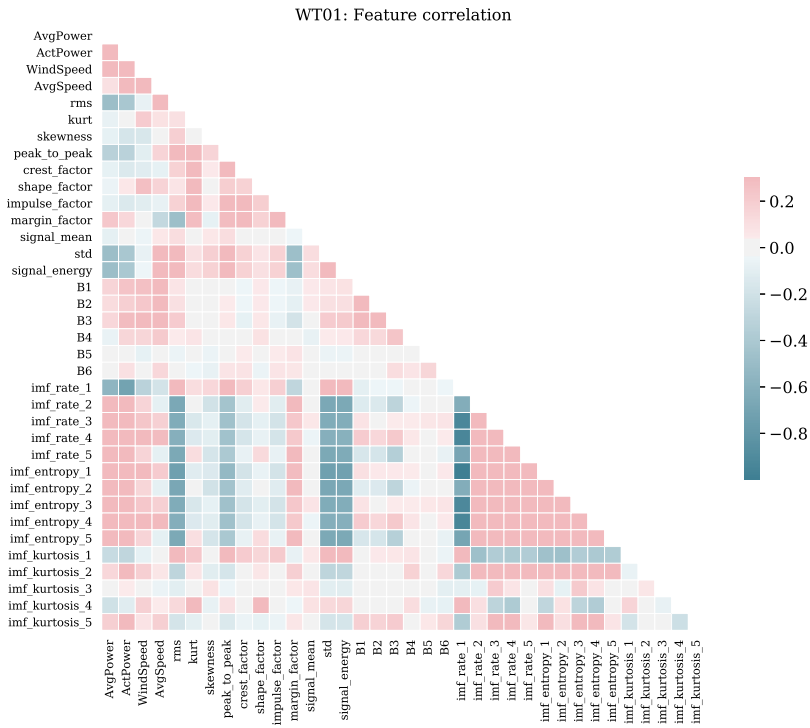
Figure B.24: WT01: Correlation plot of all the 36 features extracted.
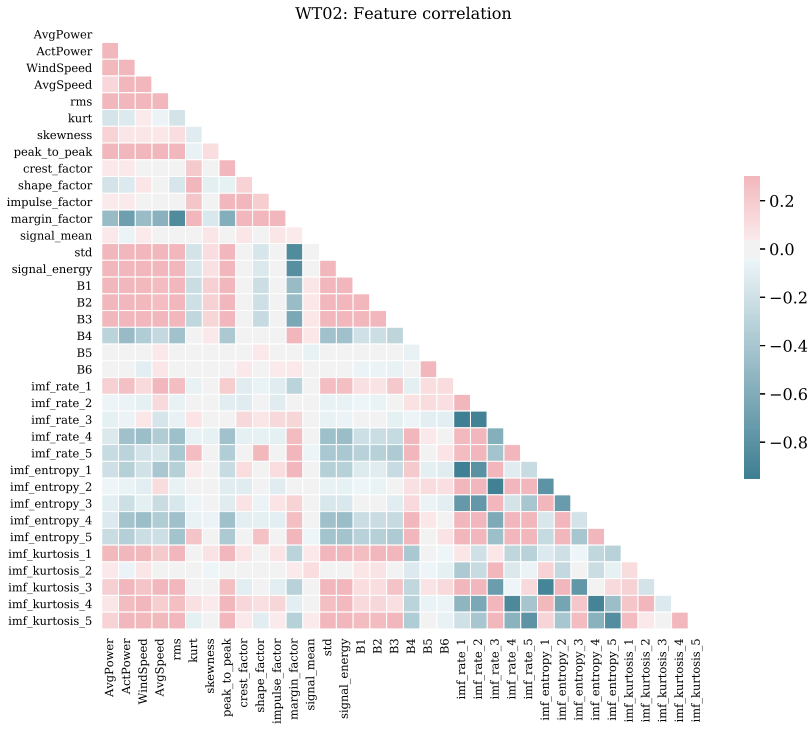
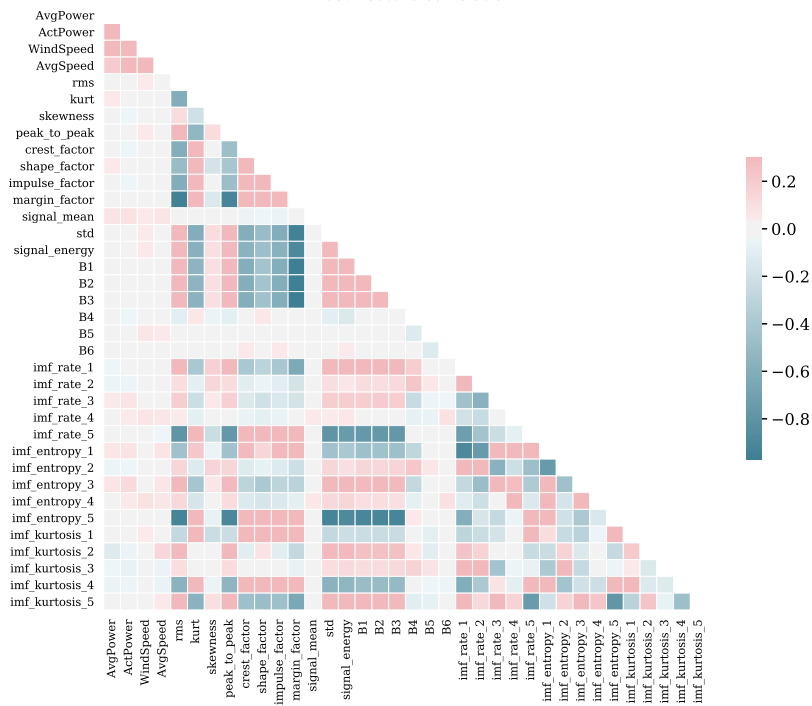**Figure B.25:** WT02: Correlation plot of all the 36 features extracted.

Figure B.26: WT03: Correlation plot of all the 36 features extracted.
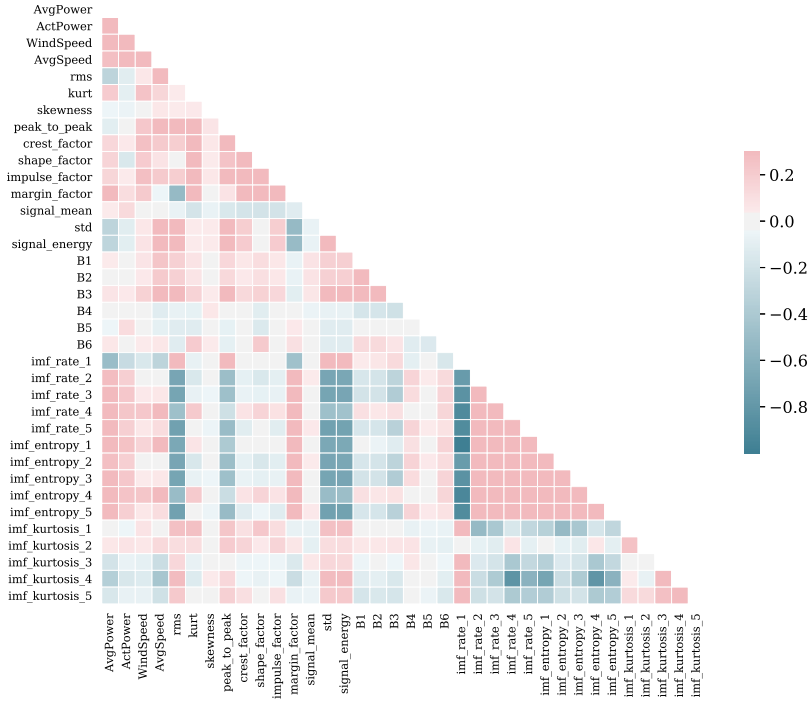
Figure B.27: WT04: Correlation plot of all the 36 features extracted.

B.4 Box Plots for Data Sets
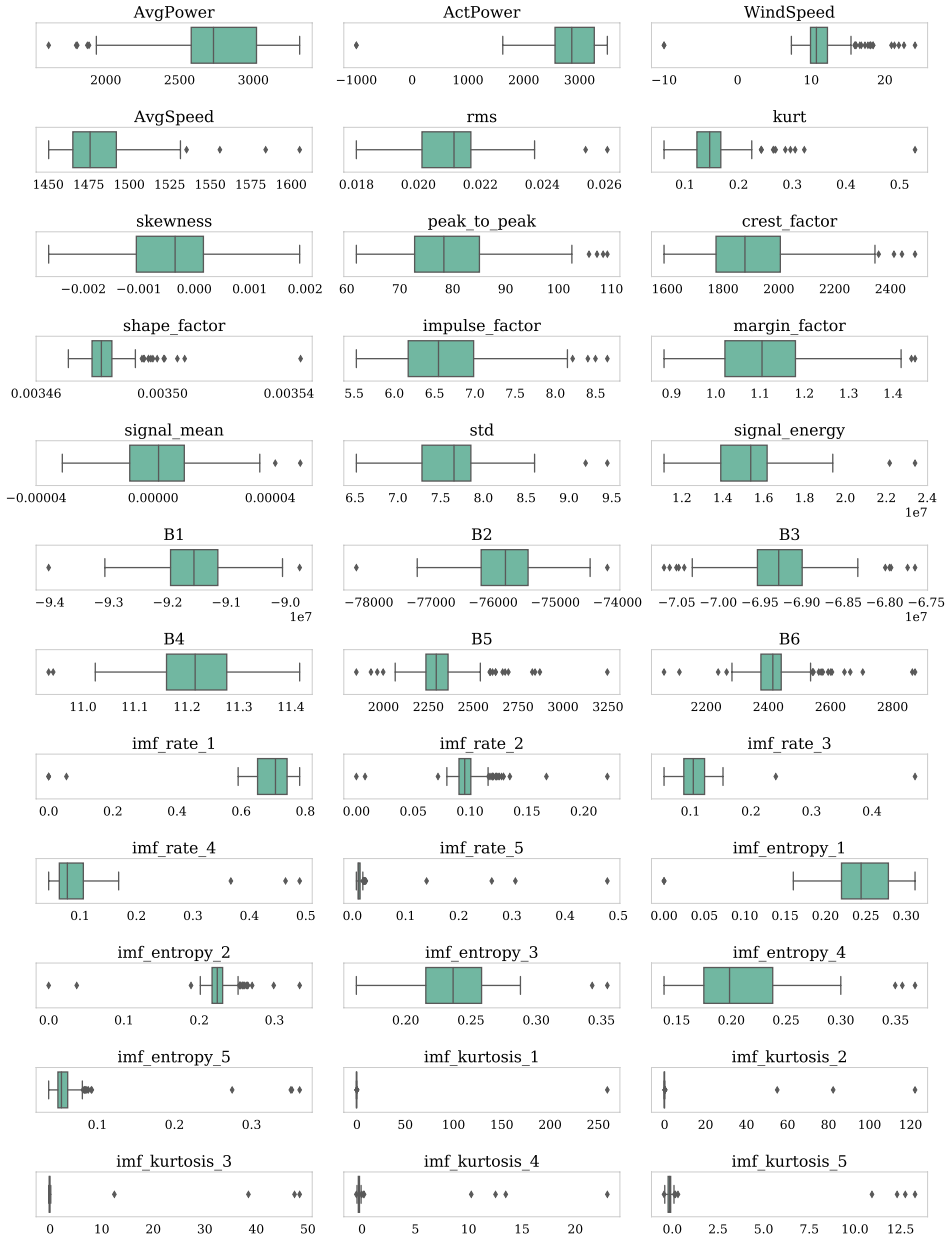
WT01: Box plot of the 36 extracted features

Figure B.28: WT01: Boxplot on the unfiltered data after extracting features.

WT02: Box plot of the 36 extracted features

Figure B.29: WT02: Boxplot on the unfiltered data after extracting features.

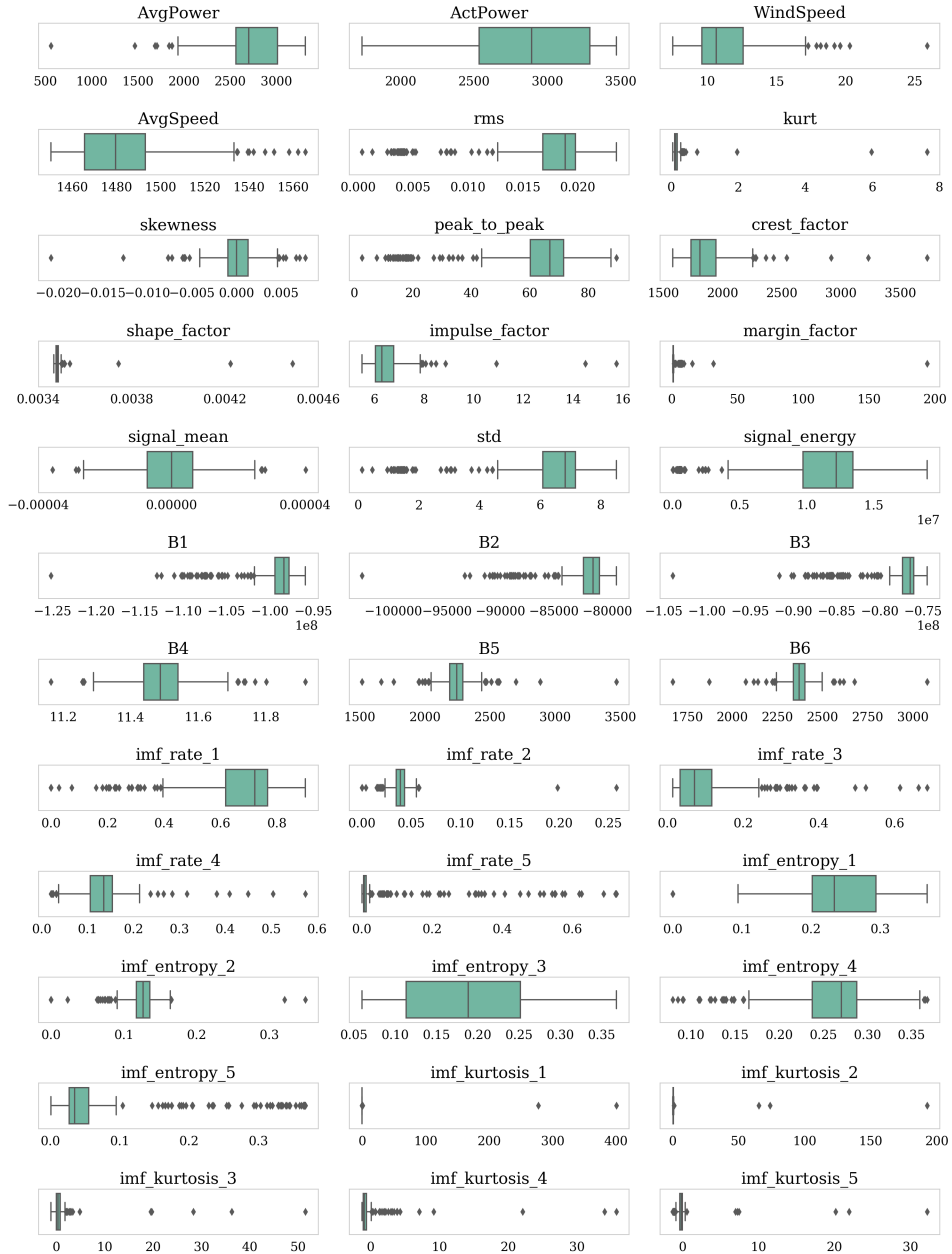# WT03: Box plot of the 36 extracted features

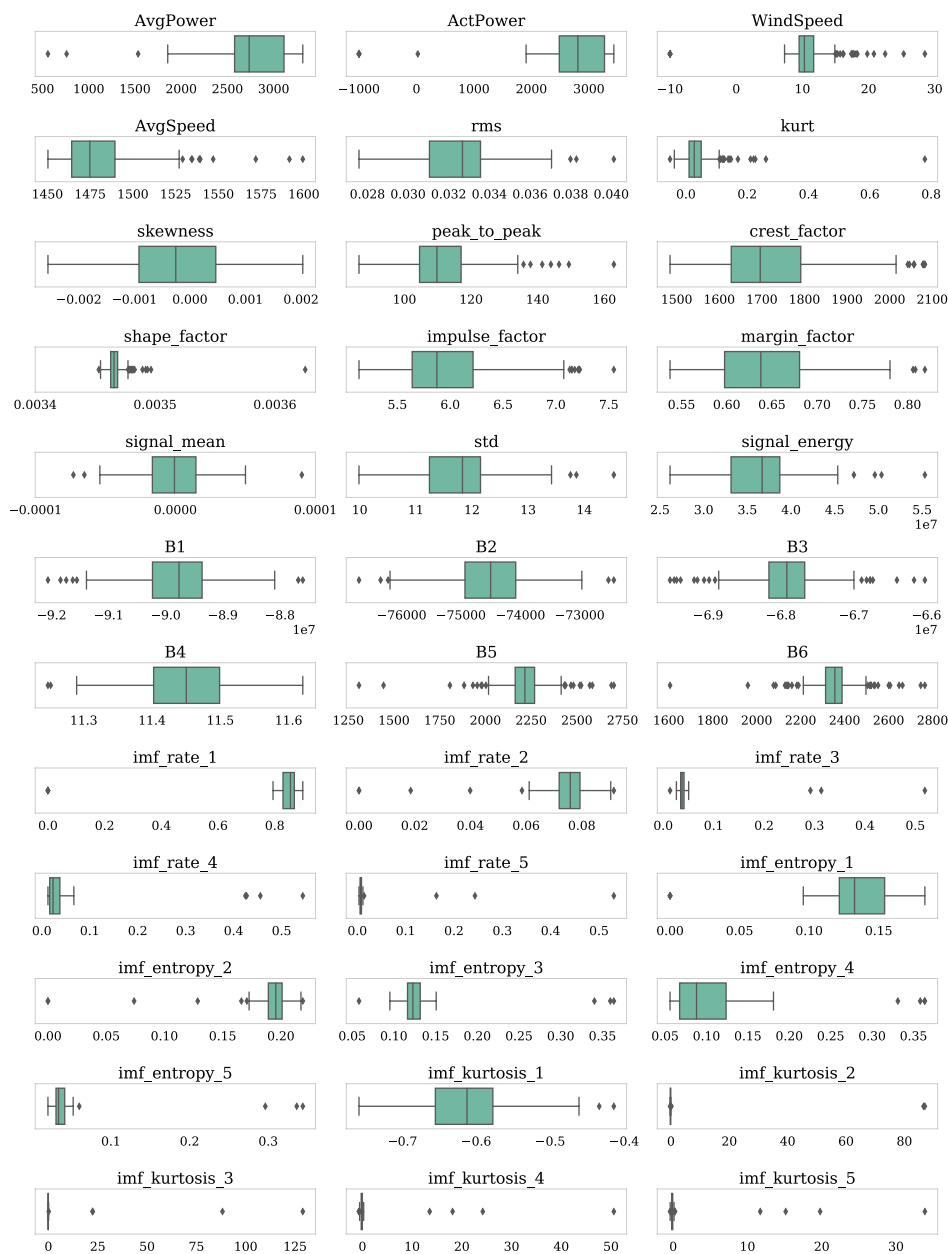**Figure B.30:** WT03: Boxplot on the unfiltered data after extracting features.

Figure B.31: WT04: Boxplot on the unfiltered data after extracting features.

Stian Ismar, Morten Olsen Osvik

Detecting Gear and Bearing Faults in Wind Turbines

NTNU
Norwegian University of
Science and Technology